BRAIN CONNECTOME IN MAJOR DEPRESSION AND PRETERM BORN INDIVIDUALS AT RISK FOR DEPRESSION

Graduate School of
Systemic Neurosciences
LMU Munich

Dissertation of the Graduate School of Systemic Neurosciences

Ludwig-Maximilians-University Munich

Submitted by Chun Meng

Defense:
Munich, November 13th, 2014

Supervisor:
Dr. Afra Wohlschläger
Dr. Christian Sorg
Prof. Dr. Hermann Müller

Examination committee:
Dr. Afra Wohlschläger
Dr. Christian Sorg
Dr. Virginia L. Flanagin
Prof. Dr. Hermann Müller

Table of contents

Outline of this thesis **3**

Abbreviations **4**

Initial summary **5**

Aim of this thesis **8**

Introduction **9**

The networked brain: *human brain connectome* 9
Connectome and connectomics *9*
Macroscopic brain connectome *11*

Current arts to explore brain connectome based on MRI 14
Measuring brain activity and gray matter's functional connectivity *17*
Measuring brain structure and white matter's connectivity *22*
Characterizing connectivity profiles *24*
Characterizing network topology *26*

Mental disorder and risk factors affect brain connectome 31

Major depression and preterm birth affect brain connectome 34
Open general questions about the connectome trajectory in major depression *39*

References 40

Paper 1 **51**

Aberrant topology of striatum's connectivity is associated with the number of episodes in depression (Brain, 2014) 51

Manuscript 1 **77**

Aberrant microstructural white matter is associated with the number of episodes in major depression

Manuscript 2 **105**

Altered functional brain connectome in very preterm born adults (submitted)

Manuscript 3 **151**

Extensive and interrelated subcortical white and gray matter alterations in preterm born adults (submitted)

Summary and discussion **199**

Brain connectome is altered in MDD, linked with depressive episodes and symptom severity 199

Brain connectome is altered in preterm born adults, linked with lesion and compensation 200

MDD and preterm born adults show overlap in subcortical regions 201

Overall conclusion 203

References 204

Acknowledgements **205**

Affidavit / Statutory declaration and statement **206**

CV **207**

List of publications and manuscripts **209**

Declaration of author contributions **210**

Outline of this thesis

Abbreviations and initial summary which describes the total picture of my PhD study are provided in the beginning.

The section aim of this thesis briefly shows my objectives.

The introduction addresses the general and methodological background of brain connectome, the neurobiology and imaging-based evidence of major depression and preterm birth, my research questions and hypothesizes.

In the main section, in order to uncover brain connectome in major depression and preterm born individuals at risk for depression for both its topological organization and underlying white matter connectivity, I have carried out separate rs-fMRI and DTI studies, which are depicted in separate publications and unpublished manuscripts.

Next, a short summary and further discussion is addressed.

In the end, acknowledgements, affidavit, CV, list of publications, and declaration of contribution are provided.

Abbreviations

MRI - Magnetic Resonance Imaging

T1 - T1-weighted MRI

fMRI - Functional MRI

rs-fMRI - resting-state fMRI

DTI - Diffusion Tensor Imaging

BOLD - Blood Oxygen Level Dependent

FC - Functional Connectivity

SC - Structural Connectivity

iFC - intrinsic FC

DMN - Default Mode Network

FA - Fractional Anisotropy

MD - Mean Diffusivity

AD - Axial Diffusivity

RD - Radial Diffusivity

TBSS - Tract-based spatial statistics

AAL - Automated Anatomical Labeling

HOA - Harvard-Oxford cortical and subcortical structural Atlases

MDD - Major Depressive Disorder

Initial summary

Our brain is a network in which external and internal information is intensively and continuously processed and transported among structurally and functionally connected regions. The brain network is complex concerning the brain's tremendous and subtle structures and functions. An emerging and promising approach for exploring the brain's structural and functional organization is to study the brain's connectome, which conceptualizes the brain network comprising the whole set of brain regions and their interconnections. Over the past decade, connectomics has become a revolution in basic brain science and put new insight into system-level understanding of fundamental organizational principles of the brain in health and disease. In the multidisciplinary research of neuroscience and brain mapping, rapidly developing methods allow the in-vivo mapping of whole brain connectivity based on anatomical white matter fibers or neural dynamics in gray matter, fine-tuned constructions of large-scale structural and functional brain networks, detailed assessments of connectivity profiles, and advanced network analyses of various topological properties in brain connectome based on graph theory. Furthermore, the brain connectome, seen as a potentially common intermediate phenotype, has been contributing to the discovery science of the structural and functional brain abnormalities associated with different neurological and psychiatric disorders as well as various risk factors.

MDD is one of the most frequent mental disorders with the disorder course in more than 50% of cases coupled with recurrent multiple depressive episodes. Preterm birth

leads to higher neonatal risk and adverse outcomes, associated with persistent neurodevelopmental deficits, long-term impaired cognition, and significantly increased risk for mental disorders particularly depression in adulthood. In short, preterm birth is a risk factor for depression.

The papers of this thesis cover resting-state fMRI and DTI studies of patients with recurrent major depressive disorder, as well as preterm born adults at risk for depression. We reported brain connectome methods to analyze functional organization featured by resting-state functional connectivity and network topology, as well as underlying structural basis featured by microstructural white matter tracts. Firstly, we investigated aberrant network topology of global and local functional integration and segregation in patients with major depressive disorder compared with healthy controls. We revealed that striatal network topology is associated with the number of episodes independent of symptom severity, which suggests the potential mechanistic link between brain connectome and the course of recurrent episodes in major depression. Secondly, we applied the same approach of functional connectome to preterm born adults who are at risk for major depressive disorder. We showed that globally comparable but locally reconfigured topological organizations in preterm born adults compared with term born controls, which pointed to lesion-like and/or compensation-like associations with effects of preterm birth and adulthood general cognitive functioning. To sum up, these findings based on fMRI studies suggest shared and distinct patterns of aberrant functional connectome in major depression and preterm born individuals at risk for depression, which might constitute the potential link between at-risk, transient state and

clinically diagnosis for major depression. Thirdly, in addition to gray matter's role for aberrant brain connectome, we investigate the microstructural features of white matter subserving dysfunctional brain connectome in patients and at-risk individuals for depression. We reported tract-based methods to assess the fractional anisotropy and diffusivity of major white matter tracts over whole brain. We showed similar pattern of widespread microstructural alterations, consistent patterns of reduced fractional anisotropy and increased diffusivity in both patients with major depression and preterm born adults at for depression. These findings based on DTI studies demonstrate the underlying structural basis for disrupted functional organization in brain connectome, which might contribute to neurobiological and mechanistic understanding of altered brain connectome in patients with major depressive disorder and individuals at risk for depression.

Taken together, current results point out the important role of brain connectome in better understanding neural correlates of major depression and early life risk factor such as preterm birth. Current work highlights that human brain embeds system-level complex organization which is robustly detectable in resting-state fMRI and DTI data via connectome analysis. Both major depression and risk factor of preterm birth can be attributed to disrupted brain connectome regarding altered functional and structural connectivity, suggesting a potentially common intermediate phenotype for brain diseases.

Aim of this thesis

Connetome analysis of resting-state fMRI data and DTI data using graph theory and tract-based spatial statistics to investigate

- Recurrent major depression and functional connectome as course predictor
- Recurrent major depression and structural connectivity as course predictor
- Preterm born adults and functional connectome
- Preterm born adults and structural connectivity
- Link between major depression and preterm birth via the discussion of overlapping changes

Introduction

The networked brain: *human brain connectome*

Connectome and connectomics

Human brain has the nature of a **network**. According to basic brain research, the human brain is estimated to have approximately 89 billion neurons and 1000-10000 times as many synapses at the micro scale (Herculano-Houzel, 2012). Extensive evidence from cognitive neuroscience demonstrates that functionally specialized and anatomically segregated areas and circuits are present in the human brain. Since brain connections and integrative processes are of vital importance for coherent cognitive and behavioral outcomes, brain function depends on not only specialized local information processing but also efficient global integration of distributed processing units (Sporns et al., 2005). Therefore, a simple but system-level conceptualization is that, **human brain is a network** of both locally segregated and globally integrated processes. To profile the characteristics of the **networked brain**, it is urged to comprehensively map the neural connections of the entire brain, so-called **connectome**, which attempts to uncover the full spectrum of brain connections and the systemic organizational principles of brain structure and function (Sporns et al., 2005). The term *connectome* was initially invoked to describe structural brain connectivity and has been adapted to refer to both structural and functional interactions between brain regions (Biswal et al., 2010). **Connectomics** is the study of connectivity in the brain, including the mapping of both structural and functional connectome, ranging in the scale from the microscopic (neuronal-level, e.g.

cytoarchitectonics, myeloarchitectonics, chemoarchitectonics) to the macroscopic (millimeter, e.g. cerebral lobes, surface landmarks, white matter tracts) (Smith et al., 2013).

Up to date, the **human connectome**, which conceptualizes the connection of the entire human brain at different scales as a complex and dynamic system, has become a revolution in the basic brain research (Sporns, 2013). Much research in the general neuroscience field is stimulated to picture and investigate the connectome architecture at different temporal (from millisecond on) and spatial resolutions (from molecular level to the macro scale of millimeter), in order to reveal the neural correlates of brain function as well as the brain-behavior relationship in the perspective of human connectome. Huge data sets of human brain are currently collected (e.g. the milestone human connectome project (Van Essen and Ugurbil, 2012). Novel and quantitative analytical tools have been rapidly translated from multiple fields (such as statistics, physics, informatics, and computer science) to studies of human connectome in contemporary multidisciplinary neuroimaging research. As for clinical neuroscience, neuroimaging and connectome research appear to offer a potentially valuable perspective, enabling the use of structural and functional brain networks as biomarkers of neuropsychiatric disorders, for diagnostic and prognostic purposes, and to provide mechanistic insights on various characteristic factors and heterogeneous behavioral phenotypes (e.g. heterogeneity in symptoms, disorder course, and early life contributors) (Castellanos et al., 2013; Filippi et al., 2013; Sporns, 2014).

Macroscopic brain connectome

Magnetic Resonance Imaging (MRI), as the cutting-edge neuroimaging technique, provides the efficient, whole-brain, in-vivo, and non-invasive mapping for both structure and function of human brains, with the best trade-off between spatial and temporal resolutions (millimeters and seconds) at the current stage (Cole et al., 2010; Kelly et al., 2012; Craddock et al., 2013). Accordingly, MRI has been extensively used in the general and clinical neuroscience, and also contributed a lot to studies of human connectome so far. For example, functional MRI (fMRI) and Diffusion Tensor Imaging (DTI) allow to assess both structural and functional connectivity of large-scale brain networks, which open up the window to investigate in-vivo macroscopic connectome of human brain's structure and function.

The **macroscopic brain connectome** has played the most important role in contemporary MRI-based human connectome research. On the one hand, at the macro scale, which refers to the spatial resolution of millimeter, human brain comprises many different regions (e.g. lobe, gyrus and sulcus, specific anatomical locations) with many structural connectivity (e.g. white matter tracts) and coupled dynamic activities (e.g. interacted neural information in the form of electrical and/or chemical signals). It is worth mentioning that, anatomically distinct brain regions and inter-regional connections represents at the macro scale represent currently most feasible organizational level for exploring human connectome (Sporns et al., 2005), considering: (*i*) Neuronal level connections are much more subject to rapid plastic changes such as synaptic rewiring and dendritic remodeling (Engert and Bonhoeffer, 1999). The

microscopic connectome is supra complex given the huge amount of nodes. In the contrary, individual brain regions maintain relatively stable connection profiles together with relatively finite number of nodes (usually 50 - 1000), resulting in contemporarily computable complexity. (*ii*) The higher-order representations that directly relate to regulatory, cognitive and affective functions can be captured at the macro scale according to numerous task-related and lesion-related studies. Meanwhile, the interpretation of macroscopic connectome findings can be easily compared with those from a broad range of other experimental approaches existing at the macro scale such as dissection, histological staining, axonal tracing (Kobbert et al., 2000). (*iii*) Currently in-vivo whole brain imaging is mostly limited to the macro scale resolution. On the other hand, large data sets on a wide range of complex systems (e.g internet, airline-net, power grid, social network, neural network) have led to a fundamental consensus that substantively different complex systems – from societies to brains – often share certain key organizational principles that display remarkably similar macroscopic behavior despite profound differences in the microscopic details of the elements of each system or their mechanisms of interaction (Bullmore and Sporns, 2009). Taken together, it is substantially important to investigate the macroscopic brain connectome, which can be quantitatively characterized by MRI and network analysis.

Simple features of macroscopic brain connetome can be assessed by uni- and bivariate analysis of the brain region and connectivity (see details in next subsections). More complex features of macroscopic brain connetome, about system-level brain organization, can be assessed by multivariate analysis, namely network analysis, which

depends largely on graph theory (see details in next subsections). In brief, brain connectome can be mathematically expressed as a graph with nodes (brain regions) and edges (brain connections between regions). Topological organization - such as small-world topology, highly-connected hubs, global integration and local clustering – can be assessed in macroscopic brain connetome in both structural and functional domains, which is owing to the complex network nature of brain connectome (Bullmore and Sporns, 2009).

In addition to the fundamental frameworks of brain connectome, it is crucial to explore distinct modifications of the macroscopic brain connetome in healthy people associated with the individual variability, for example, cognitive functioning (Li et al., 2009; van den Heuvel et al., 2009), emotional and attentional task performance (Kinnison et al., 2012; Giessing et al., 2013), gender (Gong et al., 2009; Ingalhalikar et al., 2014), genetic factors (Glahn et al., 2013; Jahanshad et al., 2013), development (Supekar et al., 2009; Power et al., 2010; Khundrakpam et al., 2013; Cao et al., 2014), aging (Wen et al., 2011; Zhou et al., 2012), and so on. On the other hand, a rapidly growing body of studies of the macroscopic brain connetome in neuropsychiatric patients emerges in the recent decade, highlighting another crucially important multidisciplinary field that combines brain imaging, clinical neuroscience, and neuroinformatics for better understanding brain health and diseases (see details in next subsections).

To sum up, human brain is a complex network. Numerous information is continuously processed and communicated between structurally and functionally

connected regions based on efficient brain organization. The MRI-based macroscopic brain connectome provides one of fundamentally important frameworks for investigating brain organization in both structural and functional domains, and elicits wide-scope interests with regard to but not limited to cognitive and clinical neuroscience.

Current arts to explore brain connectome based on MRI

With the help of modern neuroimaging techniques, like electroencephalography (EEG), magnetoencephalography (MEG), positron emission tomography (PET), and magnetic resonance imaging (MRI), neuroscientists are able to examine human brain much more than before. Particularly **MRI** provides an in vivo, noninvasive, and convenient way to map the macroscopic whole brain with the best trade-off between spatial and temporal resolutions at the current stage (i.e. a voxel of millimeters in a time-window of seconds). Different MRI protocols enable to acquire specific aspect of brain information. For example, **T1-weighted MRI (T1)** mainly delineates morphometric features of brain structure, like tissue identification, regional gray matter's intensity and volume (see Figure 1); **functional MRI (fMRI)** can measure dynamic signals related to neuronal activity underlying brain function, mainly focusing on gray matter; inside, conventional **task-based fMRI** mainly examines the specific functional activity during the performance of a cognitive task or a designed experiment with specific stimulus, like detecting which brain regions become active when the task is performed; newly developed **resting-state fMRI (rs-fMRI)** focuses on the ongoing spontaneous activity

when the brain is just at rest (see Figure 2), gradually becoming an impacting field of brain research, like mapping intrinsic functional connectivity, large-scale functional brain networks and fundamental brain organization; Diffusion-weighted MRI or **Diffusion Tensor Imaging (DTI)** mainly measure microstructural features of white matter pathways in the brain via properties of water diffusion, also playing an important role in connectome research, like mapping white matter integrity and white matter fiber connections. Moreover, for the same individual brain, post-analysis of MRI allows information fusion across different modalities to obtain intact picture and comprehensive understanding combining brain structure and function. For example, both rs-fMRI and DTI can be used to infer brain connectivity.

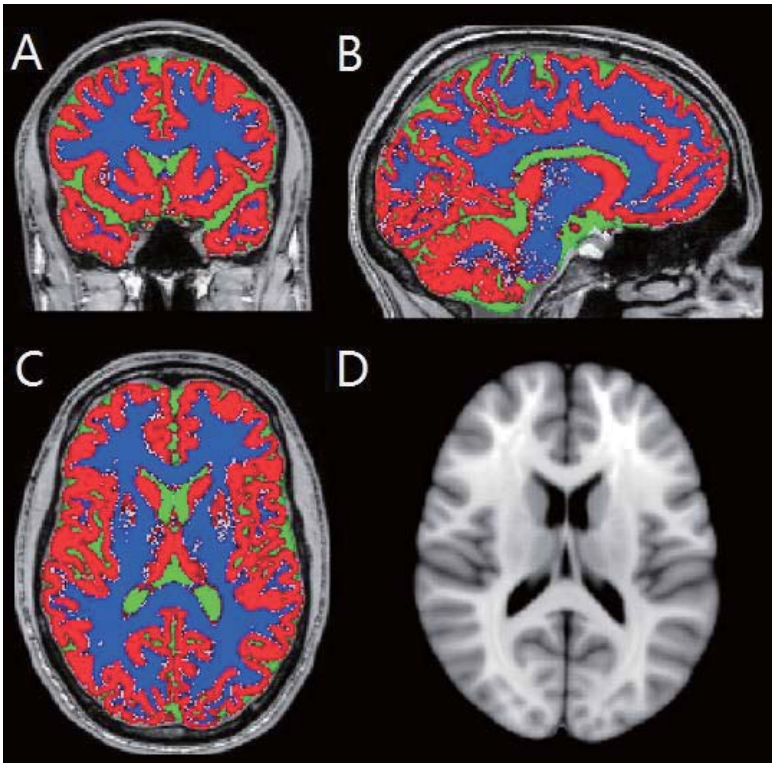

Figure 1. T1-based segmented brain tissues (A – C) (data based on (Meng et al., 2014)) and FSL's standard T1 template (Jenkinson et al., 2012)

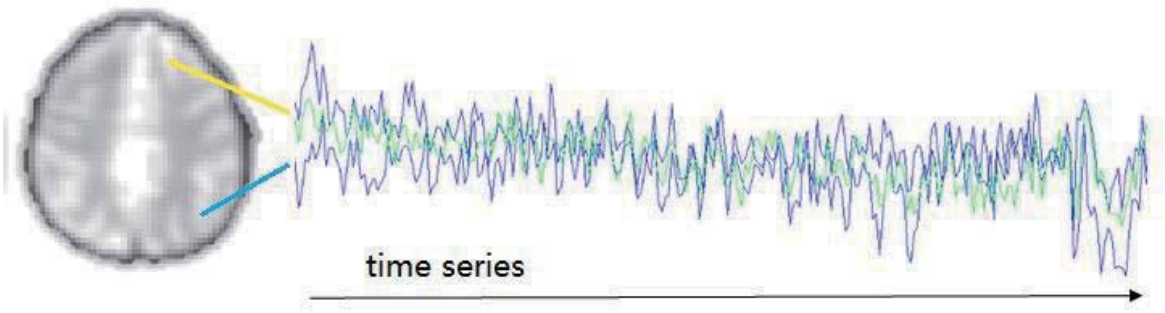

Figure 2. The resting-state fMRI image and preprocessed time series (data based on (Meng et al., 2014))

After acquiring data of human brain based on MRI, various analytical pipelines can be employed typically consisting of preprocessing, feature extraction and calculation, and group-level statistical inference. Firstly, the data preprocessing aims to reduce noises and artifacts such as induced by movement, and to normalize individual brains into standardized space if multiple subjects need to be compared with each other or analyzed all together. Secondly, for the feature in MRI-based data analysis, the measure can be univariate like voxelwise gray matter volume from T1 (see Figure 1, gray matter is colored by red), bivariate like Pearson's correlation of time series from a pair of brain regions (see Figure 2), multivariate like integrative skeleton-based white matter metrics or graph-based network metrics (see following subsections). Thirdly, within- or between-group comparisons are frequently utilized to identify group commonalities or differences, for example, in discovery science of disease-related brain abnormalities, cross-sectional design is usually employed for patient and healthy control groups. Fourthly, obtained brain imaging measures is used to link with other data such as

behavioral measures (e.g. cognitive performance) and clinical characteristics (e.g. disease symptom) due to detailed research questions.

Specifically, the brain connectome can be constructed based on MRI data like rs-fMRI and DTI by defining appropriate nodes (e.g brain regions) and links (e.g functional or structural connectivity). To explore brain connectome, important features refer to connectivity profile and network topology. This described next.

Measuring brain activity and gray matter's functional connectivity

Brain function depends on large-scale brain networks with respect to brain connectome (Deco et al., 2011; Bullmore and Sporns, 2012). Functional connectivity (FC) is defined as the synchronization of neurophysiological activities between spatially remote brain areas (Friston et al., 1993). Different measures can be related to brain activity of the physiological function such as **blood-oxygen-level-dependent (BOLD)**, cerebral blood flow, and glucose metabolism, of which BOLD is the predominantly used in current fMRI. The brain activity consumes energy, which is provided by the transport of glucose and hemoglobin-bound oxygen in the blood (Shulman et al., 2004). Because hemoglobin is diamagnetic in its oxygenated state but paramagnetic in its deoxygenated state (Pauling and Coryell, 1936), Ogawa et al. firstly demonstrated that by applying distinct MRI sequences, the level of blood oxygenation could be depicted in image contrasts (Ogawa et al., 1990) and most importantly it is related to neuronal activity and change of functional brain states in vivo (Ogawa et al., 1992). Therefore it has been proved that BOLD-based fMRI can infer the brain function since the returned signal is

an indirect measure of brain activity. Until now BOLD has fascinated numerous studies in basic and clinical neuroscience.

While conventional task-based fMRI mainly examines synchronous responses to extrinsic stimulation or tasks in single brain regions, **resting-state fMRI (rs-fMRI)** investigates the ongoing spontaneous activity, particularly between-region low-frequency (0.01 – 0.1 Hz) synchronized activity that defines **intrinsic functional connectivity (iFC)** (Biswal et al., 1995; Raichle et al., 2001; Fox et al., 2005). The iFC represents continuous synchronization among different regions in the brain supporting brain function as it has been well documented that the brain continuously maintains a remarkably high level of intrinsic activity and the brain function is continuously active during the resting state (Snyder and Raichle, 2012; Sadaghiani and Kleinschmidt, 2013). The baseline metabolism of the human brain measured during resting state represents about 20% of the total energy consumption of human body, which highlights the rich and continuously present set of spontaneous, correlated activities in the resting brain (Raichle, 2006; Smith et al., 2013). For example, the default mode network (DMN) of the human brain represents a remarkable success of discovery science with functional connectome (Buckner et al., 2008). This network originally referred to a set of brain regions including the posterior cingulate, hippocampus, medial prefrontal and inferior parietal cortex which are functionally connected (Greicius et al., 2003) and reliably deactivated during most externally focused tasks (Shulman et al., 1997) but exhibits elevated metabolism during internal cognitive processes (Raichle et al., 2001). The function of the DMN has been related to self-processing (Qin and Northoff, 2011),

autobiographical memories and introspective self-directed thinking (Catani et al., 2013), mentalizing and social interaction (Schilbach et al., 2013; Li et al., 2014), mind wandering (Mason et al., 2007) and various traits (Adelstein et al., 2011; Volkow et al., 2011). On the other hand, DMN alterations have been widely found in neuropsychiatric diseases like Major Depressive Disorder (MDD) (Greicius, 2008; Broyd et al., 2009; Zhu et al., 2012). As for other resting-state networks (RSNs), task-based fMRI and resting-state fMRI studies have converged on similar definitions of 8 – 10 spatially and functionally distinct networks such as primary visual, auditory, motor, executive control, attention, and default mode networks, which suggests that the full repertoire of functional networks utilized by the brain in action is continuously and dynamically active even at rest (Smith et al., 2012).

Given the biological and organizational significance of brain activity at rest, rs-fMRI is emerging as a mainstream approach to construct MRI-based macroscopic brain connectome for characterizing normal brain functions, behavior-brain associations, and various mental disorders (Snyder and Raichle, 2012; Castellanos et al., 2013; Smith et al., 2013). A typical resting-state fMRI dataset can be obtained in 5 – 15 minutes while the participant is told to lie still in the MRI scanner, keep awake, and think of nothing in particular. The brain connectome, conceptualized by graph of linked nodes, is constructed based on rs-fMRI in the following steps. Firstly, the whole brain can be divided into different brain regions (i.e. nodes, ~ 100 or even more) based on anatomical landmarks and parcellation, such as Automated Anatomical Labeling (AAL) and Harvard-Oxford cortical and subcortical structural atlases (HOA) (Stanley et al., 2013).

There also exist other methods to define nodes based on meta-analysis of task-based fMRI studies and data-driven approaches like hierarchical clustering, independent component analysis. Secondly, the link for a pair of nodes can be defined by their functional connectivity, which is commonly estimated from bivariate tests for statistical dependency between dynamic activities observed in distributed brain regions (Friston et al., 1993). The nodal activity is derived from regional mean time series. Some clean-up approaches are necessary to carry out to remove confounding variation (e.g. time series of white matter and cerebrospinal fluid, global signal across all gray matter, and time series related to head motion) (Power et al., 2012). The meaningful low-frequency time series can be extracted by temporal band-pass filtering or wavelet-based decomposition (Cordes et al., 2001; Bullmore et al., 2004). Pearson's correlation is commonly employed to estimate linear dependence between pairs of time series and primarily utilized for inferring functional connectivity while other methods are also used in relevant fields (Zhou et al., 2009). In the end, the brain connectome is represented by the generated FC matrix that can be visualized as a graph of linked nodes.

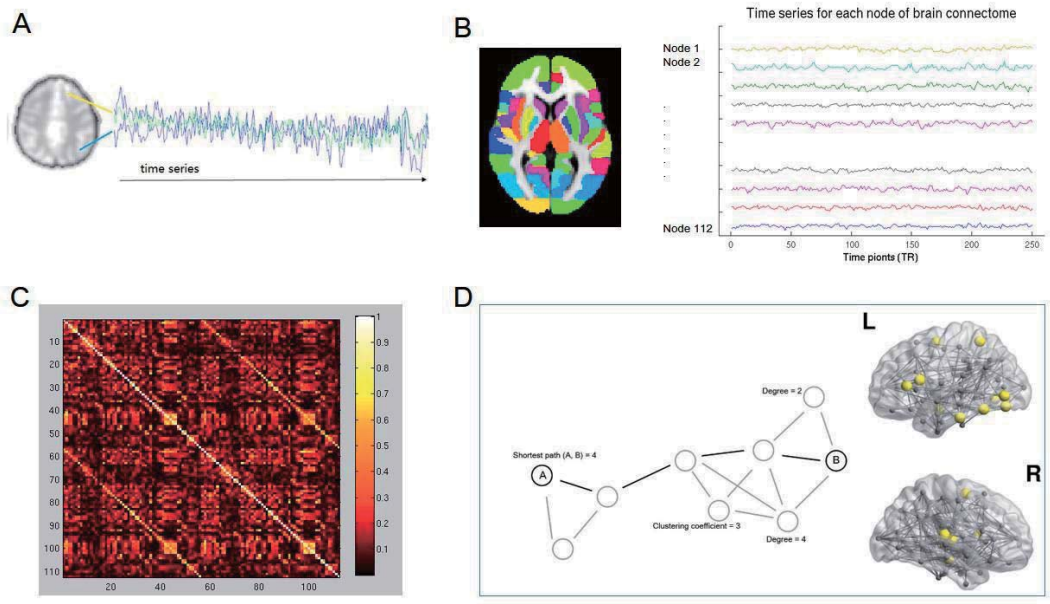

Figure 3. The illustration of brain connectome's construction and analysis. After preprocessing rs-fMRI data, low-frequency intrinsic functional activity is extracted (A). The whole brain can be subdivided into a number of regions, which are defined as nodes (e.g. 112 nodes derived from FSL's Harvard-Oxford cortical and subcortical atlases (Jenkinson et al., 2012)) and then provide regional mean time series for each node (B). The edges are defined by statistical dependence between nodal brain activities (e.g. Pearson's correlation coefficient), resulting in individual brain's connectivity matrix, which is brain connectome (C). The brain connectome can be investigated by graph-based network analysis, resulting in quantitative metrics of network topology, such as degree, hub, shortest path length, clustering coefficient and so on, which demonstrate global and nodal functional integration and segregation to evaluate the brain's complex organization and disease-related changes. The illustration was based on data of my PhD work.

Measuring brain structure and white matter's connectivity

It is crucially important to understand the structural basis of brain function in the context of brain connectome. Both T1 and DTI can measure brain structure, respectively on gray matter and white matter. The macroscopic structural brain connectome can be constructed based on the cross-subject gray matter's covariance by using T1, or the anatomical connectivity of myelinated nerve fibers corresponding to white matter tracts by using DTI (Griffa et al., 2013). Up to date, DTI-based white matter's connectivity is the most popular approach to explore individual structural brain connectome.

DTI is a MRI technique that provides a noninvasive, in vivo, and millimeter-resolution mapping of white matter tracts. By using specified sequence to capture and trace the diffusive motion of water molecules in the brain, DTI enables to reconstruct white matter fiber pathways for characterizing microstructural properties, anatomical connectivity, and brain connectome (Iturria-Medina et al., 2007). In principle, water diffusion in white matter is restricted in myelinated fibers and occurs primarily along the path of neuronal axons, while it occurs almost equally in all directions in gray matter and cerebral spinal fluid. Therefore, such diffusion anisotropy can distinguish white matter and delineate the tract-based pathways. A typical DTI dataset contains a set of direction-related gradient images (from 15 to 32 or even more) together with non-directional reference images (so called B0). Combining B0 and gradient images, the magnitudes of water diffusion in different directions can be estimated at each point of the whole brain. Via diffusion tensor calculation, the orientations of white matter fibers

passing through each voxel of white matter can be estimated, which can shape white matter tracts across voxels. By propagating continuous three-dimensional trajectories across neighboring voxels, fiber tractography enables to estimate the determinative or probabilistic distribution of white matter fibers and point-to-point structural connectivity over the whole brain.

After obtaining the tract-based information of white matter, the microstructural integrity can be typically profiled by fractional anisotropy (FA) as well as mean, axial, and radial diffusivity (MD, AD, and RD) of white matter, which is frequently used to explore the structural basis underlying brain function and to associate with brain diseases. Furthermore, brain connectome can be constructed using white matter's structural connectivity in the same way with gray matter's functional connectivity.

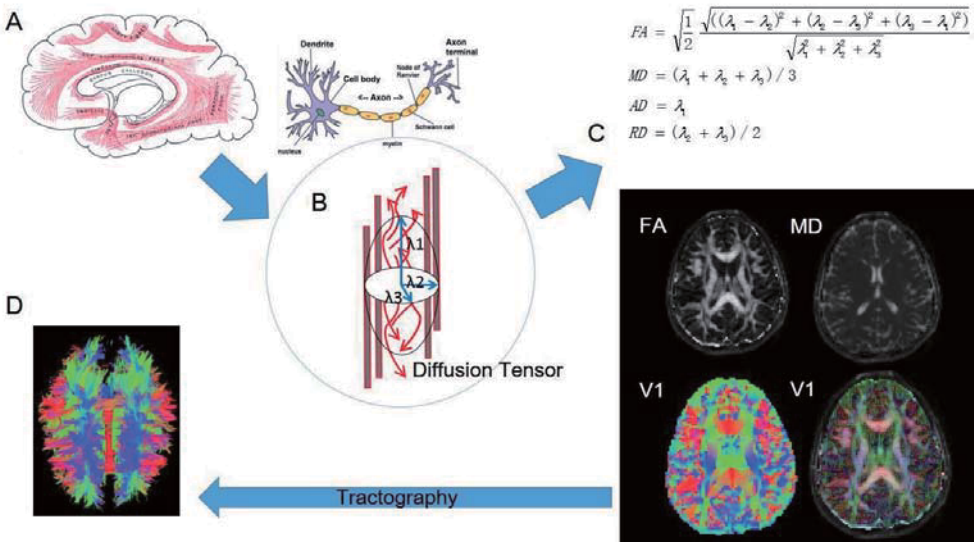

Figure 4. The illustration of DTI methods. The brain's white matter tracts/pathways (A), neuronal axon fiber and modelled diffusion tensor (B) are illustrated (The diagram of the white matter tracts/pathways and the neuron was from the internet). Based on

diffusion tensor model and definition formulas, FA, MD, AD and RD maps can be computed (Basser and Pierpaoli, 1996) (C). To note, the V1 map shows the first principle directions of diffusion tensors by color and directional lines (the left-right is colored by red, up-down by blue, and posterior-anterior by green). By using the tractography, white matter's connectivity can be estimated for whole brain resulting in various commissural, projection and association fibers (D).

Characterizing connectivity profiles

Macroscopic brain connectivity is defined by inter-regional correlated functional activity and/or white matter tracts. Despite single connectivity strength, global connectivity profiles reflect more integrative information about the brain connectome, such as global strength, diversity, and integration. The global strength and diversity are estimated as the mean and variance of connectivity matrix of brain connectome (Lynall et al., 2010). The global integration is estimated by the ratio of the first eigenvalue to the sum of all other eigenvalues from principal component analysis on connectivity matrix (Tononi et al., 1994). Altered global functional connectivity has been identified in schizophrenia (Lynall et al., 2010), depression (Bohr et al., 2012), and Alzheimer's disease (Liu et al., 2014).

For DTI and white matter, an integrative approach, tract-based spatial statistics (TBSS), has been developed to profile whole brain white matter tracts that is the structural basis of brain connectome. Owing to multifold complexity of various

direction-sensitive white matter tracts, it is compromised to align individual white matter maps (e.g. FA) across subjects using any standard registration algorithm and do subsequent voxelwise analysis. TBSS adopts the nonlinear registration for FA maps, identifies common skeleton mask at the center of major white matter tracts, integrates the individual microstructural measures surrounding the skeleton by projecting and combining them onto the skeleton, and finally provides the alignment-invariant tract representation, i.e. skeletonized FA, MD, AD, RD maps (Smith et al., 2006) (See Figure 5). After that, TBSS carries out voxelwise permutation-based statistical tests on the generated skeleton across all subjects, providing estimated P value that is necessarily corrected for multiple comparison by applying methods preferably like threshold-free cluster enhancement (TFCE). TFCE uses cluster-based thresholding that is more sensitive than voxel-wise thresholding, and minimizes the pitfall of arbitrary defining the initial cluster-forming threshold (Smith and Nichols, 2009) (See Figure 5). To draw the final result from TBSS analysis, for example, significant FA reductions can be identified in patients compared with healthy controls (See Figure 5).

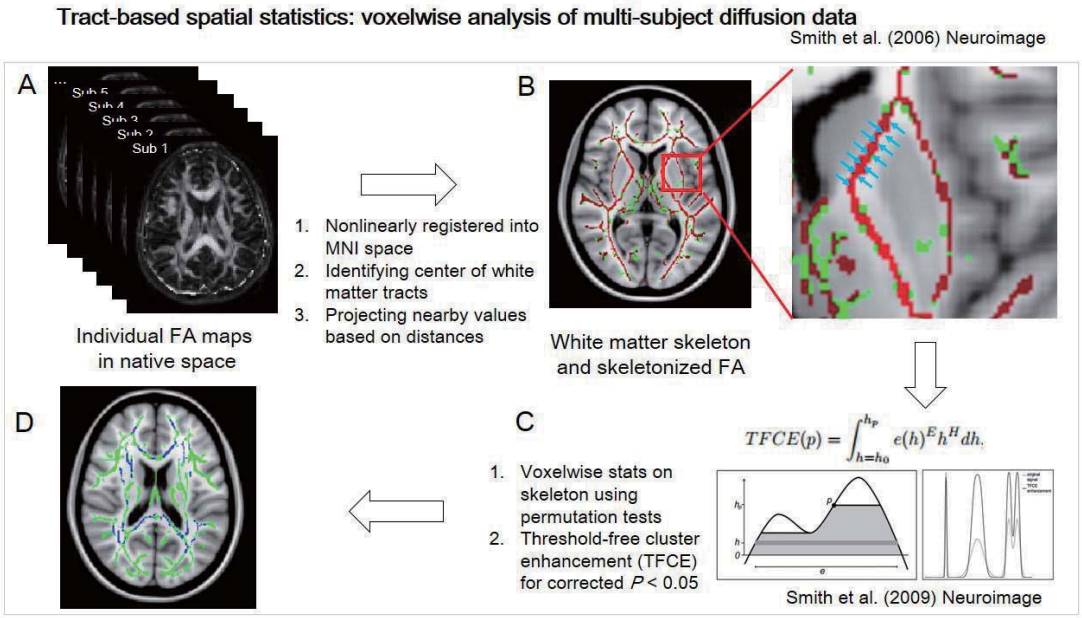

Figure 5. Flowchart of TBSS analysis of DTI data, according to (Smith et al., 2006; Smith and Nichols, 2009)

Since TBSS analysis remarkably improves the sensitivity, objectivity and interpretability of analysis of multi-subject DTI studies, it is widely used related to plastic training (Sampaio-Baptista et al., 2013), development and aging (Ball et al., 2013; Glahn et al., 2013), and brain diseases such as Major Depressive Disorder (Korgaonkar et al., 2011) and Schizophrenia (Douaud et al., 2007).

Characterizing network topology

It is important to examine the brain connectome as a network due to its complex organization including functional segregation and integration. Such brain organization can be characterized by network topology and graph theory in a quantitative perspective translated from evaluation of large complex social, physical, and biological systems

(Bullmore and Sporns, 2009). Graph theory provides a rich repertoire of mathematical tools and concepts that can be used to characterize diverse topological organization of the brain connectome (Craddock et al., 2013; Fornito et al., 2013). Using graph theory, the brain connectome can be mathematically depicted as a binary or weighted, undirected or directed graph and subsequently assessed for various topological properties about network topology (Rubinov and Sporns, 2010).

Binary undirected graph is the conventional simplest model, which consists of a set of nodes (e.g. brain regions) connected by a lot of binary edges. Binary edges denote the presence or absence of connections between brain regions by applying a weight threshold on estimated structural or functional connectivity, for example, proportional thresholding based on network cost (Rubinov and Sporns, 2010). The network cost is defined by the number of present edges in the graph as a percentage of the maximum number of possible edges in brain connectome, which reflects the topological wiring cost of brain connectome related to the economy of the brain network organization (Bullmore and Sporns, 2012). Additional thresholding can be used to guarantee that all nodes in the graph are connected even at the lowest cost, for example, minimum spanning tree algorithm (Alexander-Bloch et al., 2012). For resulting graphs, topological measures, which is also called network metrics, can be calculated for each node and whole graph with respect to nodal and global topological properties such as clustering, shortest path length, centrality, modularity, small-world and rich-club organization (Sporns, 2014).

The brain development and organization is characterized by an optimal balance

between functional segregation and integration (Tononi et al., 1994; Fair et al., 2007). On the one hand, functional integration of brain connectome is the ability of efficient information processing and combining over distributed brain regions, which can be assessed by nodal centrality metrics (e.g. nodal degree, betweenness, and efficiency) and global metrics (e.g characteristic path length and network global efficiency of whole network) (Rubinov and Sporns, 2010). On the other hand, functional segregation of brain connectome is the ability of local specialized processing within densely interconnected groups of brain regions, which can be assessed by nodal metric (e.g. nodal local efficiency) and global metrics (e.g. clustering coefficient and network local efficiency of whole network) (Rubinov and Sporns, 2010) (See Figure 6).

As for functional integration, *degree* is defined as the number of edges connected with the given node. The path between a pair of nodes is the edges in the graph connecting the two nodes. *Shortest path length* is defined by the smallest number of edges that must be passed to connect a pair of nodes. *Nodal shortest path length* is the mean length of all shortest paths connecting given node and other nodes. *Betweenness* is defined as the fraction of all shortest paths (the smallest number of intermediate edges) between all other nodes that pass through the given node in the network (Rubinov and Sporns, 2010). *Efficiency* is a measure of the capacity for global parallel information process and transfer, estimated by the inverse of harmonic mean of shortest path lengths between the given node and all other nodes in the network (Latora and Marchiori, 2001). So nodal efficiency is inversely related to the path length and a node featured by higher efficiency will play a more central role in the integrated organization of the network.

Therefore, degree, betweenness, and efficiency all quantify nodal *centrality* in a network. The brain connectome includes a minority of highly connected *hub* nodes, which are typically with high centrality, high cost, and high value for network topology (Crossley et al., 2014).

As for functional segregation, *nodal clustering coefficient* is defined as the number of existing connections among the node's neighbors divided by all their possible connections while *nodal local efficiency* is a measure of the capacity for local information exchange between the nearest neighbors of the given node, defined by averaged efficiency of subgraph comprising neighboring nodes of the given node (Rubinov and Sporns, 2010). It is worth mentioning, nodal local efficiency is highly related to nodal clustering coefficient, which implies the extent of segregated organization (Watts and Strogatz, 1998). So a node featured by higher local efficiency will contribute more to the cliquish organization of the network (Giessing et al., 2013).

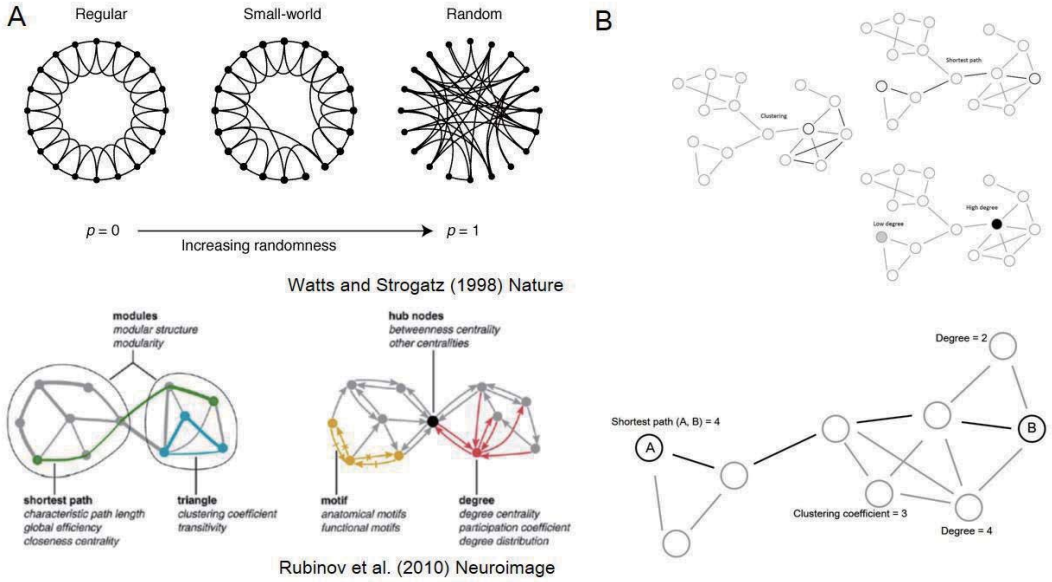

Figure 6. Illustrations for small-world network and graph-based network metrics by

examples (Watts and Strogatz, 1998; Rubinov and Sporns, 2010)

As for the global network topology, the *characteristic path length* of a network is defined as the average shortest path length between all pairs of nodes in the network (Watts and Strogatz, 1998). The *clustering coefficient* of a network is defined as mean clustering coefficient across all nodes (Watts and Strogatz, 1998). *Global efficiency* and *local efficiency* of a network is computed by averaging efficiency and local efficiency of all nodes in the network, which is respectively related to characteristic path length and clustering coefficient, and frequently evaluated for global network topology (Rubinov and Sporns, 2010). As Watt et al. described the fundamental feature of small-world organization (See Figure 6), it is also present in brain connection. The *small-worldness* is defined as the ratio of clustering coefficient against characteristic path length of a network compared with random networks with the same number of nodes, edges and degree distribution, which can describe the small-world property of high local specialization and high global integration in brain connectome (Watts and Strogatz, 1998). As recent studies revealed the of rich-club organization in brain connectome, *rich-club coefficient* is computed as the ratio of connections present between hub nodes against the maximum of their possible connections, which should be normalized by the coefficient derived from randomized networks to obtain valid estimation (van den Heuvel and Sporns, 2011). The brain's rich-club organiztion demonstrates that high-degree brain hubs are more densely connected among themselves than other non-hub nodes, forming a rich club and playing an important role in global communication and

backbone network of brain connectome.

For the application of network topology in disease-related brain connectome, so far altered network topology and disrupted brain connectiome has been manifested in major psychiatric disorders (Filippi et al., 2013; Crossley et al., 2014), such as schizophrenia (Fornito et al., 2012), depression (Zhang et al., 2011), obsessive compulsive disorder (Taylor, 2014), ADHD (Wang et al., 2009), autism (Di Martino et al., 2013), mild cognitive impairment and Alzheimer's disease (Xie and He, 2011). The emerging and accumulating evidence of brain-connectome-based delineation of psychiatric disorders links abnormal brain connectome with intermediate phenotype of psychiatric disorders (Bullmore and Sporns, 2009; Rubinov and Bullmore, 2013).

Mental disorder and risk factors affect brain connectome

Mental disorders are characterized by aberrant thinking, volition, feeling and actions that reach such a severity that the patient's social, occupational, and psychological functioning is severely compromised, resulting in long-term influence on the patient's life and adverse burden on the society (American Psychiatric Association, 2000). According to the World Health Organization (WHO)'s "global burden of disease study 2010", mental disorders are becoming more and more frequent in the modern times with an increasing population prevalence, currently accounting for 22.7% of years lived with diseases (YLD), regardless of age, gender, social status or geographical origin (Vos et al., 2012). Therefore, it is an urgent and critical challenge to understand the neural

underpins of mental disorders including onset, remitted and recurrent course, and risk factors, in order to develop better intervention and treatment.

With the advance of modern neuroimaging, it has become possible to map the patient's brain in an in vivo non-invasive way. Over the past decades, researchers have applied such as rs-fMRI and DTI to uncover neural correlates regarding the brain's structural and functional abnormalities in mental disorders, aiming to find valid biomarkers for mental disorders such as schizophrenia and depression. The discovery and validation of biomarkers is central to the development of MRI-based clinical applications. The biomarker is defined as a characteristic that is objectively measured and evaluated as an indicator of normal biological processes, pathogenic processes, or pharmacologic responses to a therapeutic intervention according to the NIH's definition (Atkinson Jr. et al., 2001). Therefore imaging-based biomarker should help determination of the presence or absence of a disease (i.e. diagnosis), staging of a disease, determination of risk prognosis, or prediction and monitoring of clinical response to an intervention, where brain connectome is postulated to offer a powerful discovery framework (Castellanos et al., 2013; Filippi et al., 2013).

Since brain is a system with complex and subtle organization subserving various functions, mental disorders are commonly attributed to disordered brain organization, for example to deficits in access, engagement and disengagement of large-scale brain networks (Menon, 2011). In principle, many disorders like Alzheimer's disease and schizophrenia can be described as disconnectivity syndromes, because their symptoms and clinical manifestations can be related to disrupted integration of spatially

distributed regions of the brain that are part of large-scale networks subserving specific functions (Catani and ffytche, 2005). Recent evidence points out that in the context of disease there exist strong links between disrupted brain network and clinical consequences (Zhou and Seeley, 2014). For example, loss of small-world network properties is identified in Alzheimer's disease and schizophrenia (Lynall et al., 2010; Liu et al., 2014). Therefore, brain connectome is becoming a common intermediate phenotype for characterizing patient groups (Bullmore and Sporns, 2009).

On the other hand, though contemporary clinical diagnosis classify mental disorders into distinct categories, they show clinical overlap (e.g. cognitive impairment, emotional dysfuntion) and familial co-aggregation (e.g. share genetic risk factors). According to an examination of genetic data from more than 60,000 people worldwide, five major mental disorders – schizophrenia, bipolar disorder, major depressive disorder, attention deficit-hyperactivity disorder (ADHD), autism spectrum disorder (ASD) – appear to share some common genetic risk factors (Smoller et al., 2013). Inside, moderate but general genetic correlation has been identified in major depressive disorder with others: between schizophrenia and major depressive disorder (0.43 ± 0.06 s.e.), bipolar disorder and major depressive disorder (0.47 ± 0.06 s.e.), ADHD and major depressive disorder (0.32 ± 0.07 s.e.), ASD and major depressive disorder (non-significant) (Lee et al., 2013). This empirical evidence of shared genetic etiology for psychiatric disorders encourages the investigation of common pathophysiological pathways from genotype to clinical phenotype and their interactions with neurodevelopment, environmental influence, learning, adaptive behaviors, and so on,

where brain connectome has emerged as the intermediate phenotype to combine with other biological data in the context of mental disorders (Medland et al., 2014).

To sum up, MRI-based macroscopic brain connectome has opened up a new era in studying large-scale brain networks and topological organization in healthy subjects, patients with mental disorders as well as individuals at high psychiatric risk. Brain-connectome-based methods are changing how researchers conceptualize and explore brain diseases, with potentially important implications for understanding mental disorders (Bullmore and Sporns, 2012; Castellanos et al., 2013; Fornito et al., 2013; Griffa et al., 2013; Menon, 2013; Rubinov and Bullmore, 2013). Therefore, brain connectome is becoming the intermediate phenotype for studying mental disorders (Filippi et al., 2013).

Major depression and preterm birth affect brain connectome

Major depressive disorder (MDD) is a disabling mental disorder associated with an intense negative interpretation of the environment, oneself and one's own future (Beck, 1967). MDD is a common and globally distributed mental health problem with a lifetime prevalence of about 16% (Kessler et al., 2003). For detailed symptoms, MDD is characterized by persistent and pervasive depressed mood, loss of interest or pleasure, feelings of sadness, guilt, and worthlessness, impaired cognition, vegetative symptoms, and suicidal tendency, with one or multiple depressive episodes (American Psychiatric Association, 2000). According to the Global Burden of Disease, Injuries, and Risk

Factors Study 2010 (GBD 2010), mental disorders were one of the leading causes of years lived with disability (YLDs) worldwide and MDD accounted for highest burden in mental disorders, about 2.8 times as anxiety disorders in the second position (Whiteford et al., 2013). Given both that MDD is becoming the most burdensome disease in the world in the 21st century and that MDD is often unresponsive to conventional pharmacologic intervention, it is urged to advance the brain research underlying MDD of first-episode, recurrent-episode, drug-naïve, treatment-resistant, early-onset, and late life (Lorenzetti et al., 2009; Hasler and Northoff, 2011; Hamilton et al., 2012).

However it remains yet unclear about the etiopathology of MDD. According to the diathesis-stress-model of MDD (Monroe and Simons, 1991), it is assumed that distinct internal and/or external stressors might trigger the onset of MDD against the background of individual vulnerability, which results from various factors including genetic factors (Kendler et al., 2006) and early life experiences (Willner et al., 2013). Recent neuroepigenetics research has shown that genetic disposition, environmental exposures, and dynamic interplay between genes and experience play important roles in the development of depression and other mental disorders (Schwahn and Grabe, 2009; Sweatt, 2013). For example, owing to Gene-by-Environment (GxE) interaction, the serotonin transporter gene (also known as 5-*HTT*) stress-sensitivity model suggests that the serotonin transporter links with polymorphic region (5-*HTTLPR*), stress sensitivity, and depression in humans (Caspi et al., 2010). The neurodevelopmental hypothesis postulates that apart from the influence of risk genes, psychosocial stress during the

perinatal period and following development into adulthood is an important trigger for MDD (Bale et al., 2010).

In humans, the last trimester of fetal development extending into the first postnatal month is a critical period of rapid brain development. Gestational age is defined by the gestational duration before the baby's delivery. Term birth is associated with the newborns of gestational age no less than 37 weeks. Preterm birth is defined by delivery before 37 weeks of gestation are completed, characterized by lower gestational age higher prematurity and associated risk. Preterm born infants ranging from very preterm (< 32 complete gestation weeks) to early preterm (< 37 complete gestation weeks) is susceptible for significant risk of growth failure, higher levels of morbidity and brain injury (e.g. intraventricular or germinal matrix hemorrhage and periventricular leukomalacia), impaired neurodevelopment (e.g. cognitive deficits), and psychiatric diagnosis in adulthood (Milligan, 2010; D'Onofrio et al., 2013; Katz et al., 2013). Recent historical population-based cohort study has reported that preterm birth is significantly associated with increased risk of psychiatric hospitalization in young adult life. Compared with term born adults (gestational age 37 – 41 weeks), preterm born adults who were born between 32 and 36 weeks were 1.3 (95% CI, 1.1 – 1.7) times more likely to have depressive disorder, and very preterm born adults (gestational age < 32 weeks) were 2.9 (95% CI, 1.8 – 4.6) times more likely to have depressive disorder, which might suggest a dose-like association between preterm birth and MDD (Nosarti et al., 2012). Therefore, preterm born individual are at the risk for depression. Taking into account that the global prevalence of preterm birth is more than 10% (i.e. about 15

million preterm newborns per year) and the rate keeps increasing in almost all countries (Blencowe et al., 2012), preterm birth is an inneglectable risk factor for depression.

Given the significant impact of both MDD and preterm birth on global health burden, relevant brain studies are heavily called to better understand underlying neural mechanism such as their brains' functional and structural abnormalities. Given the potential link between MDD and preterm birth, it is necessary to apply the same investigation on their underlying neural correlates and link emerging evidence together.

Aberrant brain connectome is present in MDD, featured by widespread structural and functional brain changes (Greicius et al., 2007; Erk et al., 2010; Sheline et al., 2010; Aizenstein et al., 2011; Lui et al., 2011; Li et al., 2012; Mwangi et al., 2012; Zeng et al., 2012), for reviews see (Savitz and Drevets, 2009; Hamilton et al., 2012; Whitfield-Gabrieli and Ford, 2012). Zhang et al. provided the first evidence about aberrant network topology of brain connectome in MDD by combining rs-fMRI and graph-based network analysis. They found lower path length and higher global efficiency as well as altered nodal centralities in thirty drug-naïve, first-episode MDD patients compared with 63 healthy controls (Zhang et al., 2011). Subsequent study reported impaired modular organization of brain connectome in first-episode or long-term therapy resistant MDD by using rs-fMRI (Tao et al., 2013). Using T1 and across-subject gray-matter-volume-based correlation, Singh et al. constructed structural brain connectome for 93 patients with first-episode or recurrent-episode MDD and reported decreased clustering and less efficient organization in MDD (Singh et al., 2013). Very recently, the first MDD study of DTI-based brain connectome was reported, showing

altered structural connectivity between nodes of the default mode network and the frontal-thalamo-caudate regions are core neurobiological features associated with MDD (Korgaonkar et al., 2014). They found Due to these findings we suggest that specific changes of intrinsic fcnT, particularly those reflecting functional integration (i.e. efficiency, centrality or modularity), may interact with the course of MDD. Taken together, emerging evidence highlights that brain connectome is affected by MDD and links with disorder duration and severity (Zhang et al., 2011). However, it is not yet known whether aberrant brain connectome underpins the course of MDD featured by multiple recurrent episodes.

Until very recently brain connectome in preterm born individuals has started to be investigated. It is reported that, structural and functional brain connectome and human brain's fundamental organization emerges and develops during early brain maturation earlier than 40 gestational weeks (Ball et al., 2014; van den Heuvel et al., 2014). According to two DTI studies, similar small-world organization is present in brain connectome of preterm and term born infants (Brown et al., 2014) but longer gestation is associated with more efficient brain organization in preterm and term born preadolescent children (Kim et al., 2014). Since brain connectome develops and reshapes along with the age (Collin and van den Heuvel, 2013; Cao et al., 2014), it is interesting to explore brain connectome in adults after preterm birth, particularly considering it might be an important transient state bridging typical/atypical brain development and mental health/disorder. However, much less is known about adult brain compared to infant brain with regard to preterm birth, despite altered gray matter's

functional connectivity and reduced white matter's fractional anisotropy in preterm born adults (Eikenes et al., 2011; White et al., 2014).

Open general questions about the connectome trajectory in major depression

For depression, there might exist an overlapped developmental trajectory for risk- and disorder- related brain connectome, which remains largely unclear.

Firstly, after the clinical diagnosis of MDD, it remains largely unknown whether specific brain connectome changes link with the course of major depression. For the disorder course, MDD is characterized by single or recurrent major depressive episodes while in 35-85% of cases the course of MDD includes the recurrence of depressive episodes (Hardeveld et al., 2010; Lewis et al., 2010; Farb et al., 2011). Especially for recurrent MDD, it is still an open question whether aberrant brain connectome may underpin the risk of recurrence and predict the number of depressive episodes.

Secondly, there is no clear preclinical state for depression like mild cognitive impairment (MCI) for Alzheimer's disease (AD). What we already know is that preterm born individuals are at risk for depression, who may have been not clinically diagnosed but with a high risk for lifetime disorder diagnosis, which might provide the potentially important information about at-risk or preclinical brain state for depression. Considering the long-term adverse vulnerability of preterm brain, it forms another open question whether aberrant brain connectome has emerged in preterm born individuals at risk for major depression and may be associated with MDD's aberrant pattern to

some extent.

These two general questions have motivated the following papers in terms of a research framework. They have been broken up into testable small piece questions as described above in the section aim of the thesis. In more detail single questions and corresponding hypotheses are motivated and specified in the beginning of each paper.

References

Adelstein JS, Shehzad Z, Mennes M, Deyoung CG, Zuo XN, Kelly C, Margulies DS, Bloomfield A, Gray JR, Castellanos FX, Milham MP (2011) Personality is reflected in the brain's intrinsic functional architecture. PloS one 6:e27633.

Aizenstein HJ, Andreescu C, Edelman KL, Cochran JL, Price J, Butters MA, Karp J, Patel M, Reynolds CF, 3rd (2011) fMRI correlates of white matter hyperintensities in late-life depression. The American journal of psychiatry 168:1075-1082.

Alexander-Bloch A, Lambiotte R, Roberts B, Giedd J, Gogtay N, Bullmore E (2012) The discovery of population differences in network community structure: new methods and applications to brain functional networks in schizophrenia. NeuroImage 59:3889-3900.

American Psychiatric Association (2000) Diagnostic and statistical manual of mental disorders, Ed 4, text revision. Washington, DC: American Psychiatric Association.

Atkinson Jr. AJ, Colburn WA, DeGruttola VG, DeMets DL, Downing GJ, Hoth DF, Oates JA, Peck CC, Schooley RT, Spilker BA, Woodcock J, Zeger SL (2001) Biomarkers and surrogate endpoints: preferred definitions and conceptual framework. Clinical pharmacology and therapeutics 69:89-95.

Bale TL, Baram TZ, Brown AS, Goldstein JM, Insel TR, McCarthy MM, Nemeroff CB, Reyes TM, Simerly RB, Susser ES, Nestler EJ (2010) Early life programming and neurodevelopmental disorders. Biological psychiatry 68:314-319.

Ball G, Srinivasan L, Aljabar P, Counsell SJ, Durighel G, Hajnal JV, Rutherford MA, Edwards AD (2013) Development of cortical microstructure in the preterm human brain. Proceedings of the National Academy of Sciences of the United States of America 110:9541-9546.

Ball G, Aljabar P, Zebari S, Tusor N, Arichi T, Merchant N, Robinson EC, Ogundipe E, Rueckert D, Edwards AD, Counsell SJ (2014) Rich-club organization of the newborn human brain. Proceedings of the National Academy of Sciences of the

United States of America 111:7456-7461.

Basser PJ, Pierpaoli C (1996) Microstructural and physiological features of tissues elucidated by quantitative-diffusion-tensor MRI. Journal of magnetic resonance Series B 111:209-219.

Beck AT (1967) Depression: Clinical, experimental, and theoretical aspects: University of Pennsylvania Press.

Biswal B, Yetkin FZ, Haughton VM, Hyde JS (1995) Functional connectivity in the motor cortex of resting human brain using echo-planar MRI. Magnetic resonance in medicine : official journal of the Society of Magnetic Resonance in Medicine / Society of Magnetic Resonance in Medicine 34:537-541.

Biswal BB et al. (2010) Toward discovery science of human brain function. Proceedings of the National Academy of Sciences of the United States of America 107:4734-4739.

Blencowe H, Cousens S, Oestergaard MZ, Chou D, Moller AB, Narwal R, Adler A, Vera Garcia C, Rohde S, Say L, Lawn JE (2012) National, regional, and worldwide estimates of preterm birth rates in the year 2010 with time trends since 1990 for selected countries: a systematic analysis and implications. Lancet 379:2162-2172.

Bohr IJ, Kenny E, Blamire A, O'Brien JT, Thomas AJ, Richardson J, Kaiser M (2012) Resting-state functional connectivity in late-life depression: higher global connectivity and more long distance connections. Frontiers in psychiatry 3:116.

Brown CJ, Miller SP, Booth BG, Andrews S, Chau V, Poskitt KJ, Hamarneh G (2014) Structural network analysis of brain development in young preterm neonates. NeuroImage.

Broyd SJ, Demanuele C, Debener S, Helps SK, James CJ, Sonuga-Barke EJ (2009) Default-mode brain dysfunction in mental disorders: a systematic review. Neuroscience and biobehavioral reviews 33:279-296.

Buckner RL, Andrews-Hanna JR, Schacter DL (2008) The brain's default network: anatomy, function, and relevance to disease. Annals of the New York Academy of Sciences 1124:1-38.

Bullmore E, Sporns O (2009) Complex brain networks: graph theoretical analysis of structural and functional systems. Nature reviews Neuroscience 10:186-198.

Bullmore E, Sporns O (2012) The economy of brain network organization. Nature reviews Neuroscience 13:336-349.

Bullmore E, Fadili J, Maxim V, Sendur L, Whitcher B, Suckling J, Brammer M, Breakspear M (2004) Wavelets and functional magnetic resonance imaging of the human brain. NeuroImage 23 Suppl 1:S234-249.

Cao M, Wang JH, Dai ZJ, Cao XY, Jiang LL, Fan FM, Song XW, Xia MR, Shu N, Dong Q, Milham MP, Castellanos FX, Zuo XN, He Y (2014) Topological organization of the human brain functional connectome across the lifespan. Developmental cognitive neuroscience 7:76-93.

Caspi A, Hariri AR, Holmes A, Uher R, Moffitt TE (2010) Genetic sensitivity to the environment: the case of the serotonin transporter gene and its implications for studying complex diseases and traits. The American journal of psychiatry

167:509-527.
Castellanos FX, Di Martino A, Craddock RC, Mehta AD, Milham MP (2013) Clinical applications of the functional connectome. NeuroImage 80:527-540.
Catani M, ffytche DH (2005) The rises and falls of disconnection syndromes. Brain : a journal of neurology 128:2224-2239.
Catani M, Dell'acqua F, Thiebaut de Schotten M (2013) A revised limbic system model for memory, emotion and behaviour. Neuroscience and biobehavioral reviews 37:1724-1737.
Cole DM, Smith SM, Beckmann CF (2010) Advances and pitfalls in the analysis and interpretation of resting-state FMRI data. Frontiers in systems neuroscience 4:8.
Collin G, van den Heuvel MP (2013) The ontogeny of the human connectome: development and dynamic changes of brain connectivity across the life span. The Neuroscientist : a review journal bringing neurobiology, neurology and psychiatry 19:616-628.
Cordes D, Haughton VM, Arfanakis K, Carew JD, Turski PA, Moritz CH, Quigley MA, Meyerand ME (2001) Frequencies contributing to functional connectivity in the cerebral cortex in "resting-state" data. AJNR American journal of neuroradiology 22:1326-1333.
Craddock RC, Jbabdi S, Yan CG, Vogelstein JT, Castellanos FX, Di Martino A, Kelly C, Heberlein K, Colcombe S, Milham MP (2013) Imaging human connectomes at the macroscale. Nature methods 10:524-539.
Crossley NA, Mechelli A, Scott J, Carletti F, Fox PT, McGuire P, Bullmore ET (2014) The hubs of the human connectome are generally implicated in the anatomy of brain disorders. Brain : a journal of neurology 137:2382-2395.
D'Onofrio BM, Class QA, Rickert ME, Larsson H, Langstrom N, Lichtenstein P (2013) Preterm birth and mortality and morbidity: a population-based quasi-experimental study. JAMA psychiatry 70:1231-1240.
Deco G, Jirsa VK, McIntosh AR (2011) Emerging concepts for the dynamical organization of resting-state activity in the brain. Nature reviews Neuroscience 12:43-56.
Di Martino A, Zuo XN, Kelly C, Grzadzinski R, Mennes M, Schvarcz A, Rodman J, Lord C, Castellanos FX, Milham MP (2013) Shared and distinct intrinsic functional network centrality in autism and attention-deficit/hyperactivity disorder. Biological psychiatry 74:623-632.
Douaud G, Smith S, Jenkinson M, Behrens T, Johansen-Berg H, Vickers J, James S, Voets N, Watkins K, Matthews PM, James A (2007) Anatomically related grey and white matter abnormalities in adolescent-onset schizophrenia. Brain : a journal of neurology 130:2375-2386.
Eikenes L, Lohaugen GC, Brubakk AM, Skranes J, Haberg AK (2011) Young adults born preterm with very low birth weight demonstrate widespread white matter alterations on brain DTI. NeuroImage 54:1774-1785.
Engert F, Bonhoeffer T (1999) Dendritic spine changes associated with hippocampal long-term synaptic plasticity. Nature 399:66-70.
Erk S, Mikschl A, Stier S, Ciaramidaro A, Gapp V, Weber B, Walter H (2010) Acute

and sustained effects of cognitive emotion regulation in major depression. The Journal of neuroscience : the official journal of the Society for Neuroscience 30:15726-15734.

Fair DA, Dosenbach NU, Church JA, Cohen AL, Brahmbhatt S, Miezin FM, Barch DM, Raichle ME, Petersen SE, Schlaggar BL (2007) Development of distinct control networks through segregation and integration. Proceedings of the National Academy of Sciences of the United States of America 104:13507-13512.

Farb NA, Anderson AK, Bloch RT, Segal ZV (2011) Mood-linked responses in medial prefrontal cortex predict relapse in patients with recurrent unipolar depression. Biological psychiatry 70:366-372.

Filippi M, van den Heuvel MP, Fornito A, He Y, Hulshoff Pol HE, Agosta F, Comi G, Rocca MA (2013) Assessment of system dysfunction in the brain through MRI-based connectomics. Lancet neurology 12:1189-1199.

Fornito A, Zalesky A, Breakspear M (2013) Graph analysis of the human connectome: Promise, progress, and pitfalls. NeuroImage 80:426-444.

Fornito A, Zalesky A, Pantelis C, Bullmore ET (2012) Schizophrenia, neuroimaging and connectomics. NeuroImage 62:2296-2314.

Fox MD, Snyder AZ, Vincent JL, Corbetta M, Van Essen DC, Raichle ME (2005) The human brain is intrinsically organized into dynamic, anticorrelated functional networks. Proceedings of the National Academy of Sciences of the United States of America 102:9673-9678.

Friston KJ, Frith CD, Liddle PF, Frackowiak RS (1993) Functional connectivity: the principal-component analysis of large (PET) data sets. Journal of cerebral blood flow and metabolism : official journal of the International Society of Cerebral Blood Flow and Metabolism 13:5-14.

Giessing C, Thiel CM, Alexander-Bloch AF, Patel AX, Bullmore ET (2013) Human brain functional network changes associated with enhanced and impaired attentional task performance. The Journal of neuroscience : the official journal of the Society for Neuroscience 33:5903-5914.

Glahn DC, Kent JW, Jr., Sprooten E, Diego VP, Winkler AM, Curran JE, McKay DR, Knowles EE, Carless MA, Goring HH, Dyer TD, Olvera RL, Fox PT, Almasy L, Charlesworth J, Kochunov P, Duggirala R, Blangero J (2013) Genetic basis of neurocognitive decline and reduced white-matter integrity in normal human brain aging. Proceedings of the National Academy of Sciences of the United States of America 110:19006-19011.

Gong G, Rosa-Neto P, Carbonell F, Chen ZJ, He Y, Evans AC (2009) Age- and gender-related differences in the cortical anatomical network. The Journal of neuroscience : the official journal of the Society for Neuroscience 29:15684-15693.

Greicius M (2008) Resting-state functional connectivity in neuropsychiatric disorders. Current opinion in neurology 21:424-430.

Greicius MD, Krasnow B, Reiss AL, Menon V (2003) Functional connectivity in the resting brain: a network analysis of the default mode hypothesis. Proceedings

of the National Academy of Sciences of the United States of America 100:253-258.

Greicius MD, Flores BH, Menon V, Glover GH, Solvason HB, Kenna H, Reiss AL, Schatzberg AF (2007) Resting-state functional connectivity in major depression: abnormally increased contributions from subgenual cingulate cortex and thalamus. Biological psychiatry 62:429-437.

Griffa A, Baumann PS, Thiran JP, Hagmann P (2013) Structural connectomics in brain diseases. NeuroImage 80:515-526.

Hamilton JP, Etkin A, Furman DJ, Lemus MG, Johnson RF, Gotlib IH (2012) Functional neuroimaging of major depressive disorder: a meta-analysis and new integration of base line activation and neural response data. The American journal of psychiatry 169:693-703.

Hardeveld F, Spijker J, De Graaf R, Nolen WA, Beekman AT (2010) Prevalence and predictors of recurrence of major depressive disorder in the adult population. Acta psychiatrica Scandinavica 122:184-191.

Hasler G, Northoff G (2011) Discovering imaging endophenotypes for major depression. Molecular psychiatry 16:604-619.

Herculano-Houzel S (2012) The remarkable, yet not extraordinary, human brain as a scaled-up primate brain and its associated cost. Proceedings of the National Academy of Sciences of the United States of America 109 Suppl 1:10661-10668.

Ingalhalikar M, Smith A, Parker D, Satterthwaite TD, Elliott MA, Ruparel K, Hakonarson H, Gur RE, Gur RC, Verma R (2014) Sex differences in the structural connectome of the human brain. Proceedings of the National Academy of Sciences of the United States of America 111:823-828.

Iturria-Medina Y, Canales-Rodriguez EJ, Melie-Garcia L, Valdes-Hernandez PA, Martinez-Montes E, Aleman-Gomez Y, Sanchez-Bornot JM (2007) Characterizing brain anatomical connections using diffusion weighted MRI and graph theory. NeuroImage 36:645-660.

Jahanshad N, Rajagopalan P, Hua X, Hibar DP, Nir TM, Toga AW, Jack CR, Jr., Saykin AJ, Green RC, Weiner MW, Medland SE, Montgomery GW, Hansell NK, McMahon KL, de Zubicaray GI, Martin NG, Wright MJ, Thompson PM (2013) Genome-wide scan of healthy human connectome discovers SPON1 gene variant influencing dementia severity. Proceedings of the National Academy of Sciences of the United States of America 110:4768-4773.

Jenkinson M, Beckmann CF, Behrens TE, Woolrich MW, Smith SM (2012) FSL. NeuroImage 62:782-790.

Katz J et al. (2013) Mortality risk in preterm and small-for-gestational-age infants in low-income and middle-income countries: a pooled country analysis. Lancet 382:417-425.

Kelly C, Biswal BB, Craddock RC, Castellanos FX, Milham MP (2012) Characterizing variation in the functional connectome: promise and pitfalls. Trends in cognitive sciences 16:181-188.

Kendler KS, Gardner CO, Prescott CA (2006) Toward a comprehensive developmental

model for major depression in men. The American journal of psychiatry 163:115-124.

Kessler RC, Berglund P, Demler O, Jin R, Koretz D, Merikangas KR, Rush AJ, Walters EE, Wang PS (2003) The epidemiology of major depressive disorder: results from the National Comorbidity Survey Replication (NCS-R). JAMA : the journal of the American Medical Association 289:3095-3105.

Khundrakpam BS, Reid A, Brauer J, Carbonell F, Lewis J, Ameis S, Karama S, Lee J, Chen Z, Das S, Evans AC (2013) Developmental changes in organization of structural brain networks. Cerebral cortex (New York, NY : 1991) 23:2072-2085.

Kim DJ, Davis EP, Sandman CA, Sporns O, O'Donnell BF, Buss C, Hetrick WP (2014) Longer gestation is associated with more efficient brain networks in preadolescent children. NeuroImage 100:619-627.

Kinnison J, Padmala S, Choi JM, Pessoa L (2012) Network analysis reveals increased integration during emotional and motivational processing. The Journal of neuroscience : the official journal of the Society for Neuroscience 32:8361-8372.

Kobbert C, Apps R, Bechmann I, Lanciego JL, Mey J, Thanos S (2000) Current concepts in neuroanatomical tracing. Progress in neurobiology 62:327-351.

Korgaonkar MS, Fornito A, Williams LM, Grieve SM (2014) Abnormal Structural Networks Characterize Major Depressive Disorder: A Connectome Analysis. Biological psychiatry.

Korgaonkar MS, Grieve SM, Koslow SH, Gabrieli JD, Gordon E, Williams LM (2011) Loss of white matter integrity in major depressive disorder: evidence using tract-based spatial statistical analysis of diffusion tensor imaging. Human brain mapping 32:2161-2171.

Latora V, Marchiori M (2001) Efficient behavior of small-world networks. Physical review letters 87:198701.

Lee SH, Ripke S, Neale BM, Faraone SV, etc. (2013) Genetic relationship between five psychiatric disorders estimated from genome-wide SNPs. Nature genetics 45:984-994.

Lewis CM et al. (2010) Genome-wide association study of major recurrent depression in the U.K. population. The American journal of psychiatry 167:949-957.

Li B, Liu L, Friston KJ, Shen H, Wang L, Zeng LL, Hu D (2012) A Treatment-Resistant Default Mode Subnetwork in Major Depression. Biological psychiatry.

Li W, Mai X, Liu C (2014) The default mode network and social understanding of others: what do brain connectivity studies tell us. Frontiers in human neuroscience 8:74.

Li Y, Liu Y, Li J, Qin W, Li K, Yu C, Jiang T (2009) Brain anatomical network and intelligence. PLoS computational biology 5:e1000395.

Liu Y, Yu C, Zhang X, Liu J, Duan Y, Alexander-Bloch AF, Liu B, Jiang T, Bullmore E (2014) Impaired long distance functional connectivity and weighted network architecture in Alzheimer's disease. Cerebral cortex (New York, NY : 1991) 24:1422-1435.

Lorenzetti V, Allen NB, Fornito A, Yucel M (2009) Structural brain abnormalities in

major depressive disorder: a selective review of recent MRI studies. Journal of affective disorders 117:1-17.

Lui S, Wu Q, Qiu L, Yang X, Kuang W, Chan RC, Huang X, Kemp GJ, Mechelli A, Gong Q (2011) Resting-state functional connectivity in treatment-resistant depression. The American journal of psychiatry 168:642-648.

Lynall ME, Bassett DS, Kerwin R, McKenna PJ, Kitzbichler M, Muller U, Bullmore E (2010) Functional connectivity and brain networks in schizophrenia. The Journal of neuroscience : the official journal of the Society for Neuroscience 30:9477-9487.

Mason MF, Norton MI, Van Horn JD, Wegner DM, Grafton ST, Macrae CN (2007) Wandering minds: the default network and stimulus-independent thought. Science (New York, NY) 315:393-395.

Medland SE, Jahanshad N, Neale BM, Thompson PM (2014) Whole-genome analyses of whole-brain data: working within an expanded search space. Nature neuroscience 17:791-800.

Meng C, Brandl F, Tahmasian M, Shao J, Manoliu A, Scherr M, Schwerthoffer D, Bauml J, Forstl H, Zimmer C, Wohlschlager AM, Riedl V, Sorg C (2014) Aberrant topology of striatum's connectivity is associated with the number of episodes in depression. Brain : a journal of neurology 137:598-609.

Menon V (2011) Large-scale brain networks and psychopathology: a unifying triple network model. Trends in cognitive sciences 15:483-506.

Menon V (2013) Developmental pathways to functional brain networks: emerging principles. Trends in cognitive sciences 17:627-640.

Milligan DW (2010) Outcomes of children born very preterm in Europe. Archives of disease in childhood Fetal and neonatal edition 95:F234-240.

Monroe SM, Simons AD (1991) Diathesis-stress theories in the context of life stress research: implications for the depressive disorders. Psychological bulletin 110:406-425.

Mwangi B, Ebmeier KP, Matthews K, Steele JD (2012) Multi-centre diagnostic classification of individual structural neuroimaging scans from patients with major depressive disorder. Brain : a journal of neurology 135:1508-1521.

Nosarti C, Reichenberg A, Murray RM, Cnattingius S, Lambe MP, Yin L, MacCabe J, Rifkin L, Hultman CM (2012) Preterm birth and psychiatric disorders in young adult life. Archives of general psychiatry 69:E1-8.

Ogawa S, Lee TM, Kay AR, Tank DW (1990) Brain magnetic resonance imaging with contrast dependent on blood oxygenation. Proceedings of the National Academy of Sciences of the United States of America 87:9868-9872.

Ogawa S, Tank DW, Menon R, Ellermann JM, Kim SG, Merkle H, Ugurbil K (1992) Intrinsic signal changes accompanying sensory stimulation: functional brain mapping with magnetic resonance imaging. Proceedings of the National Academy of Sciences of the United States of America 89:5951-5955.

Pauling L, Coryell CD (1936) The Magnetic Properties and Structure of Hemoglobin, Oxyhemoglobin and Carbonmonoxyhemoglobin. Proceedings of the National Academy of Sciences of the United States of America 22:210-216.

Power JD, Fair DA, Schlaggar BL, Petersen SE (2010) The development of human functional brain networks. Neuron 67:735-748.

Power JD, Barnes KA, Snyder AZ, Schlaggar BL, Petersen SE (2012) Spurious but systematic correlations in functional connectivity MRI networks arise from subject motion. NeuroImage 59:2142-2154.

Qin P, Northoff G (2011) How is our self related to midline regions and the default-mode network? NeuroImage 57:1221-1233.

Raichle ME (2006) Neuroscience. The brain's dark energy. Science (New York, NY) 314:1249-1250.

Raichle ME, MacLeod AM, Snyder AZ, Powers WJ, Gusnard DA, Shulman GL (2001) A default mode of brain function. Proceedings of the National Academy of Sciences of the United States of America 98:676-682.

Rubinov M, Sporns O (2010) Complex network measures of brain connectivity: uses and interpretations. NeuroImage 52:1059-1069.

Rubinov M, Bullmore E (2013) Fledgling pathoconnectomics of psychiatric disorders. Trends in cognitive sciences 17:641-647.

Sadaghiani S, Kleinschmidt A (2013) Functional interactions between intrinsic brain activity and behavior. NeuroImage 80:379-386.

Sampaio-Baptista C, Khrapitchev AA, Foxley S, Schlagheck T, Scholz J, Jbabdi S, DeLuca GC, Miller KL, Taylor A, Thomas N, Kleim J, Sibson NR, Bannerman D, Johansen-Berg H (2013) Motor skill learning induces changes in white matter microstructure and myelination. The Journal of neuroscience : the official journal of the Society for Neuroscience 33:19499-19503.

Savitz J, Drevets WC (2009) Bipolar and major depressive disorder: neuroimaging the developmental-degenerative divide. Neuroscience and biobehavioral reviews 33:699-771.

Schilbach L, Timmermans B, Reddy V, Costall A, Bente G, Schlicht T, Vogeley K (2013) Toward a second-person neuroscience. The Behavioral and brain sciences 36:393-414.

Schwahn C, Grabe HJ (2009) Gene-environment interactions and depression. JAMA : the journal of the American Medical Association 302:1860-1861; author reply 1861-1862.

Sheline YI, Price JL, Yan Z, Mintun MA (2010) Resting-state functional MRI in depression unmasks increased connectivity between networks via the dorsal nexus. Proceedings of the National Academy of Sciences of the United States of America 107:11020-11025.

Shulman GL, Fiez JA, Corbetta M, Buckner RL, Miezin FM, Raichle ME, Petersen SE (1997) Common Blood Flow Changes across Visual Tasks: II. Decreases in Cerebral Cortex. Journal of cognitive neuroscience 9:648-663.

Shulman RG, Rothman DL, Behar KL, Hyder F (2004) Energetic basis of brain activity: implications for neuroimaging. Trends in neurosciences 27:489-495.

Singh MK, Kesler SR, Hadi Hosseini SM, Kelley RG, Amatya D, Hamilton JP, Chen MC, Gotlib IH (2013) Anomalous gray matter structural networks in major depressive disorder. Biological psychiatry 74:777-785.

Smith SM, Nichols TE (2009) Threshold-free cluster enhancement: addressing problems of smoothing, threshold dependence and localisation in cluster inference. NeuroImage 44:83-98.

Smith SM, Jenkinson M, Johansen-Berg H, Rueckert D, Nichols TE, Mackay CE, Watkins KE, Ciccarelli O, Cader MZ, Matthews PM, Behrens TE (2006) Tract-based spatial statistics: voxelwise analysis of multi-subject diffusion data. NeuroImage 31:1487-1505.

Smith SM, Vidaurre D, Beckmann CF, Glasser MF, Jenkinson M, Miller KL, Nichols TE, Robinson EC, Salimi-Khorshidi G, Woolrich MW, Barch DM, Ugurbil K, Van Essen DC (2013) Functional connectomics from resting-state fMRI. Trends in cognitive sciences 17:666-682.

Smith SM, Miller KL, Moeller S, Xu J, Auerbach EJ, Woolrich MW, Beckmann CF, Jenkinson M, Andersson J, Glasser MF, Van Essen DC, Feinberg DA, Yacoub ES, Ugurbil K (2012) Temporally-independent functional modes of spontaneous brain activity. Proceedings of the National Academy of Sciences of the United States of America 109:3131-3136.

Smoller JW, Ripke S, etc. (2013) Identification of risk loci with shared effects on five major psychiatric disorders: a genome-wide analysis. Lancet 381:1371-1379.

Snyder AZ, Raichle ME (2012) A brief history of the resting state: the Washington University perspective. NeuroImage 62:902-910.

Sporns O (2013) The human connectome: origins and challenges. NeuroImage 80:53-61.

Sporns O (2014) Contributions and challenges for network models in cognitive neuroscience. Nature neuroscience 17:652-660.

Sporns O, Tononi G, Kotter R (2005) The human connectome: A structural description of the human brain. PLoS computational biology 1:e42.

Stanley ML, Moussa MN, Paolini BM, Lyday RG, Burdette JH, Laurienti PJ (2013) Defining nodes in complex brain networks. Frontiers in computational neuroscience 7:169.

Supekar K, Musen M, Menon V (2009) Development of large-scale functional brain networks in children. PLoS biology 7:e1000157.

Sweatt JD (2013) The emerging field of neuroepigenetics. Neuron 80:624-632.

Tao H, Guo S, Ge T, Kendrick KM, Xue Z, Liu Z, Feng J (2013) Depression uncouples brain hate circuit. Molecular psychiatry 18:101-111.

Taylor SF (2014) Using graph theory to connect the dots in obsessive-compulsive disorder. Biological psychiatry 75:593-594.

Tononi G, Sporns O, Edelman GM (1994) A measure for brain complexity: relating functional segregation and integration in the nervous system. Proceedings of the National Academy of Sciences of the United States of America 91:5033-5037.

van den Heuvel MP, Sporns O (2011) Rich-club organization of the human connectome. The Journal of neuroscience : the official journal of the Society for Neuroscience 31:15775-15786.

van den Heuvel MP, Stam CJ, Kahn RS, Hulshoff Pol HE (2009) Efficiency of functional brain networks and intellectual performance. The Journal of

neuroscience : the official journal of the Society for Neuroscience 29:7619-7624.

van den Heuvel MP, Kersbergen KJ, de Reus MA, Keunen K, Kahn RS, Groenendaal F, de Vries LS, Benders MJ (2014) The Neonatal Connectome During Preterm Brain Development. Cerebral cortex (New York, NY : 1991).

Van Essen DC, Ugurbil K (2012) The future of the human connectome. NeuroImage 62:1299-1310.

Volkow ND, Tomasi D, Wang GJ, Fowler JS, Telang F, Goldstein RZ, Alia-Klein N, Woicik P, Wong C, Logan J, Millard J, Alexoff D (2011) Positive emotionality is associated with baseline metabolism in orbitofrontal cortex and in regions of the default network. Molecular psychiatry 16:818-825.

Vos T, Flaxman AD, Naghavi M, etc. (2012) Years lived with disability (YLDs) for 1160 sequelae of 289 diseases and injuries 1990-2010: a systematic analysis for the Global Burden of Disease Study 2010. Lancet 380:2163-2196.

Wang L, Zhu C, He Y, Zang Y, Cao Q, Zhang H, Zhong Q, Wang Y (2009) Altered small-world brain functional networks in children with attention-deficit/hyperactivity disorder. Human brain mapping 30:638-649.

Watts DJ, Strogatz SH (1998) Collective dynamics of 'small-world' networks. Nature 393:440-442.

Wen W, Zhu W, He Y, Kochan NA, Reppermund S, Slavin MJ, Brodaty H, Crawford J, Xia A, Sachdev P (2011) Discrete neuroanatomical networks are associated with specific cognitive abilities in old age. The Journal of neuroscience : the official journal of the Society for Neuroscience 31:1204-1212.

White TP, Symington I, Castellanos NP, Brittain PJ, Froudist Walsh S, Nam KW, Sato JR, Allin MP, Shergill SS, Murray RM, Williams SC, Nosarti C (2014) Dysconnectivity of neurocognitive networks at rest in very-preterm born adults. NeuroImage Clinical 4:352-365.

Whiteford HA, Degenhardt L, Rehm J, Baxter AJ, Ferrari AJ, Erskine HE, Charlson FJ, Norman RE, Flaxman AD, Johns N, Burstein R, Murray CJ, Vos T (2013) Global burden of disease attributable to mental and substance use disorders: findings from the Global Burden of Disease Study 2010. Lancet 382:1575-1586.

Whitfield-Gabrieli S, Ford JM (2012) Default mode network activity and connectivity in psychopathology. Annual review of clinical psychology 8:49-76.

Willner P, Scheel-Kruger J, Belzung C (2013) The neurobiology of depression and antidepressant action. Neuroscience and biobehavioral reviews 37:2331-2371.

Xie T, He Y (2011) Mapping the Alzheimer's brain with connectomics. Frontiers in psychiatry 2:77.

Zeng LL, Shen H, Liu L, Wang L, Li B, Fang P, Zhou Z, Li Y, Hu D (2012) Identifying major depression using whole-brain functional connectivity: a multivariate pattern analysis. Brain : a journal of neurology 135:1498-1507.

Zhang J, Wang J, Wu Q, Kuang W, Huang X, He Y, Gong Q (2011) Disrupted brain connectivity networks in drug-naive, first-episode major depressive disorder. Biological psychiatry 70:334-342.

Zhou D, Thompson WK, Siegle G (2009) MATLAB toolbox for functional connectivity. NeuroImage 47:1590-1607.

Zhou J, Seeley WW (2014) Network dysfunction in Alzheimer's disease and frontotemporal dementia: implications for psychiatry. Biological psychiatry 75:565-573.

Zhou J, Gennatas ED, Kramer JH, Miller BL, Seeley WW (2012) Predicting regional neurodegeneration from the healthy brain functional connectome. Neuron 73:1216-1227.

Zhu X, Wang X, Xiao J, Liao J, Zhong M, Wang W, Yao S (2012) Evidence of a dissociation pattern in resting-state default mode network connectivity in first-episode, treatment-naive major depression patients. Biological psychiatry 71:611-617.

Paper 1

Aberrant topology of striatum's connectivity is associated with the number of episodes in depression (Brain, 2014)

doi:10.1093/brain/awt290 Brain 2014: 137; 598–609 | 598

BRAIN
A JOURNAL OF NEUROLOGY

Aberrant topology of striatum's connectivity is associated with the number of episodes in depression

Chun Meng,[1,2,3,*] Felix Brandl,[1,2,*] Masoud Tahmasian,[1,2,4] Junming Shao,[1,2] Andrei Manoliu,[1,2,5] Martin Scherr,[5,6] Dirk Schwerthöffer,[5] Josef Bäuml,[5] Hans Förstl,[5] Claus Zimmer,[1] Afra M. Wohlschläger,[1,2,3,7] Valentin Riedl[1,2,4] and Christian Sorg[1,2,5]

1 Department of Neuroradiology, Technische Universität München TUM, Ismaninger Strasse 22, 81675 Munich, Germany
2 TUM-Neuroimaging Centre of Klinikum rechts der Isar, Technische Universität München TUM, Ismaninger Strasse 22, 81675 Munich, Germany
3 Graduate School of Systemic Neurosciences GSN, Ludwig-Maximilians-Universität München LMU, Biocenter, Großhaderner Strasse 2, 82152 Munich, Germany
4 Department of Nuclear Medicine, Technische Universität München TUM, Ismaninger Strasse 22, 81675 Munich, Germany
5 Department of Psychiatry, Technische Universität München TUM, Ismaninger Strasse 22, 81675 Munich, Germany
6 Department of Neurology, Christian Doppler Klinik, Paracelsus Medical University Salzburg, Ignaz-Harrer-Straße 79, 5020 Salzburg, Austria
7 Department of Neurology, Technische Universität München TUM, Ismaninger Strasse 22, 81675 Munich, Germany

*These authors contributed equally to this work.

Correspondence to: Christian Sorg,
Department of Psychiatry and Neuroradiology,
Klinikum rechts der Isar,
Technische Universität München,
Ismaninger Strasse 22,
81675 Munich,
Germany
E-mail: c.sorg@lrz.tu-muenchen.de

In major depressive disorder, depressive episodes reoccur in ~60% of cases; however, neural mechanisms of depressive relapse are poorly understood. Depressive episodes are characterized by aberrant topology of the brain's intrinsic functional connectivity network, and the number of episodes is one of the most important predictors for depressive relapse. In this study we hypothesized that specific changes of the topology of intrinsic connectivity interact with the course of episodes in recurrent depressive disorder. To address this hypothesis, we investigated which changes of connectivity topology are associated with the number of episodes in patients, independently of current symptoms and disease duration. Fifty subjects were recruited including 25 depressive patients (two to 10 episodes) and 25 gender- and age-matched control subjects. Resting-state functional magnetic resonance imaging, Harvard-Oxford brain atlas, wavelet-transformation of atlas-shaped regional time-series, and their pairwise Pearson's correlation were used to define individual connectivity matrices. Matrices were analysed by graph-based methods, resulting in outcome measures that were used as surrogates of intrinsic network topology. Topological scores were subsequently compared across groups, and, for patients only, related with the number of depressive episodes and current symptoms by partial correlation analysis. Concerning the whole brain connectivity network of patients, small-world topology was preserved but global efficiency was reduced and global betweenness-centrality increased. Aberrant nodal efficiency and centrality of regional connectivity was found in the dorsal striatum, inferior frontal and orbitofrontal cortex as well as in the occipital and somatosensory cortex. Inferior frontal changes were associated with current symptoms, whereas aberrant right putamen network topology was associated with the number of episodes. Results were controlled for effects of total grey matter volume, medi-

Received January 24, 2013. Revised August 20, 2013. Accepted September 2, 2013. Advance Access publication October 26, 2013
© The Author (2013). Published by Oxford University Press on behalf of the Guarantors of Brain. All rights reserved.
For Permissions, please email: journals.permissions@oup.com

Downloaded from http://brain.oxfordjournals.org/ at Universitaetsbibliothek Muenchen on August 26, 2014

cation, and total disease duration. This finding provides first evidence that in major depressive disorder aberrant topology of the right putamen's intrinsic connectivity pattern is associated with the course of depressive episodes, independently of current symptoms, medication status and disease duration. Data suggest that the reorganization of striatal connectivity may interact with the course of episodes in depression thereby contributing to depressive relapse risk.

Keywords: major depressive disorder; recurrent episodes; striatum; intrinsic functional connectivity; graph analysis

Abbreviation: HAM-D = Hamilton Rating Scale for Depression

Introduction

Major depressive disorder is one of the most frequent psychiatric disorders with a lifetime prevalence of ~16% (Kessler *et al.*, 2003). Major depression is characterized by single or recurrent major depressive episodes, which include depressed mood, reduced energy, impaired cognition, vegetative symptoms, and suicidal tendency with suicide rates of 4% (American Psychiatric Association, 2000). In 35–85% of cases the course of major depression includes the recurrence of depressive episodes (Hardeveld *et al.*, 2010; Lewis *et al.*, 2010; Farb *et al.*, 2011). However, our knowledge about factors and mechanisms contributing to episode relapse is only fragmentary.

Depressive episodes are associated with widespread structural and functional brain changes (Greicius *et al.*, 2007; Erk *et al.*, 2010; Sheline *et al.*, 2010; Aizenstein *et al.*, 2011; Lui *et al.*, 2011; Li *et al.*, 2012; Mwangi *et al.*, 2012; Zeng *et al.*, 2012; for review Savitz and Drevets, 2009; Hamilton *et al.*, 2012; Whitfield-Gabrieli and Ford, 2012). For example, aberrant resting-state functional connectivity, which has been proved to separate patients from healthy control subjects by pattern classification, was found in the default mode network, salience network, occipital areas, subcortical areas and the cerebellum (Zeng *et al.*, 2012). Particularly, connectivity changes in the default mode and salience networks, which are both intrinsic networks of synchronous ongoing activity (Greicius *et al.*, 2007; Seeley *et al.*, 2007), have been linked with patients' impaired self-focused processing and aberrant emotional reactivity (Sheline *et al.*, 2010; Hamilton *et al.*, 2011, 2012; Whitfield-Gabrieli and Ford, 2012). These widespread functional brain changes, which are detectable even during rest, indicate altered large-scale organization of intrinsic brain activity in depressive episodes. Graph-based network analysis allows us to map such brain organization changes by quantifying topological properties of functional networks consisting of nodes (i.e. brain regions) and edges (i.e. functional connectivity between regions) (Bullmore and Sporns, 2009). Using resting-state functional MRI and graph-based methods, Zhang *et al.* (2011) found aberrant global efficiency of the whole brain intrinsic functional connectivity network as well as changed nodal centrality of specific brain regions' connectivity in patients with first depressive episode. Such aberrant topology of connectivity during episodes is modulated by early life experience such as childhood neglect (Wang *et al.*, 2013), and its modularity (i.e. the organization in ensembles of regions with strong within-module functional connectivity) is distinctively changed depending on whether patients suffer from their first or long-term therapy resistant episode (Tao *et al.*, 2013). Because of these findings we hypothesized that specific changes of the topology of intrinsic connectivity, particularly those reflecting functional integration (i.e. efficiency, centrality or modularity), may interact with the course of major depression.

Besides sub-depressive residuals, the number of previous depressive episodes has strongest influence on the course of major depression (Kendler *et al.*, 2001; Hardeveld *et al.*, 2010; Moylan *et al.*, 2013). A recent meta-analysis demonstrated the number of episodes to be one of the best predictors for the episode relapse risk in major depression (Hardeveld *et al.*, 2010). However, it remains poorly understood which neural mechanisms might contribute to such relationship (Robinson and Sahakian, 2008). Because of the course-sensitive aberrant topology of brain connectivity during episodes, we hypothesized that selective changes of intrinsic connectivity, which reflect altered functional integration, interact with the course of episodes in major depression. In more detail, we aimed to address the question whether and how the topology of intrinsic functional connectivity is related to the number of episodes in patients with recurrent major depression, independently of current symptoms and the total duration of the disease.

Therefore, patients with recurrent major depression and healthy control subjects were assessed by resting-state functional MRI and graph-based analysis. Resting-state blood oxygenation level-dependent signal fluctuations were used as a surrogate for intrinsic brain activity (Fox and Raichle, 2007; Raichle, 2010). Graph-based topological scores were restricted to measures of functional integration (i.e. estimates reflecting the efficiency of the interaction between distributed brain areas) and centrality (i.e. degree and betweenness-centrality both reflecting the importance of nodes for functional integration) (Rubinov and Sporns, 2010). We used the Harvard-Oxford brain atlas and functional connectivity across regions to determine each subject's functional connectivity matrix. Topological scores were derived from these matrices, compared across groups and, in patients only, related to the number of depressive episodes and current depressive symptoms by partial correlation analysis. Because of previous findings that demonstrate a link between structural changes and the course of major depression (Sheline *et al.*, 1999; MacQueen *et al.*, 2003; Frodl *et al.*, 2008; Kronmuller *et al.*, 2009), we controlled analyses for structural changes. In addition, effects of medication, disease duration, and accumulated stress, which may interact with the course of depression (Robinson and Sahakian, 2008; Hardeveld *et al.*, 2010), were controlled.

Downloaded from http://brain.oxfordjournals.org/ at Universitaetsbibliothek Muenchen on August 26, 2014

Materials and methods

Subjects

Twenty-five patients with recurrent major depression (two to 10 depressive episodes; mean age of 48.8 years; 13 female) and 25 healthy persons (mean age of 44.0 years; 14 female) participated in this study (Table 1). All participants provided informed consent in accordance with the Human Research Committee guidelines of the Klinikum rechts der Isar, Technische Universität München. Patients were recruited from the Department of Psychiatry by treating psychiatrists, healthy control subjects from the area of Munich by word-of-mouth advertizing. Participants' examination included medical history, psychiatric interview, and psychometric assessment. Psychiatric diagnoses were based on Diagnostic and Statistical Manual of Mental Disorders-IV (DSM-IV; American Psychiatric Association, 2000). The Structured Clinical Interview for DSM-IV (SCID) was used to assess the presence of psychiatric diagnoses (Spitzer *et al.*, 1992). Severity of clinical symptoms was measured with the Hamilton Rating Scale for Depression (HAM-D; Hamilton, 1960). The global level of social, occupational, and psychological functioning was measured with the Global Assessment of Functioning Scale (Spitzer *et al.*, 1992). Psychiatrists D.S. and M.S. performed clinical-psychometric assessment; they have been professionally trained for SCID interviews with inter-rater reliability for diagnoses and scores of >95%.

Recurrent major depression was the primary diagnosis for all patients. Patients with recurrent major depression constitute a heterogeneous clinical group, varying in severity of current symptoms, age of disorder onset, duration of the disorder, number of depressive episodes, family history of major depression, co-morbidity of other disorders, and type of medication. Since the goal of the present study was to determine the relationship between the topology of the brain's functional connectivity network and the course of major depression common to most patients with recurrent major depression, we adopted selection criteria from a previous study on recurrent major depression to obtain a clinically representative patient sample (Hennings *et al.*, 2009). Recurrence implies the return of an entirely new episode after clinical recovery. Due to the unreliable self-report in major depression because of patients' potential memory problems, the determination of episode number was based on the review of patients' medical records. Only patients whose records enabled us to determine a consistent episode number were included in the study. The number of episodes of all patients ranged from two to 10 following a continuous distribution (Supplementary Fig. 1). All patients met criteria for a current depressive episode with an average episode length of 16.6 weeks [standard deviation (SD) 6.6] and an averaged HAM-D score of 22 (SD 7.1). The average age of major depression onset was 32 years (SD 8), and all patients experienced their first episode before 45 years of age. The average duration of major depression was 16.7 years (SD 10.2) and on average, patients had experienced five to six episodes (mean 5.6, SD 2.5). On average 1.7 episodes (SD 1.1) were triggered by stressful life events; episodes triggered by a stressful life event were defined as episodes that started within 1 month after a stressful life event. Four patients had a positive family history of major depression. Fourteen patients had psychiatric co-morbidities: six generalized anxiety disorder, three somatization disorder, and five avoidant or dependent personality disorders. Patients with psychotic symptoms, schizophrenia, schizoaffective disorder, bipolar disorder, and substance abuse were excluded from this study. Additional exclusion criteria were pregnancy, neurological or severe internal systemic diseases, and general contraindications for MRI. One patient was free of any psychotropic medication during MRI assessment. Seven patients were treated by antidepressant mono-therapy [three cases: citalopram 30 mg/d (mean dose); three cases: sertraline 200 mg/d; one case: mirtazapine 30 mg/d]; 12 patients by dual-therapy (five cases: citalopram 37.5 mg/d + mirtazapine 30 mg/d; two cases: citalopram 40 mg/d + venlafaxine 225 mg/d; one case: citalopram 30 mg/d + quetiapine 200 mg/d; one case: sertraline 200 mg/d + mirtazapine 30 mg/d; three cases: venlafaxine 225 mg/d + mirtazapine 30 mg/d); and five patients by triple-therapy (two cases: citalopram 30 mg/d + venlafaxine 187.5 mg/d + amisulprid 200 mg/d; two cases: citalopram 30 mg/d + mirtazapine 30 mg/d + quetiapine 200 mg/d; 1 case: venlafaxine 22 mg/d + mirtazapine 30 mg/d + quetiapine 200 mg/d). All healthy control subjects were free of any current or past neurological or psychiatric disorder or psychotropic medication.

Table 1 Demographic, clinical and psychometric data

	Patients with major depression	Healthy controls	*P*-value
Subjects [total number]	25	25	
Age [years]	48.76 (14.83)	44.08 (14.78)	>0.05
Gender	13F/12M	14F/11M	>0.05
Number of episodes	5.6 (2.5)	NA	
Duration of major depression [years]	16.7 (10.2)	NA	
Current episode			
Duration [weeks]	16.6 (6.6)	NA	
HAM-D	22 (7.1)	0	<0.001
GAF	50 (10.5)	99.5 (1.1)	<0.001

Group comparisons: two-sample *t*-tests for age, HAM-D, and GAF; χ^2-test for gender. Data are presented as mean and SD (in brackets). GAF = Global Assessment of Functioning.

Data acquisition and preprocessing

All participants underwent 10 min of resting-state functional MRI with the instruction to keep their eyes closed and not to fall asleep. We verified that subjects stayed awake by interrogating via intercom immediately after the resting-state functional MRI scan. No patient dropped out during the scanning session.

Data acquisition

MRI was performed on a 3 T MR scanner (Achieva, Philips) using an 8-channel phased-array head coil. For co-registration and volumetric analysis, T_1-weighted anatomical data were obtained by using a MP-RAGE sequence (echo time = 4 ms, repetition time = 9 ms, inversion time = 100 ms, flip angle = 5°, field of view = 240 × 240 mm^2, matrix = 240 × 240, 170 slices, slice thickness = 1 mm, and 0 mm interslice gap, voxel size = 1 × 1 × 1 mm^3). Functional MRI data were obtained by using a gradient echo EPI sequence (echo time = 35 ms, repetition time = 2000 ms, flip angle = 82°, field of view = 220 × 220 mm^2, matrix = 80 × 80, 32 slices, slice thickness = 4 mm, and 0 mm interslice gap, voxel size = 2.75 × 2.75 × 4 mm^3; 300 volumes).

Preprocessing

The first three functional images of each subject's data set were discarded because of magnetization effects. The remaining resting-state functional MRI data were preprocessed by SPM8 (Wellcome Department of Cognitive Neurology, London) including head motion correction, spatial normalization into the standard stereotactic space of

Downloaded from http://brain.oxfordjournals.org/ at Universitaetsbibliothek Muenchen on August 26, 2014

the Montreal Neurological Institute with isotropic voxel of $3 \times 3 \times 3\,mm^3$, and spatial smoothing with a $6 \times 6 \times 6\,mm^3$ Gaussian kernel to reduce spatial noise. To ensure data quality, particularly concerning motion-induced artefacts, temporal signal-to-noise ratio and point-to-point head motion were estimated for each subject (Murphy *et al.*, 2007; Van Dijk *et al.*, 2012). Excessive head motion (cumulative motion translation or rotation >3 mm or 3° and mean point-to-point translation or rotation >0.15 mm or 0.1°) was applied as an exclusion criterion. Point-to-point motion was defined as the absolute displacement of each brain volume compared with its previous volume. None of the participants had to be excluded. Two-sample *t*-tests yielded no significant differences between groups regarding mean point-to-point translation or rotation of any direction ($P > 0.10$) as well as temporal signal-to-noise ratio ($P > 0.50$). Further control for head motion effects was carried out in the network construction procedure.

Topological analysis of whole brain functional connectivity network

Network construction

For each subject, the whole brain functional connectivity network was constructed from preprocessed resting-state functional MRI data. We defined 112 nodes by anatomical parcellation of the whole brain using Harvard-Oxford atlas (Supplementary Table 1; FSL, Oxford University). Time series of functional MRI signal were extracted from each voxel and subsequently averaged within each region of interest. The regional time courses were then regressed against confounding covariates (comprising six time courses of head motion and signals derived from whole grey matter, white matter and CSF). Maximal overlap discrete wavelet transform was applied to decompose the residual regional time series into the following four frequency scales: scale 1 (0.125–0.250 Hz), scale 2 (0.060–0.125 Hz), scale 3 (0.030–0.060 Hz) and scale 4 (0.015–0.030 Hz) (Percival and Walden, 2000). Absolute wavelet correlation coefficients at the low-frequency scale 2 (0.060–0.125 Hz) were used for further analysis according to previous studies (Lynall *et al.*, 2010; Alexander-Bloch *et al.*, 2012). Finally, a 112×112 connectivity matrix representing individual whole brain functional connectivity network was obtained for each subject.

Network analysis

To prepare graph-based topological analysis of the functional connectivity network, binary networks were generated for the cost range from 0.05–0.50 (with intervals of 0.01) using Prim's algorithm of minimum spanning tree in-line with previous work (Alexander-Bloch *et al.*, 2012). The cost of a network is defined as the number of existing edges divided by the number of all possible edges and serves as a basic 'economical' constraint on brain networks (Bullmore and Sporns, 2012). Cost range 0.05–0.5 was selected because networks with cost <0.05 are too sparse to obtain stable network topology and those with cost >0.50 become increasingly random and lose their small-world property that is characteristic for human brains (Humphries *et al.*, 2006; Lynall *et al.*, 2010). In addition, to investigate the impact of costs on network topology, four arbitrary quasi-equidistant cost sub-ranges (i.e. 0.05–0.14, 0.15–0.24, 0.25–0.34 and 0.35–0.50) were defined.

Graph analysis of binary networks was carried out in Matlab using the Brain Connectivity Toolbox (Rubinov and Sporns, 2010). Global topological properties of characteristic path length, global efficiency, and global betweenness-centrality (all reflecting functional integration; Rubinov and Sporns, 2010), and clustering coefficient and small-worldness (reflecting functional segregation and its relation to functional integration; Rubinov and Sporns, 2010) were calculated (Supplementary Methods) and averaged across costs for each subject. Group comparison was carried out for each cost sub-range by permutation test (100 000 iterations; $P < 0.05$) controlling for age, gender and total grey matter volume (Supplementary Methods, grey matter volume was provided by structural voxel-based morphometry analysis). Correspondingly, to analyse the topology of nodal connectivity, nodal efficiency and centrality (represented by nodal degree and betweenness-centrality; Rubinov and Sporns, 2010) were calculated and compared across groups (permutation test, 100 000 iterations, $P < 0.05$). One should note that, although efficiency, degree and betweenness-centrality reflect different aspects of functional integration, they are not completely independent among each other (i.e. they correlate significantly for specific nodes (Valente *et al.*, 2008; Lynall *et al.*, 2010; Bassett *et al.*, 2012; Zuo *et al.*, 2012). Nodal analysis was restricted to scores of centrality and efficiency within the low cost sub-range (0.05–0.14) due to results of global property analysis. After previous studies, false positive correction for *N*-node statistical comparison was applied using 1 / (amount of nodes) = 1 / 112 = 0.009 as significance threshold (Lynall *et al.*, 2010).

Partial correlation analysis for topology scores, number of depressive episodes and current symptoms

To analyse the relationship of both the course of major depression and current depressive symptoms with topological properties of nodal connectivity independently of each other, we calculated the partial correlation coefficients between topological scores and both the number of depressive episodes and HAM-D scores in patients ($P < 0.009$, false positive correction); partial correlation analysis was controlled for several variables including particularly structural changes, medication and disease duration (see below). Partial correlation analysis was used because it allows for measuring the degree of association between two random variables (i.e. topological score and number of episodes), with the effect of controlling variables removed (e.g. current symptoms reflected by HAM-D). In more detail, the partial correlation between a given topological score and the number of depressive episodes given controlling variables Z = (HAM-D, age, gender, grey matter volume, duration, medication), written as ρ(Top score, Number of depressive episodes;·Z), is the correlation between the residuals R(Top score) and R(Number of depressive episodes) resulting from the linear regression of Top score with Z and of Number of depressive episodes with Z, respectively. Therefore, a partial correlation-based approach enables the analysis of the relationship between a topological property and the course of major depression while controlling for the effect of current symptoms and vice versa.

To control for potential confounding effects, we included age, gender, grey matter volume, medication, accumulated stress, and disease duration as covariates-of-no-interest into our partial correlation approach. First, the functional connectivity of intrinsic brain networks depends on widespread structural integrity of polysynaptic pathways (Lu *et al.*, 2011). As we focus on changes of functional integration among the whole brain network that are independent of structural changes (MacQueen *et al.*, 2003; Frodl *et al.*, 2008; Kronmuller *et al.*, 2009), we included total grey matter volume scores as covariate-of-no-interest in the above mentioned functional connectivity analyses to control for this influence of structural variations (for structural changes in patients see voxel-based morphometry analysis in the Supplementary Methods). Second, patients of our study were treated by antidepressant medication, which has been demonstrated to affect intrinsic functional connectivity (Delaveau *et al.*, 2011). Therefore,

Downloaded from http://brain.oxfordjournals.org/ at Universitaetsbibliothek Muenchen on August 26, 2014

control for medication effects is necessary. Different from antipsychotic drugs, which can be compared by chlorpromazine equivalents, no comparable approach exists currently for antidepressants. We developed two ways to control for antidepressant effects and evaluated them among each other and with previous findings: (i) we divided applied antidepressants and augmentation medication into four classes (selective serotonin reuptake inhibitor, serotonin-norepinephrine reuptake inhibitor, noradrenergic and specific serotonergic antidepressants, and atypical antipsychotics); then we defined a medication covariate by the number of different classes a patient received in the partial correlation analysis; (ii) in a validation analysis, we defined four covariates (i.e. one for each medication class) with numbers 1 or 0: 1 means the patient was treated by this medication class whereas 0 means they were not. Third, as we were interested in the relationship between nodal connectivity topology and number of episodes independent of disease duration and accumulated stress, we included disease duration and the number of episodes triggered by stressful life events as additional covariates. Thereby we assume that the number of such stress-triggered episodes reflects patient's accumulated stress relevant for depression course.

Results

Global and regional atrophy in patients

Patients' total grey matter volume was reduced; regional brain volume reduction was found in the anterior cingulate cortex, dorsal prefrontal cortex, and hippocampus amongst other areas (Supplementary Fig. 2 and Supplementary Table 2). This result is in line with previous findings (Savitz and Drevets, 2009).

Aberrant global functional integration in patients

For the first cost-sub-range from 0.05 to 0.14, all subjects had small-worldness scores >1.22, demonstrating for all subjects brain networks with small-world property (Supplementary Table 3). Across groups, small-worldness and global clustering coefficient did not differ significantly (Fig. 1 and Table 2). In patients, global efficiency was reduced, global betweenness-centrality and characteristic path length were increased (Fig. 1 and Table 2). Cost range analysis revealed that changes of global topological scores were mainly driven by the low-cost sub-range (0.05–0.14), i.e. by connections of strong functional connectivity (Fig. 1).

Aberrant nodal efficiency and centrality in patients

Altered nodal centrality and efficiency of node-centred connectivity was found for several regions in patients (Fig. 2 and Table 3). In the striatum, patients had increased nodal betweenness-centrality in the right putamen and decreased nodal degree and efficiency in the caudate. In the frontal cortex, patients had decreased nodal degree in the inferior frontal gyrus pars triangularis and decreased nodal efficiency in the orbital gyrus. Furthermore, patients had increased nodal degree in the occipito-temporal cortex and decreased nodal betweenness-centrality in the postcentral gyrus.

Depressive symptoms were associated with the nodal connectivity topology of areas known to be part of the salience and default mode networks

To investigate the relationship among connectivity topology, disease course and depressive symptoms, we applied partial correlation analysis of corresponding scores with additional covariates of age, gender, grey matter volume, medication, accumulated stress and disease duration. To control for medication effects, we used two different ways to model medication influences; as results of both models differed only marginally, we report only results of the first model in which the number of medication classes administered to the patient constituted the medication covariate. To facilitate comprehensive evaluation of partial correlation results, we first examined the relationship among covariates by Pearson's correlation: HAM-D and the number of depressive episodes were not correlated ($r = 0.041$, $P = 0.844$); number of depressive episodes was correlated with disease duration ($r = 0.784$, $P < 0.001$), and HAM-D with the number of medication classes administered to the patient ($r = 0.569$, $P = 0.003$). No further covariate showed significant correlation with number of depressive episodes or HAM-D ($P > 0.05$). Additionally, total grey matter volume was significantly correlated with age ($r = -0.649$, $P = 0.0004$) and disease duration was also correlated with age ($r = 0.459$, $P = 0.021$). For partial correlation results regarding connectivity topology, critically, we found that patients' HAM-D scores were negatively correlated with nodal degree of the inferior frontal gyrus and positively correlated with nodal betweenness-centrality of the posterior supramarginal gyrus (Table 4). The inferior frontal gyrus is a hub of the salience network, and the posterior supramarginal gyrus of the default mode network.

The number of depressive episodes is associated with aberrant topology of striatal connectivity independently of current symptoms

In patients' right putamen, the number of depressive episodes was positively correlated with nodal efficiency of connectivity, independently of current symptoms, medication status, disease duration and additional covariates (Fig. 3 and Table 4). In addition, significant association between nodal degree of the nucleus accumbens' connectivity and number of depressive episodes was found (Fig. 3 and Table 4).

Discussion

To analyse how the topology of the brain's intrinsic functional connectivity network is linked with the course of depressive episodes in major depression, we applied resting-state functional MRI and

Downloaded from http://brain.oxfordjournals.org/ at Universitaetsbibliothek Muenchen on August 26, 2014

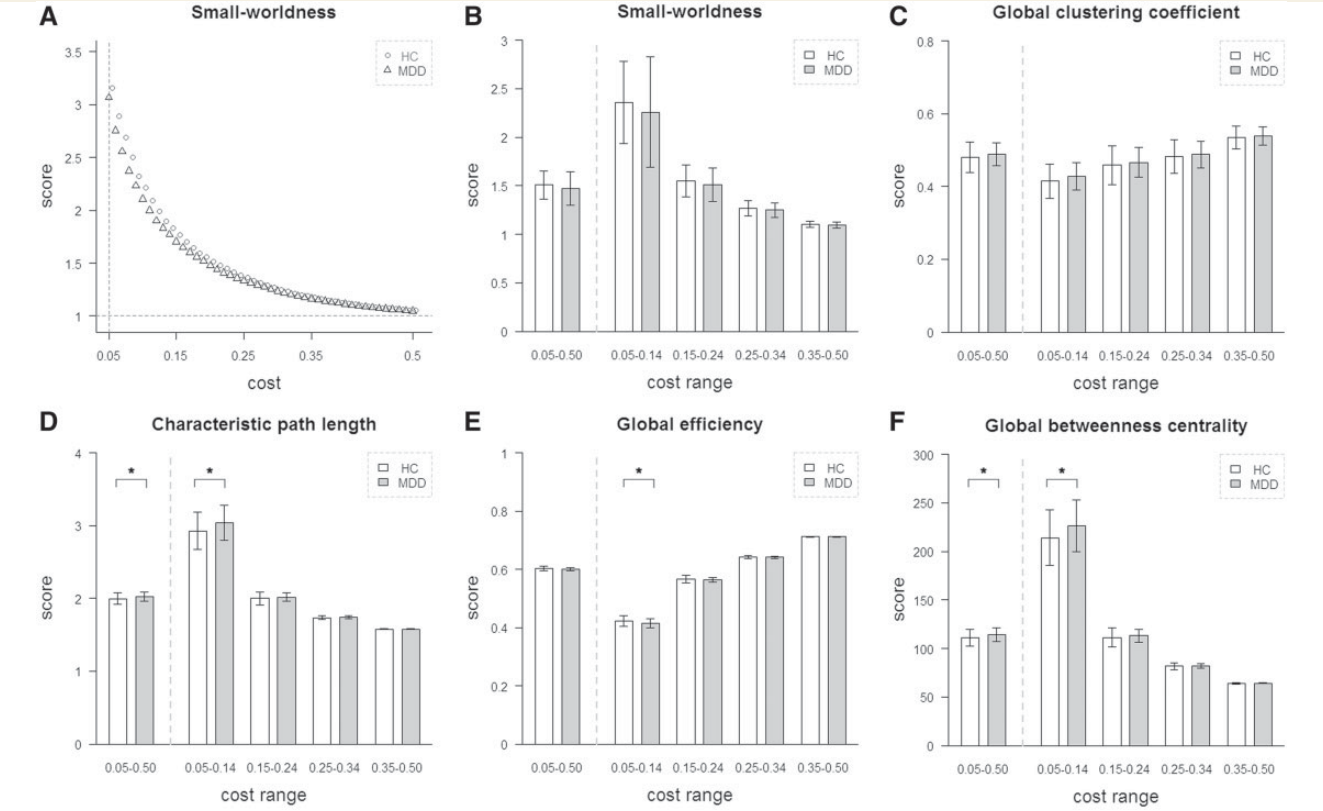

Figure 1 Global network topology in recurrent major depression. Group comparisons were based on permutation tests controlled for age, gender, and grey matter, $P < 0.05$, 100 000 permutations. (**A**) For both groups of healthy control subjects (HC) and patients with recurrent major depression (MDD), whole brain intrinsic functional connectivity networks had small-world architecture (>1.22) for the investigated cost range (0.05–0.50). Small-world properties decrease with increasing network costs. At the cost of 0.14, averaged small-worldness was 1.77 in major depression and 1.83 in control subjects. (**B** and **C**) Small-worldness and global clustering coefficient were not significantly different across groups. (**D–F**) Significant group differences were found for characteristic path length ($P = 0.029$), global efficiency ($P = 0.029$), and global betweenness-centrality ($P = 0.029$) for the cost sub-range (0.05–0.14) (i.e. for networks of spatially sparse but strong functional connectivity). *Significant group difference.

Table 2 Global topological network properties in recurrent major depression

	Healthy controls	Patients with MDD	P-Value
Small-worldness	2.344 ± 0.407	2.271 ± 0.570	0.300
Global clustering coefficient	0.412 ± 0.044	0.431 ± 0.037	0.055
Characteristic path length	2.923 ± 0.244	3.049 ± 0.215	0.029*
Global efficiency	0.423 ± 0.018	0.414 ± 0.014	0.029*
Global betweenness-centrality	213.492 ± 27.086	227.438 ± 23.841	0.029*

Group comparisons: permutation tests (100 000 permutations); *Significant result for $P < 0.05$; group comparisons were controlled for age, gender, and total grey matter volume. Global network scores are reported as mean and SD for cost sub-range 0.05-0.14. MDD = major depressive disorder.

graph-based network analysis in patients with recurrent major depression, and healthy control subjects. We found selective association between aberrant topology of the right putamen's connectivity and patients' number of depressive episodes, independently of current depressive symptoms, medication status, accumulated stress and disease duration. This result provides first evidence that intrinsic functional network organization is linked with the course of major depression, more specifically that the aberrant topology of striatal connectivity is associated with the number of episodes in depression. Data suggest that striatum's connectivity may interact with the course of depressive episodes, potentially contributing to depressive relapse risk in major depression.

Aberrant topology of striatal connectivity is associated with the course of major depression

Topology of striatal connectivity was found to be associated with the course of depressive episodes in patients with recurrent major

Downloaded from http://brain.oxfordjournals.org/ at Universitaetsbibliothek Muenchen on August 26, 2014

depression (Fig. 3, Tables 3 and 4). Specifically, we found a positive correlation between the number of episodes of major depression and nodal efficiency of right putamen intrinsic connectivity in patients (Fig. 3 and Table 4). Right putamen's centrality was significantly increased in patients (Fig. 2 and Table 3), i.e. the stronger the putamen's hubness, the more depressive episodes. Both efficiency and centrality (the latter comprising degree and betweenness-centrality) reflect functional integration in the brain i.e. the ability to rapidly combine information from distributed brain regions (Bullmore and Sporns, 2009; Rubinov and Sporns, 2010). Furthermore, we found correspondent results for the ventral striatum (Fig. 3 and Table 4) (i.e. we found a positive correlation between nucleus accumbens' centrality and the number of depressive episodes), suggesting that the topology of whole striatum's connectivity is associated with the course of episodes in major depression. Findings were not explained by age, gender, medication effects or total grey matter changes, for which we controlled statistically. Findings were also controlled for total disease duration and number of episodes triggered by stressful life events, suggesting that specifically the number of episodes and not disease duration or accumulated stress is linked with the topology of striatal connectivity. Importantly, results were also controlled for the degree of current symptoms, indicating that the topology of striatal connectivity reflects major depression's course rather than its symptoms.

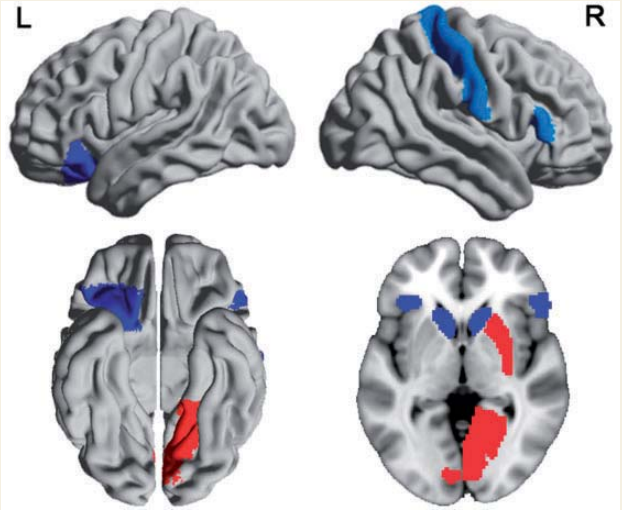

Figure 2 Brain regions with aberrant nodal efficiency and centrality in recurrent major depression. Group comparisons were based on permutation tests controlled for age, gender and grey matter volume, $P < 0.009$ based on false positive correction for multiple testing, 100 000 permutations. Coloured regions indicate significantly changed nodal intrinsic functional connectivity network topology (i.e. nodal efficiency or centrality) in patients. Blue/red indicates decrease/increase of a topological property in patients. For more details see Table 3. L = left; R = right. This figure was visualized with the BrainNet Viewer (http://www.nitrc.org/projects/bnv/).

Between-group differences of nodal network topology included bilateral caudate and right putamen (Fig. 2 and Table 3). Putamen's intrinsic functional connectivity pattern is preferentially linked with the insula and anterior cingulate cortex, i.e. with key regions of the salience network, whereas the caudate's connectivity links more with areas of the default mode network (such as the medial prefrontal and posterior cingulate cortex) (Di Martino *et al.*, 2008). Both salience and default mode networks are strongly involved in major depression (Greicius *et al.*, 2007; Sheline *et al.*, 2010; Hamilton *et al.*, 2011; for review Whitfield-Gabrieli and Ford, 2012; Hamilton *et al.*, 2013). A previous study reported increased putamen and caudate centrality/efficiency in first-episode major depression patients (Zhang *et al.*, 2011). Concerning putamen we found consistent results in patients with recurrent major depression, and concerning caudate we found reduced centrality and efficiency in patients with recurrent major depression. It might be that within the dorsal striatum, network topology of sub-areas (like putamen and caudate) develops distinctively in the course of recurrent major depression potentially because of a specific intrinsic connectivity pattern (see further

Table 3 Nodal network topology in recurrent major depression

Lobe	Node / Region of interest	Side	Mode	Healthy controls	Patients with MDD	*P*-Value
Patients with MDD > Healthy controls						
Subcortical	Putamen	R	BC	175.898 ± 126.037	346.133 ± 230.110	<0.001
Occipital	Intracalcarine cortex	R	Deg	7.672 ± 4.071	11.031 ± 4.838	0.006
		L	Deg	7.615 ± 4.095	12.446 ± 5.376	<0.001
	Lingual gyrus	R	Deg	8.649 ± 4.593	12.801 ± 6.334	0.005
Patients with MDD < Healthy controls						
Subcortical	Caudate	R	E_{nodal}	0.390 ± 0.071	0.319 ± 0.088	0.002
		L	Deg	9.162 ± 5.632	5.071 ± 4.237	0.002
			E_{nodal}	0.402 ± 0.074	0.325 ± 0.081	0.001
Frontal	Frontal orbital cortex	L	E_{nodal}	0.462 ± 0.048	0.417 ± 0.059	0.003
	Inferior frontal gyrus, pars triangularis	R	Deg	10.010 ± 5.859	6.158 ± 3.543	0.003
Sensorimotor	Postcentral gyrus	R	BC	234.044 ± 154.870	138.132 ± 78.231	0.004

Group comparisons: permutation tests (100 000 permutations); reported results are significant for $P < 0.009$ based on false positive correction for multiple testing; group comparisons were controlled for age, gender and total grey matter volume. Nodal network scores are reported for cost sub-range 0.05-0.14 as mean and SD. MDD = major depressive disorder; R = right; L = left; BC = nodal betweenness-centrality; Deg = nodal degree; E_{nodal} = nodal efficiency.

Downloaded from http://brain.oxfordjournals.org/ at Universitaetsbibliothek Muenchen on August 26, 2014

Table 4 Nodal network topology: partial correlation with depressive symptoms (HAM-D) and major depression course (number of depressive episodes), respectively

Lobe	Node / Region of interest	Side	Mode	r-Value	*P*-value
Association between nodal network topology and depressive symptoms					
Frontal	Inferior frontal gyrus, pars triangularis	R	Deg	−0.614	0.005
Parietal	Supramarginal gyrus, posterior division	R	BC	0.688	0.001
Association between nodal network topology and number of depressive episodes					
Subcortical	Putamen	R	E_{nodal}	0.588	0.008
	Accumbens	R	Deg	0.586	0.008

Partial correlation analyses were corrected for age, gender, total grey matter volume, disease duration, and medication effects; reported results are significant for $P < 0.009$ based on false positive correction for multiple comparison. Regional network scores are based on cost sub-range 0.05–0.14. R = right; L = left; Deg = nodal degree; E_{nodal} = nodal efficiency; BC = nodal betweenness-centrality.

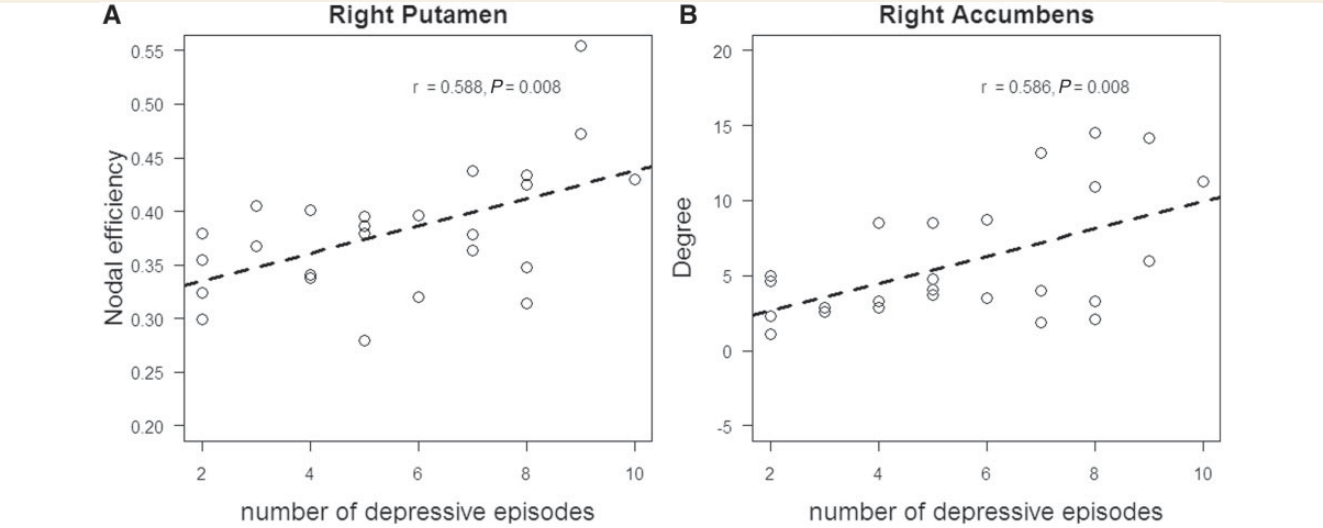

Figure 3 Association between striatal connectivity topology and number of depressive episodes in patients with recurrent major depression, independently of current symptoms and disease duration. Partial correlation analysis of nodal topological scores and number of depressive episodes, including additional covariates of current symptoms, age, gender, grey matter brain volume, medication effects and disease duration, $P < 0.009$ based on false positive correction for multiple testing. Scatter plots reflect significant correlations between different striatal network scores and the number of depressive episodes in patients with recurrent major depression.

support for this argument below). However, we cannot exclude the potential influence of methodological differences between the previous and our study [e.g. Zhang *et al*. (2011) applied a brain atlas different from that of our study; such atlas-based parcellation change may shift the network topology result; Wang *et al.* (2009)]. Future studies, which should be designed to study explicitly data of both first and recurrent episode major depression, are necessary to compare directly network topology changes within one methodological framework.

Two lines of research highlight the importance of the striatum (particularly of the right putamen) for major depression: (i) Impaired emotion processing in major depression: a recent meta-analysis in major depression, which integrated PET-based metabolic resting-state findings with functional MRI data of emotional stimulation, found that patients' aberrant striatal activity might prevent critically the regulatory impact of the prefrontal cortex on increased emotional processing in limbic-insular areas (Hamilton *et al.*, 2012). The authors suggest that changes of striatal connectivity (particularly of the dorsal striatum) may contribute to this regulatory deficit, potentially because of lowered striatal dopamine levels (Hamilton *et al.*, 2012). Our result is consistent with this idea, highlighting explicitly the important role of increasingly changed topology of striatal connectivity for the course of major depression; and (ii) Impaired emotional learning in major depression: furthermore, dopamine-dependent striatal activity is essential for reinforcement learning (Liljeholm and O'Doherty, 2012). This type of learning is impaired in major depression (Eshel and Roiser, 2010). For example, during reversal learning, right putamen responses for unexpected reward were selectively reduced in patients with major depression (Robinson *et al.*, 2012). The authors suggest that a reward-related dysfunction of the right putamen within a striatum-centred prefrontal-limbic circuit may inhibit the learning of appreciating and enjoying positive life experience; such positive experience, in turn, is critical for depressive

Downloaded from http://brain.oxfordjournals.org/ at Universitaetsbibliothek Muenchen on August 26, 2014

recovery. Our result is consistent with this idea, specifying that right putamen's connectivity topology might be relevant for such adaptive processes in major depression. In summary, aberrant topology of striatal connectivity and its link with the course of depressive episodes are consistent with models of impaired emotion regulation and dopamine-dependent reward learning in major depression.

Aberrant topology of striatal connectivity and depressive relapse risk

Aberrant topology of striatal connectivity might be a potential mechanism to mediate the relapse risk in major depression. Depressive episodes are associated with both the change of network topology (Figs 1 and 2) and the increase of episode relapse risk (Hardeveld *et al.*, 2010). Here we found that the amount of episodes is specifically linked with aberrant topology of striatal connectivity (Fig. 3). This link suggests striatal topology as neural correlate for the course of episodes in major depression, and therefore of episode relapse. This argument makes topology of striatal connectivity a potential biomarker to evaluate depressive recurrence risk.

Aberrant nodal network topology in areas of the salience network is associated with current depressive symptoms

Beyond the striatum, aberrant nodal centrality and efficiency was found in the inferior frontal gyrus, the orbitofrontal cortex as well as in the occipital and somatosensory cortex (Fig. 2 and Table 3). This finding was not influenced by age, gender, medication status, or total grey matter reduction. With respect to affected regions, our result matches perfectly previous findings in first-episode major depression (Zhang *et al.*, 2011); as mentioned above for the caudate, the direction of changes was different for some regions (e.g. patients' lingual or calcarine centrality was reduced in the previous but increased in our study). Nodal degree and efficiency of inferior frontal gyrus' and posterior supramarginal gyrus' connectivity, respectively, was specifically associated with depressive symptoms measured by the HAM-D (Table 4). These areas are key regions of the salience and default mode network, which both are critically involved in depressive symptoms such as rumination or aberrant emotional reactivity (Greicius *et al.*, 2007; Sheline *et al.*, 2010; Hamilton *et al.*, 2011, 2013; Whitfield-Gabrieli and Ford, 2012). Aberrant network topology and the association of network topology with depressive symptom severity overlapped in the inferior frontal gyrus of the salience network (Tables 3 and 4). This result suggests that topological changes of the cortical salience network reflect major depression symptoms, whereas those of the subcortical striatum are associated with the course of major depression. This finding is in line with the more general idea about cortex-basal-ganglia (including striatum)-thalamus-cortex loops, where the cortex itself initially generates action/cognition/affective candidates, between which the basal ganglia then arbitrate (likely based on their learned reinforcement probabilities) to facilitate (gate) the 'best' one (for review see Maia and Frank, 2011).

Aberrant global network topology in recurrent major depression: impact on the backbone network

Concerning global topology of functional connectivity, we found selectively aberrant functional integration (decreased global efficiency and increased global betweenness-centrality) in patients, whereas other topological properties (small-worldness and clustering coefficient) were not significantly different across groups (Fig. 1 and Table 2). In general, global topological scores are derived from correspondent nodal scores by different forms of averaging. Because of the correspondence of decreased global efficiency/decreased caudate efficiency and increased global betweenness-centrality/increased putamen betweenness-centrality, selective reorganization of global functional integration seems to depend mainly on the reorganization of striatal connectivity in major depression, emphasizing the prominent role of striatal connectivity in recurrent major depression.

Furthermore, changes of global network topology are driven by low-cost networks i.e. by networks that include edges of particularly strong intrinsic functional connectivity. Across investigated cost-sub-ranges, significant group differences of network topology focus on the cost-sub-range of 0.05–0.14, which is related to sparse networks and strong connectivity (Fig. 1). This means that recurrent major depression is selectively associated with changes in widespread (whole brain) strong (top 14%) functional connections, which are supposed to constitute the backbone of the brain network. Previous studies found that backbone networks consist mainly of both network hubs and strong long-distance edges (Serrano *et al.*, 2009; van den Heuvel *et al.*, 2012; Markov *et al.*, 2013). Correspondingly, we found global and nodal centrality, which are both related to such hubness, to be altered in patients. Taken together, these data indicate that major depression is particularly associated with changes in the brain's backbone network.

Methodological issues and limitations

To evaluate results of the current study appropriately, some methodological issues have to be considered. Issues concerning patient sample and chosen graph approach are discussed below and, issues concerning study design and imaging data analysis are discussed in the Supplementary Discussion.

Medication

Patients in our study were treated by antidepressant medication. Although recent studies suggest that antidepressants normalize brain function (Anand *et al.*, 2005; Fu *et al.*, 2007; Heller *et al.*, 2013), the impact of antidepressants on intrinsic functional connectivity is so far incompletely understood (Bruhl *et al.*, 2010; Delaveau *et al.*, 2011). To control for potential impact of medication, we modelled medication effects and added corresponding covariates into statistical analyses. As no canonical way to account

Downloaded from http://brain.oxfordjournals.org/ at Universitaetsbibliothek Muenchen on August 26, 2014

for antidepressants effects is available, we tested two different models, which yielded almost identical results. Further, we found that medication status was associated with the degree of current symptoms but not with the number of episodes, suggesting that at least during a current episode the amount of applied antidepressants is independent of the previous disorder course but dependent on symptom severity. In summary, these findings and the coherence of our results with previous studies (Zhang *et al.*, 2011; Wang *et al.*, 2013), suggest that medication may not critically influence results of our study. Nevertheless, data should be interpreted carefully because of potential medication confounds. Future studies in non-medicated patients are necessary; however, such studies in drug-free patients of recurrent major depression might implicate strong practical and ethical problems.

Binary graph approach

In this study, instead of weighted graphs, the binary undirected graph-based framework was used to analyse the brain's intrinsic functional connectivity network. Binary undirected graphs are defined by edges of either 1 or 0 (i.e. they reflect the presence or absence of connections due to a given threshold), whereas weighted graphs reflect connection strengths by continuous edge scores (Rubinov and Sporns, 2010). The binary approach was chosen for the following reasons: (i) Backbone network and weaker connection analysis: in contrast to weighted graph approaches (Rubinov and Sporns, 2011), binary approaches enable a cost analysis (i.e. an edge density analysis) to evaluate separately the brain's backbone network (defined by strongest edges for all nodes) and the influence of weaker connections (i.e. edges of weaker connectivity strength) on network topology. In particular, we found that major depression is associated with changes in the backbone network; (ii) Comparability between binary and weighted graph approaches: cost integration within binary approaches (i.e. averaging of graph metrics across costs) provides results that are comparable with those derived from weighted graph approaches (Ginestet *et al.*, 2011); and (iii) Comparability with other studies: previous studies of brain network topology in major depression relied on binary undirected graphs (Jin *et al.*, 2011; Zhang *et al.*, 2011; Tao *et al.*, 2013). We used the same framework to enable comparisons among studies. Nevertheless, it should be noted that weighted approaches conserve more information about the whole distribution of edge weights than binary approaches do. Future complementary studies using weighted graphs might be helpful to understand more comprehensively brain organization changes in major depression.

Conclusion

In recurrent major depression aberrant topology of striatal connectivity is associated with the course of depressive episodes independently of current symptoms, medication status, accumulated stress, and disease duration. Therefore, the topology of striatum's intrinsic connectivity may have the potential to predict episode relapse risk in major depression.

Acknowledgements

We are grateful to the participants of the study and the staff of the Department of Psychiatry and Neuroradiology for their help in recruitment and data collection.

Funding

This work was supported by the Chinese Scholar Council (CSC), File No: 2010604026 (C.M.), the German Federal Ministry of Education and Research (BMBF 01EV0710 to A.M.W., BMBF 01ER0803 to C.S.) and the Kommission für Klinische Forschung, Technische Universität München (KKF 8765162 to C.S).

Supplementary material

Supplementary material is available at *Brain* online.

References

Aizenstein HJ, Andreescu C, Edelman KL, Cochran JL, Price J, Butters MA, et al. fMRI correlates of white matter hyperintensities in late-life depression. Am J Psychiatry 2011; 168: 1075–82.

Alexander-Bloch A, Lambiotte R, Roberts B, Giedd J, Gogtay N, Bullmore E. The discovery of population differences in network community structure: new methods and applications to brain functional networks in schizophrenia. Neuroimage 2012; 59: 3889–900.

American Psychiatric Association. Diagnostic and statistical manual of mental disorders. 4th edn, text revision. Washington, DC: American Psychiatric Association; 2000.

Anand A, Li Y, Wang Y, Wu J, Gao S, Bukhari L, et al. Activity and connectivity of brain mood regulating circuit in depression: a functional magnetic resonance study. Biol Psychiatry 2005; 57: 1079–88.

Bassett DS, Nelson BG, Mueller BA, Camchong J, Lim KO. Altered resting state complexity in schizophrenia. Neuroimage 2012; 59: 2196–207.

Bruhl AB, Kaffenberger T, Herwig U. Serotonergic and noradrenergic modulation of emotion processing by single dose antidepressants. Neuropsychopharmacology 2010; 35: 521–33.

Bullmore E, Sporns O. Complex brain networks: graph theoretical analysis of structural and functional systems. Nat Rev Neurosci 2009; 10: 186–98.

Bullmore E, Sporns O. The economy of brain network organization. Nat Rev Neurosci 2012; 13: 336–49.

Delaveau P, Jabourian M, Lemogne C, Guionnet S, Bergouignan L, Fossati P. Brain effects of antidepressants in major depression: a meta-analysis of emotional processing studies. J Affect Disord 2011; 130: 66–74.

Di Martino A, Scheres A, Margulies DS, Kelly AM, Uddin LQ, Shehzad Z, et al. Functional connectivity of human striatum: a resting state FMRI study. Cereb Cortex 2008; 18: 2735–47.

Erk S, Mikschl A, Stier S, Ciaramidaro A, Gapp V, Weber B, et al. Acute and sustained effects of cognitive emotion regulation in major depression. J Neurosci 2010; 30: 15726–34.

Eshel N, Roiser JP. Reward and punishment processing in depression. Biol Psychiatry 2010; 68: 118–24.

Farb NA, Anderson AK, Bloch RT, Segal ZV. Mood-linked responses in medial prefrontal cortex predict relapse in patients with recurrent unipolar depression. Biol Psychiatry 2011; 70: 366–72.

Fox MD, Raichle ME. Spontaneous fluctuations in brain activity observed with functional magnetic resonance imaging. Nat Rev Neurosci 2007; 8: 700–11.

Downloaded from http://brain.oxfordjournals.org/ at Universitaetsbibliothek Muenchen on August 26, 2014

Frodl T, Jager M, Born C, Ritter S, Kraft E, Zetzsche T, et al. Anterior cingulate cortex does not differ between patients with major depression and healthy controls, but relatively large anterior cingulate cortex predicts a good clinical course. Psychiatry Res 2008; 163: 76–83.

Fu CH, Williams SC, Brammer MJ, Suckling J, Kim J, Cleare AJ, et al. Neural responses to happy facial expressions in major depression following antidepressant treatment. Am J Psychiatry 2007; 164: 599–607.

Ginestet CE, Nichols TE, Bullmore ET, Simmons A. Brain network analysis: separating cost from topology using cost-integration. PloS One 2011; 6: e21570.

Greicius MD, Flores BH, Menon V, Glover GH, Solvason HB, Kenna H, et al. Resting-state functional connectivity in major depression: abnormally increased contributions from subgenual cingulate cortex and thalamus. Biol Psychiatry 2007; 62: 429–37.

Hamilton JP, Chen MC, Gotlib IH. Neural systems approaches to understanding major depressive disorder: an intrinsic functional organization perspective. Neurobiol Dis 2013; 52: 4–11.

Hamilton JP, Etkin A, Furman DJ, Lemus MG, Johnson RF, Gotlib IH. Functional neuroimaging of major depressive disorder: a meta-analysis and new integration of base line activation and neural response data. Am J Psychiatry 2012; 169: 693–703.

Hamilton JP, Furman DJ, Chang C, Thomason ME, Dennis E, Gotlib IH. Default-mode and task-positive network activity in major depressive disorder: implications for adaptive and maladaptive rumination. Biol Psychiatry 2011; 70: 327–33.

Hamilton M. A rating scale for depression. J Neurol Neurosurg Psychiatry 1960; 23: 56–62.

Hardeveld F, Spijker J, De Graaf R, Nolen WA, Beekman AT. Prevalence and predictors of recurrence of major depressive disorder in the adult population. Acta Psychiatrica Scandinavica 2010; 122: 184–91.

Heller AS, Johnstone T, Light SN, Peterson MJ, Kolden GG, Kalin NH, et al. Relationships between changes in sustained fronto-striatal connectivity and positive affect in major depression resulting from antidepressant treatment. Am J Psychiatry 2013; 170: 197–206.

Hennings JM, Owashi T, Binder EB, Horstmann S, Menke A, Kloiber S, et al. Clinical characteristics and treatment outcome in a representative sample of depressed inpatients - findings from the Munich Antidepressant Response Signature (MARS) project. J Psychiatric Res 2009; 43: 215–29.

Humphries MD, Gurney K, Prescott TJ. The brainstem reticular formation is a small-world, not scale-free, network. Proc Biol Sci 2006; 273: 503–11.

Jin C, Gao C, Chen C, Ma S, Netra R, Wang Y, et al. A preliminary study of the dysregulation of the resting networks in first-episode medication-naive adolescent depression. Neurosci Lett 2011; 503: 105–9.

Kendler KS, Thornton LM, Gardner CO. Genetic risk, number of previous depressive episodes, and stressful life events in predicting onset of major depression. Am J Psychiatry 2001; 158: 582–6.

Kessler RC, Berglund P, Demler O, Jin R, Koretz D, Merikangas KR, et al. The epidemiology of major depressive disorder: results from the National Comorbidity Survey Replication (NCS-R). JAMA 2003; 289: 3095–105.

Kronmuller KT, Schroder J, Kohler S, Gotz B, Victor D, Unger J, et al. Hippocampal volume in first episode and recurrent depression. Psychiatry Res 2009; 174: 62–6.

Lewis CM, Ng MY, Butler AW, Cohen-Woods S, Uher R, Pirlo K, et al. Genome-wide association study of major recurrent depression in the U.K. population. Am J Psychiatry 2010; 167: 949–57.

Li B, Liu L, Friston KJ, Shen H, Wang L, Zeng LL, et al. A treatment-resistant default mode subnetwork in major depression. Biol Psychiatry 2012; 74: 48–54.

Liljeholm M, O'Doherty JP. Contributions of the striatum to learning, motivation, and performance: an associative account. Trends Cogn Sci 2012; 16: 467–75.

Lu J, Liu H, Zhang M, Wang D, Cao Y, Ma Q, et al. Focal pontine lesions provide evidence that intrinsic functional connectivity reflects polysynaptic anatomical pathways. J Neurosc 2011; 31: 15065–71.

Lui S, Wu Q, Qiu L, Yang X, Kuang W, Chan RC, et al. Resting-state functional connectivity in treatment-resistant depression. Am J Psychiatry 2011; 168: 642–8.

Lynall ME, Bassett DS, Kerwin R, McKenna PJ, Kitzbichler M, Muller U, et al. Functional connectivity and brain networks in schizophrenia. J Neurosci 2010; 30: 9477–87.

MacQueen GM, Campbell S, McEwen BS, Macdonald K, Amano S, Joffe RT, et al. Course of illness, hippocampal function, and hippocampal volume in major depression. Proc Natl Acad Sci USA 2003; 100: 1387–92.

Maia TV, Frank MJ. From reinforcement learning models to psychiatric and neurological disorders. Nat Neurosci 2011; 14: 154–62.

Markov NT, Ercsey-Ravasz M, Lamy C, Ribeiro Gomes AR, Magrou L, Misery P, et al. The role of long-range connections on the specificity of the macaque interareal cortical network. Proc Natl Acad Sci USA 2013; 110: 5187–92.

Moylan S, Maes M, Wray NR, Berk M. The neuroprogressive nature of major depressive disorder: pathways to disease evolution and resistance, and therapeutic implications. Mol Psychiatry 2013; 18: 595–606.

Murphy K, Bodurka J, Bandettini PA. How long to scan? The relationship between fMRI temporal signal to noise ratio and necessary scan duration. Neuroimage 2007; 34: 565–74.

Mwangi B, Ebmeier KP, Matthews K, Steele JD. Multi-centre diagnostic classification of individual structural neuroimaging scans from patients with major depressive disorder. Brain 2012; 135 (Pt 5): 1508–21.

Percival D, Walden A. Wavelet methods for time series analysis. Cambridge, UK: Cambridge University Press; 2000.

Raichle ME. Two views of brain function. Trends Cogn Sci 2010; 14: 180–90.

Robinson OJ, Cools R, Carlisi CO, Sahakian BJ, Drevets WC. Ventral striatum response during reward and punishment reversal learning in unmedicated major depressive disorder. Am J Psychiatry 2012; 169: 152–9.

Robinson OJ, Sahakian BJ. Recurrence in major depressive disorder: a neurocognitive perspective. Psychol Med 2008; 38: 315–8.

Rubinov M, Sporns O. Complex network measures of brain connectivity: uses and interpretations. Neuroimage 2010; 52: 1059–69.

Rubinov M, Sporns O. Weight-conserving characterization of complex functional brain networks. Neuroimage 2011; 56: 2068–79.

Savitz J, Drevets WC. Bipolar and major depressive disorder: neuroimaging the developmental-degenerative divide. Neurosci Biobehav Rev 2009; 33: 699–771.

Seeley WW, Menon V, Schatzberg AF, Keller J, Glover GH, Kenna H, et al. Dissociable intrinsic connectivity networks for salience processing and executive control. J Neurosci 2007; 27: 2349–56.

Serrano MA, Boguna M, Vespignani A. Extracting the multiscale backbone of complex weighted networks. Proc Natl Acad Sci USA 2009; 106: 6483–8.

Sheline YI, Price JL, Yan Z, Mintun MA. Resting-state functional MRI in depression unmasks increased connectivity between networks via the dorsal nexus. Proc Natl Acad Sci USA 2010; 107: 11020–5.

Sheline YI, Sanghavi M, Mintun MA, Gado MH. Depression duration but not age predicts hippocampal volume loss in medically healthy women with recurrent major depression. J Neurosci 1999; 19: 5034–43.

Spitzer RL, Williams JB, Gibbon M, First MB. The Structured Clinical Interview for DSM-III-R (SCID). I: history, rationale, and description. Arch Gen Psychiatry 1992; 49: 624–9.

Tao H, Guo S, Ge T, Kendrick KM, Xue Z, Liu Z, et al. Depression uncouples brain hate circuit. Mol Psychiatry 2013; 18: 101–11.

Valente TW, Coronges K, Lakon C, Costenbader E. How correlated are network centrality measures? Connect (Tor) 2008; 28: 16–26.

van den Heuvel MP, Kahn RS, Goni J, Sporns O. High-cost, high-capacity backbone for global brain communication. Proc Natl Acad Sci USA 2012; 109: 11372–7.

Van Dijk KR, Sabuncu MR, Buckner RL. The influence of head motion on intrinsic functional connectivity MRI. Neuroimage 2012; 59: 431–8.

Downloaded from http://brain.oxfordjournals.org/ at Universitaetsbibliothek Muenchen on August 26, 2014

Wang J, Wang L, Zang Y, Yang H, Tang H, Gong Q, et al. Parcellation-dependent small-world brain functional networks: a resting-state fMRI study. Hum Brain Mapp 2009; 30: 1511–23.

Wang L, Dai Z, Peng H, Tan L, Ding Y, He Z, et al. Overlapping and segregated resting-state functional connectivity in patients with major depressive disorder with and without childhood neglect. Hum Brain Mapp 2013, Advance Access published on February 13, 2013, doi: 10.1002/hbm.22241.

Whitfield-Gabrieli S, Ford JM. Default mode network activity and connectivity in psychopathology. Annu Rev Clin Psychol 2012; 8: 49–76.

Zeng LL, Shen H, Liu L, Wang L, Li B, Fang P, et al. Identifying major depression using whole-brain functional connectivity: a multivariate pattern analysis. Brain 2012; 135 (Pt 5): 1498–507.

Zhang J, Wang J, Wu Q, Kuang W, Huang X, He Y, et al. Disrupted brain connectivity networks in drug-naive, first-episode major depressive disorder. Biol Psychiatry 2011; 70: 334–42.

Zuo XN, Ehmke R, Mennes M, Imperati D, Castellanos FX, Sporns O, et al. Network centrality in the human functional connectome. Cereb Cortex 2012; 22: 1862–75.

Downloaded from http://brain.oxfordjournals.org/ at Universitaetsbibliothek Muenchen on August 26, 2014

Supplementary Material of

"Aberrant topology of striatum's connectivity is associated with the number of episodes in depression"

by Chun Meng et al.

Supplementary Methods: 2

Voxel-based morphometry (VBM) analysis

Definition of topological scores

Supplementary Discussion: 1

Methodological issues and limitations: study design and imaging data analysis

Supplementary References

Supplementary Figures: 2

Figure S1. Distribution of episode number in patients with recurrent major depression

Figure S2. Regional grey matter volume reduction in patients with recurrent major depression

Supplementary Tables: 3

Table S1. Regions-of-Interest derived from Harvard-Oxford atlas

Table S2. Regional VBM decrease in patients with recurrent major depression

Table S3. Small-worldness range for all subjects referring to different cost ranges

Supplementary Methods:

Voxel-based morphometry (VBM) analysis.

The functional connectivity of intrinsic brain activity depends on widespread structural integrity of polysynaptic pathways (Lu *et al.*, 2011). Since we focus on changes of intrinsic functional connectivity within the whole brain functional network, we included total grey matter volume as covariate-of-no-interest in functional network analyses to control for the influence of structural variations. As described recently (Sorg *et al.*, 2013), we used the VBM8 toolbox (http://dbm.neuro.uni-jena.de/vbm.html) to analyze brain structure. T1-weighted images were corrected for bias-field inhomogeneity, registered using linear (12-parameter affine) and nonlinear transformations, and tissue-classified into grey matter (GM), white matter, and cerebrospinal fluid within the same generative model. The resulting GM images were modulated to account for volume changes resulting from the normalization process. Here, we only considered non-linear volume changes so that further analyses did not have to account for differences in head size. Finally images were smoothed with a Gaussian kernel of 8mm (FWHM). For group comparisons, voxel-wise two-sample t-tests were performed ($p<0.001$, cluster extent 50) controlling for age and gender. Total grey matter volume GMV was derived from the first segmentation process, normalized by total brain size, and compared across groups by two-sample t-tests ($p<0.05$).

Definition of network topology scores.

A brain network consists of nodes and edges. A node is specified by a brain region. An edge is the connection between two nodes (i.e. here intrinsic functional connectivity). In binary undirected networks, edges are either 1 or 0, indicating

whether a connection exists or not (due to a specific threshold). In the current study both global and nodal network topology scores were calculated for binary undirected networks at each cost in line with previous literature (Rubinov and Sporns, 2010).

The clustering coefficient (C) of a node is defined as the fraction of the given node's neighbors that are also neighbors of each other, indicating the extent of functional segregation in brain network. Globally, clustering coefficient of the network is defined as mean clustering coefficient across all nodes (Watts and Strogatz, 1998; Rubinov and Sporns, 2010).

The characteristic path length (L) of a network is defined as the average shortest path length between all pairs of nodes in the network, indicating the extent of functional integration of specialized information from distributed brain regions (Watts and Strogatz, 1998; Rubinov and Sporns, 2010).

The global efficiency of a network is defined as the average inverse shortest path length between all pairs of nodes, representing a further measure of information integration in brain networks. Global efficiency is proportional to path length in form of a hyperbolic curve. In general, global efficiency is primarily influenced by short-range paths while characteristic path length by long-range paths (Rubinov and Sporns, 2010).

A brain network with small-world property (i.e. a highly segregated *and* integrated network) should be more clustered (i.e. larger clustering coefficient) than random networks and its characteristic path length should be comparable with those of

random networks (Watts and Strogatz, 1998). Small-worldness (S) is defined to delineate such feature:

$$S = (C/C_{rand}) / (L/L_{rand})$$

where C_{rand} and L_{rand} are the clustering coefficient and the characteristic path length, respectively, of corresponding random networks. Small-world networks are characterized by $S \gg 1$(Watts and Strogatz, 1998; Rubinov and Sporns, 2010).

Nodal centrality refers to nodal degree and betweenness-centrality in this study. Nodal degree is defined as the number of edges connected with the given node while betweenness-centrality of a node is defined as the fraction of all shortest paths between all other nodes that pass through the given node in the network (Rubinov and Sporns, 2010). Global betweenness-centrality is defined as averaged betweenness-centrality across all nodes.

Nodal efficiency is defined as average inverse shortest path length between the given node and all other nodes (Zhang *et al.*, 2011).

Supplementary Discussion:

Methodological issues and limitations.

Study design. Our study's hypothesis was that specific changes of the brain's intrinsic connectivity (as measured by connectivity topology) interact with the course of episodes (as measured by the number of episodes) in recurrent depressive disorder. Concerning basic study design, at least two ways are possible to address this hypothesis. One way might be to investigate brain connectivity in remitted patients and to link connectivity topology scores with the number of previous episodes. An advantage of this approach is that results are largely independent of confounding effects of current symptoms. A potential result might represent changed topology of intrinsic connectivity that is associated with the amount of episodes the patient has suffered from. However, for such type of result, it remains unclear whether observed changes somehow "stem from" brain changes that occur during an episode or in other words: whether specific intrinsic connectivity changes of an episode are relevant for the course of the disorder i.e. for depressive relapse. Therefore, we chose an alternative way to address our hypothesis: we investigated patients during a current episode and linked connectivity topology with episode numbers while controlling statistically for effects of current symptoms. This approach enabled us to identify episode-associated connectivity changes that are relevant for the course of the disorder and thereby to get some ideas about a potential pathophysiology relevant for relapse risk. However, by doing so, we are not able to decide whether such course-relevant changes are also present when patients are remitted. To overcome these limitations, future longitudinal studies in remitted and acute patients with recurrent major depression are necessary.

The current study focused on the relationship between aberrant functional

integration of intrinsic brain activity and the number of episodes in major depression. Previous studies investigating neural correlates of depressive relapse found a dependence of regional brain volume changes mainly in limbic areas on the course of major depression; in these studies, major depression course was represented by either the number of depressive episodes (Kronmuller *et al.*, 2009), the number of hospitalizations (Frodl *et al.*, 2008) or the estimated total duration of illness (MacQueen *et al.*, 2003). These findings implicated several consequences for the current study's design: (i) Due to the potential impact of structural changes on both major depression's course and functional connectivity in general (Lu *et al.*, 2011), we controlled for such structural effects on topological scores and their relationship with episodes; since topological scores are based on connectivity among the whole brain's grey matter, we used total grey matter volumes as corresponding covariate-of-no-interest. (ii) We focused on episode number for two reasons: the number of depressive episodes was found to be the best predictor for the episode recurrence risk in major depression (Hardeveld *et al.*, 2010); observed network topology changes in major depression refer to changes during episodes; both findings together suggest an interaction between the course of episodes and changed brain network topology, basically representing the objective of our study. (iii) Since the number of episodes was related to the total disease duration, we controlled for disease duration effects to specify our result with respect to depressive episodes and their number.

Spatial smoothing. In the current study we performed spatial smoothing during preprocessing of fMRI data. In graph-based brain network analysis, the application of spatial smoothing is extensively discussed. On the one hand, smoothing increases inter-voxel dependency of signals which may confound local connectivity strength

(especially when using small ROIs like voxel-based parcellation) (van den Heuvel *et al.*, 2008; Hayasaka and Laurienti, 2010); on the other hand, smoothing is an important step in fMRI data preprocessing to reduce the influence of spatial noise and misregistrations of anatomical neighbor regions during spatial normalization. Correspondent with this trade-off, several previous graph-based studies applied spatial smoothing (e.g. Lynall *et al.*, 2010; Liu *et al.*, 2013) while others did not (e.g. Achard *et al.*, 2006; Zhang *et al.*, 2011). When using spatial smoothing, the use of Gaussian kernels to smooth the data provided high reliability for topological scores (Guo *et al.*, 2012). Based on these data and the fact that brain atlas regions we used are rather large compared to voxel-wise resolution, we decided to apply spatial smoothing based on modest Gaussian kernel of 6mm, which was equal to the size of 2 voxels (Guo *et al.*, 2012).

Supplementary References:

Achard S, Salvador R, Whitcher B, Suckling J, Bullmore E. A resilient, low-frequency, small-world human brain functional network with highly connected association cortical hubs. The Journal of neuroscience : the official journal of the Society for Neuroscience. 2006;26(1):63-72.

Frodl T, Jager M, Born C, Ritter S, Kraft E, Zetzsche T, et al. Anterior cingulate cortex does not differ between patients with major depression and healthy controls, but relatively large anterior cingulate cortex predicts a good clinical course. Psychiatry research. 2008;163(1):76-83.

Guo CC, Kurth F, Zhou J, Mayer EA, Eickhoff SB, Kramer JH, et al. One-year test-retest reliability of intrinsic connectivity network fMRI in older adults. NeuroImage. 2012;61(4):1471-83.

Hayasaka S, Laurienti PJ. Comparison of characteristics between region-and voxel-based network analyses in resting-state fMRI data. NeuroImage. 2010;50(2):499-508.

Hardeveld F, Spijker J, De Graaf R, Nolen WA, Beekman AT. Prevalence and predictors of recurrence of major depressive disorder in the adult population. Acta psychiatrica Scandinavica. 2010;122(3):184-91.

Kronmuller KT, Schroder J, Kohler S, Gotz B, Victor D, Unger J, et al. Hippocampal volume in first episode and recurrent depression. Psychiatry research. 2009;174(1):62-6.

Liu Y, Yu C, Zhang X, Liu J, Duan Y, Alexander-Bloch AF, et al. Impaired Long Distance Functional Connectivity and Weighted Network Architecture in

Alzheimer's Disease. Cerebral cortex (New York, NY : 1991). 2013.
Lu J, Liu H, Zhang M, Wang D, Cao Y, Ma Q, et al. Focal pontine lesions provide evidence that intrinsic functional connectivity reflects polysynaptic anatomical pathways. The Journal of neuroscience : the official journal of the Society for Neuroscience. 2011;31(42):15065-71.
Lynall ME, Bassett DS, Kerwin R, McKenna PJ, Kitzbichler M, Muller U, et al. Functional connectivity and brain networks in schizophrenia. The Journal of neuroscience : the official journal of the Society for Neuroscience. 2010;30(28):9477-87.
MacQueen GM, Campbell S, McEwen BS, Macdonald K, Amano S, Joffe RT, et al. Course of illness, hippocampal function, and hippocampal volume in major depression. Proceedings of the National Academy of Sciences of the United States of America. 2003;100(3):1387-92.
Rubinov M, Sporns O. Complex network measures of brain connectivity: uses and interpretations. NeuroImage. 2010;52(3):1059-69.
Sorg C, Manoliu A, Neufang S, Myers N, Peters H, Schwerthoffer D, et al. Increased intrinsic brain activity in the striatum reflects symptom dimensions in schizophrenia. Schizophrenia bulletin. 2013;39(2):387-95.
van den Heuvel MP, Stam CJ, Boersma M, Hulshoff Pol HE. Small-world and scale-free organization of voxel-based resting-state functional connectivity in the human brain. NeuroImage. 2008;43(3):528-39.
Watts DJ, Strogatz SH. Collective dynamics of 'small-world' networks. Nature. 1998;393(6684):440-2.
Zhang J, Wang J, Wu Q, Kuang W, Huang X, He Y, et al. Disrupted brain connectivity networks in drug-naive, first-episode major depressive disorder. Biological psychiatry. 2011;70(4):334-42.

Supplementary Figures:

Figure S1. Distribution of number of episodes in patients with recurrent major depression.

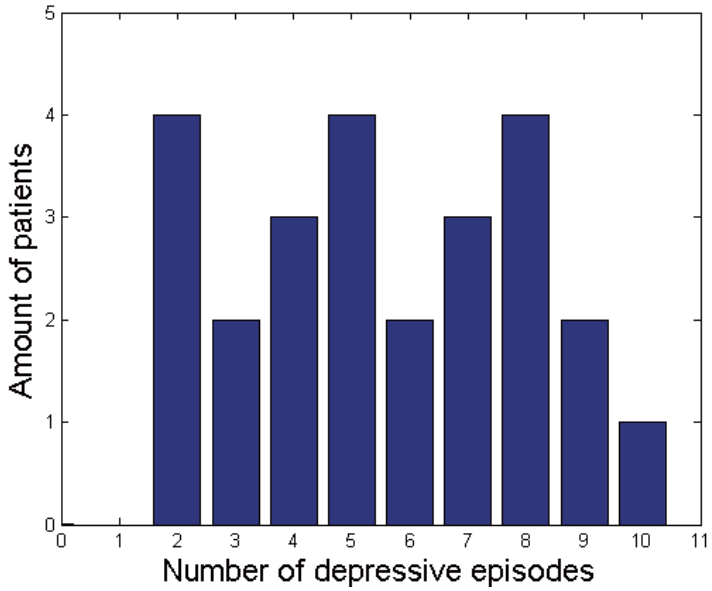

Figure S1. The bar plot reflects the frequency distribution of the number of depressive episodes across current study's patients of recurrent major depression. A bar represents the amount of patients (y-axis), who have suffered from a given number of depressive episodes.

Figure S2. Regional grey matter volume reduction in patients with recurrent major depression.

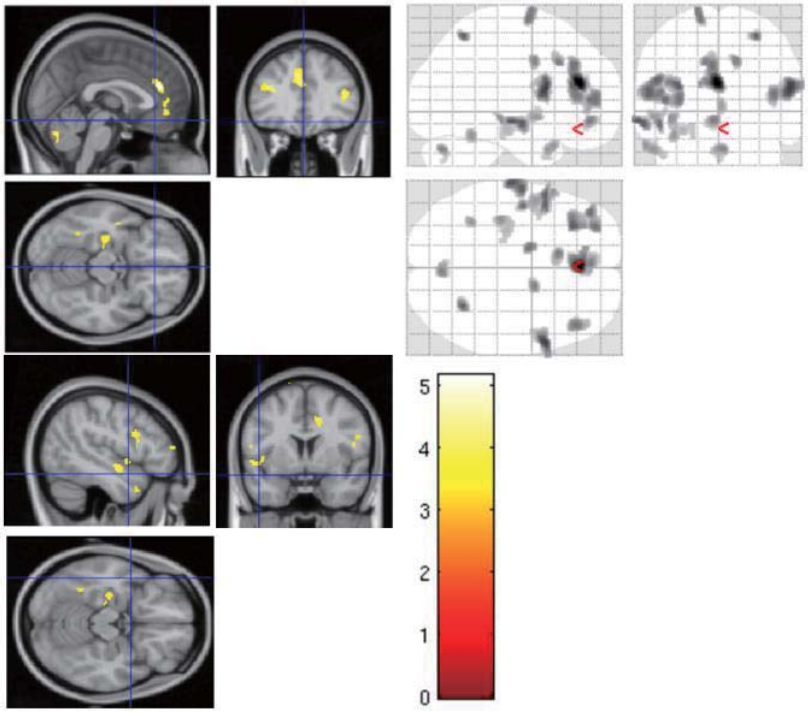

Figure S2. Colored brain regions showed significantly reduced voxel-based morphometry in patients with major depression (two-sample t-test, $p<0.001$, cluster extent threshold 50). For details see Tab. S2.

Supplementary Tables:

Table S1. Regions of Interest (ROIs) derived from Harvard-Oxford brain atlas

Index [a]	Brain regions	Index [a]	Brain regions [a]
1	Frontal Pole	29	Cingulate Gyrus, anterior division
2	Insular Cortex	30	Cingulate Gyrus, posterior division
3	Superior Frontal Gyrus	31	Precuneous Cortex
4	Middle Frontal Gyrus	32	Cuneal Cortex
5	Inferior Frontal Gyrus, pars triangularis	33	Frontal Orbital Cortex
6	Inferior Frontal Gyrus, pars opercularis	34	Parahippocampal Gyrus, anterior division
7	Precentral Gyrus	35	Parahippocampal Gyrus, posterior division
8	Temporal Pole	36	Lingual Gyrus
9	Superior Temporal Gyrus, anterior division	37	Temporal Fusiform Cortex, anterior division
10	Superior Temporal Gyrus, posterior division	38	Temporal Fusiform Cortex, posterior division
11	Middle Temporal Gyrus, anterior division	39	Temporal Occipital Fusiform Cortex
12	Middle Temporal Gyrus, posterior division	40	Occipital Fusiform Gyrus
13	Middle Temporal Gyrus, temporooccipital part	41	Frontal Operculum Cortex
14	Inferior Temporal Gyrus, anterior division	42	Central Opercular Cortex
15	Inferior Temporal Gyrus, posterior division	43	Parietal Operculum Cortex
16	Inferior Temporal Gyrus, temporooccipital part	44	Planum Polare
17	Postcentral Gyrus	45	Heschl's Gyrus (includes H1 and H2)
18	Superior Parietal Lobule	46	Planum Temporale
19	Supramarginal Gyrus, anterior division	47	Supracalcarine Cortex
20	Supramarginal Gyrus, posterior division	48	Occipital Pole
21	Angular Gyrus	49	Amygdala
22	Lateral Occipital Cortex, superior division	50	Hippocampus
23	Lateral Occipital Cortex, inferior division	51	Caudate
24	Intracalcarine Cortex	52	Putamen
25	Frontal Medial Cortex	53	Pallidum
26	Juxtapositional Lobule Cortex (formerly Supplementary Motor Cortex)	54	Thalamus
27	Subcallosal Cortex	55	N. accumbens
28	Paracingulate Gyrus	56	Brainstem

[a] The order of ROIs is consistent with Harvard-Oxford Atlas indices (HarvardOxford-cort-maxprob-thr25-2mm). Subcortical ROIs are added at the end. Left and right hemispheres have the same set of ROIs so that finally 112 ROIs were involved in this study.

Table S2. Regional VBM reduction in patients with recurrent major depression (refers to Fig. S1).

Lobe	L/R	Region	Cluster (voxel)	MNI coordinates (mm)			T value
				x	y	z	
Frontal	L	Superior Frontal Gyrus	110	-15	-1.5	73.5	4.124
	L	Middle Frontal Gyrus	781	-31.5	33	19.5	4.321
	L	Inferior Frontal Gyrus, Pars triangularis					
	L	Inferior Frontal Gyrus, Pars opercularis	430	-55.5	10.5	15	4.292
	L	Inferior Frontal Gyrus, Pars triangularis					
	R	Inferior Frontal Gyrus, Pars opercularis	548	57	10.5	18	4.561
	R	Precentral Gyrus					
	R	Rolandic Operculum					
	R	Inferior Frontal Gyrus, Pars triangularis	286	43.5	34.5	13.5	4.134
	R	Middle Frontal Gyrus					
	L	Medial Frontal Gyrus	663	-1.5	37.5	22.5	5.169
	L	Anterior Cingulate Gyrus					
	R	Anterior Cingulate Gyrus					
	R	Middle Cingulate Gyrus	100	13.5	1.5	39	4.03
	L	Medial Frontal Gyrus	137	-10.5	21	37.5	4.057
	L	Middle Cingulate Gyrus					
	L	Supplementary Motor Area					
	L	Medial Orbital Frontal Gyrus	277	-3	46.5	-7.5	4.102
	R	Anterior Cingulate Gyrus					
	L	Anterior Cingulate Gyrus					
Temporal	L	Superior Temporal Gyrus	278	-48	-7.5	-10.5	4.177
	L	Insula					
	L	Middle Temporal Gyrus	279	-64.5	-16.5	-7.5	4.38
	L	Middle Temporal Pole	176	-58.5	18	-27	3.826
	L	Fusiform Gyrus	75	-36	-49.5	-18	3.82
	L	Hippocampus	222	-37.5	-25.5	-6	3.858
Parietal	R	Superior Parietal Lobule	96	30	-55.5	58.5	4.286
	L/R	Cerebellar vermis	128	3	-72	-28.5	4.001

Group comparison: two-sample t-test, $p<0.001$, cluster extent 50.

Table S3. Small-worldness range for all subjects referring to different cost ranges

Cost range	0.05 – 0.50	0.05 – 0.14
HC	1.024543 - 4.691944	1.380449 - 4.691944
MDD	1.026928 - 5.784881	1.222477 - 5.784881

HC healthy controls; MDD major depressive disorder.

Manuscript 1

Aberrant microstructural white matter is associated with the number of episodes in major depression

Title page:

Title:

Aberrant microstructural white matter is associated with the number of episodes in major depression

Running title:

Altered white matter integrity in depression

Authors and Affiliations:

Chun Meng[1,5,6], Felix Brandl[1,5], Martin Scherr[2,7], Dirk Schwerthöffer[2], Josef Bäuml[2], Hans Förstl[2], Claus Zimmer[1], Afra M. Wohlschläger[1,4,5,6], Valentin Riedl[1,3,5], Christian Sorg[1,2,5]

Departments of [1]Neuroradiology, [2]Psychiatry, [3]Nuclear Medicine, [4]Neurology, [5]TUM-Neuroimaging Center of Klinikum rechts der Isar, Technische Universität München TUM, Ismaninger Strasse 22, 81675 Munich, Germany; [6]Graduate School of Systemic Neurosciences GSN, Ludwig-Maximilians-Universität, Biocenter, Großhaderner Strasse 2, 82152 Munich, Germany; [7]Department of Neurology, Christian Doppler Klinik, Paracelsus Medical University Salzburg, Ignaz-Harrer-Straße 79, 5020 Salzburg, Austria

Corresponding Author:

Christian Sorg, Department of Psychiatry and Neuroradiology, Klinikum rechts der Isar, Ismaninger Strasse 22, 81675 Munich, Germany, phone: +49 89 4140-7631, fax: -7665, c.sorg@lrz.tu-muenchen.de

Abstract:

The number of recurrent episodes in major depressive disorder (MDD) has been shown to be associated with a disrupted topology of striatum's whole-brain functional connectivity. This result suggests the re-organization of functional connectivity as factor of depressive relapse; however, little is known about the underlying structural basis. In this study we tested the hypothesis that white matter (WM) microstructure relates to the number of episodes in MDD.

We examined diffusion tensor imaging (DTI) correlates of WM structural connectivity in 24 patients with MDD (2 – 10 episodes) and 25 demographically similar healthy controls. Tract-based spatial statistics (TBSS) was applied to uncover voxel-level changes in fractional anisotropy (FA), and mean (MD), axial (AD) and radial (RD) diffusivity in major WM pathways in MDD patients compared with controls. Subsequently, for affected WM tracts and within MDD group, partial correlation analysis was employed to assess the relationships between WM alterations and the number of depressive episodes as well as symptom severity of current episode.

MDD group showed widespread significant FA reductions in corpus callosum, superior and inferior longitudinal fasciculus, inferior fronto-occipital fasciculus, cingulum and corticospinal tracts ($P < 0.05$, TFCE corrected). MDD group also showed similarly extensive patterns of increased MD and RD. Across MDD patients, partial correlation relationships were found between FA and the number of depressive episodes independent of depressive symptom severity of current episode in affected

WM tracts connecting frontal, occipital, and temporal cortices while other tracts demonstrated associations with symptom severity ($P < 0.005$, uncorrected).

Results provide first evidence that altered white matter connectivity is associated with the course of depressive episodes in MDD, independently of current symptoms. Our findings imply that differential re-organization of structural connectivity in fronto-occipital and fronto-temopral circuits may contribute to depressive relapse risk.

Key words:

Major depressive disorder, recurrent episodes, DTI, TBSS

Introduction:

Major depressive disorder (MDD) is one of the most frequent psychiatric disorders with a lifetime prevalence of about 16% (Kessler et al., 2003). MDD is characterized by single or recurrent major depressive episodes, which include depressed mood, reduced energy, impaired cognition, vegetative symptoms, and suicidal tendency with suicide rates of about 4% (American Psychiatric Association, 2000). In 35-85% of cases the course of major depression includes the recurrence of depressive episodes (Hardeveld et al., 2010; Lewis et al., 2010; Farb et al., 2011). However, detailed neurobiological pathway of the episode relapse remains poorly understood.

Over past decades, accumulative evidences of in-vivo imaging research in MDD have shown that depressive episodes are associated with altered brain structure and function regarding both gray and white matter ((Greicius et al., 2007; Erk et al., 2010; Sheline et al., 2010; Aizenstein et al., 2011; Korgaonkar et al., 2011; Lui et al., 2011; Li et al., 2012; Mwangi et al., 2012; Zeng et al., 2012; Grieve et al., 2013); for reviews (Savitz and Drevets, 2009; Murphy and Frodl, 2011; Hamilton et al., 2012; Whitfield-Gabrieli and Ford, 2012)). Particularly, depressive symptoms and durations are reported to associate with aberrant patterns of gray matter's functional connectivity (Zhang et al., 2011) and white matter's structural connectivity (Henderson et al., 2013). On the other hand, recent study has started to examine the link between aberrant functional brain network and the course of recurrent episodes (Meng et al., 2014). Besides sub-depressive residuals, the number of previous depressive episodes has strongest influence on the course of major depression

(Kendler et al., 2001; Hardeveld et al., 2010; Moylan et al., 2012). The number of episodes is suggested as one of the best predictors for the episode relapse risk in major depression (Hardeveld et al., 2010). Our prior work showed that striatal functional connectivity and network topology associated with the number of depressive episodes independent of symptom severity in recurrent MDD, which provide new insight into the specific mechanistic link between MDD-realted brain changes and relapsed risk of depressive episodes (Meng et al., 2014). However, it remains unclear about the structural basis underlying such mechanistic associations. To our best knowledge, no previous study has used Diffusion Tensor Imaging (DTI) to map the characteristic alterations of white matter tracts in relation to the course of MDD featured by the number of depressive episodes.

The goal of the present study was to map the white matter microstructural changes specifically linked with the course of depressive episdoes in MDD. Therefore, patients with recurrent major depression and healthy controls were assessed by DTI and Tract-Based Spatial Statistics (TBSS). White matter integrity scores were derived from the major white matter tracts, compared across groups, and related to the number of depressive episodes and current depressive symptoms by within-MDD-group partial correlation analysis.

Methods and Materials:

Subjects.

Twenty-four patients with recurrent major depression (mean age of 48.04 years; 11 males) and twenty-five healthy persons (mean age of 44.08 years; 11 males) were analyzed in this study (Table 1). One patient from the same cohort in our prior fMRI study dropped out of the DTI scan (Meng et al., 2014). All participants provided informed consent in accordance with the Human Research Committee guidelines of the Klinikum rechts der Isar, Technische Universität München. Patients were recruited from the Department of Psychiatry, healthy controls from the area of Munich by word-of-mouth advertising. Participants' examination included medical history, psychiatric interview, and psychometric assessment. Psychiatric diagnoses were based on DSM-IV (American Psychiatric Association, 2000). The Structured Clinical Interview for DSM-IV (SCID) was used to assess the presence of psychiatric diagnoses (Spitzer et al., 1992). Severity of clinical symptoms was measured with the Hamilton Rating Scale for Depression (HAM-D) (Hamilton, 1960). The global level of social, occupational, and psychological functioning was measured with the Global Assessment of Functioning Scale (Spitzer et al., 1992). Psychiatrists D.S. and M.S. performed clinical-psychometric assessment; they have been professionally trained for SCID interviews with inter-rater reliability for diagnoses and scores of more than 95%.

Recurrent major depression was the primary diagnosis for all patients. Patients with recurrent major depression constitute a heterogeneous clinical group, varying in

severity of current symptoms, age of disorder onset, duration of the disorder, number of depressive episodes, family history of major depression, co-morbidity of other disorders, and type of medication. Since the goal of the present study was to determine the relationship between the topology of the brain's functional connectivity network and the course of major depression common to most patients with recurrent major depression, we adopted selection criteria from a prior work on recurrent major depression in order to obtain a clinically representative patient sample (Hennings et al., 2009). Recurrence implies the return of an entirely new episode after clinical recovery. Due to the unreliable self-report in major depression because of patients' potential memory problems, the determination of episode number was based on the review of patients' medical records. Only patients whose records enabled us to determine a consistent episode number were included in the study. The number of episodes of all patients ranged from two to ten following a continuous distribution. All patients met criteria for a current depressive episode with an average episode length of 16.5 weeks (SD 6.8) and an averaged HAM-D score of 22.3 (SD 7.2). The average age of major depression onset was 32.1 years (SD 13.9). The average duration of major depression was 16.0 years (SD 9.7) and on average, patients had experienced 5-6 episodes (mean 5.5, SD 2.5). Four patients had a positive family history of major depression. Fourteen patients had psychiatric co-morbidities: six generalized anxiety disorder, three somatization disorder, and five avoidant or dependent personality disorders. Patients with psychotic symptoms, schizophrenia, schizoaffective disorder, bipolar disorder, and substance abuse were already excluded

from this study. Additional exclusion criteria were pregnancy, neurological or severe internal systemic diseases, and general contraindications for MRI.

Data acquisition and preprocessing.

Whole brain T1-weighted MRI and DTI data were acquired on a 3 T MR scanner (Achieva, Philips, Netherland) using an 8-channel phased-array head coil. Diffusion images were acquired using a single-shot spin-echo echo-planar imaging sequence, resulting in one non-diffusion weighted image (b = 0 s/mm2) and 15 diffusion weighted images (b = 800 s/mm2, 15 non-colinear gradient directions) covering whole brain with: echo time (TE) = 60 ms, repetition time (TR) = 6516 ms, flip angle = 90°, field of view = 224 x 224 mm², matrix = 128 x 128, 75 transverse slices, slice thickness = 2 mm, and 0 mm interslice gap, voxel size = 1.75 x 1.75 x 2 mm^3. A whole-head, high-resolution T1-weighted image was acquired using a magnetization-prepared rapid acquisition gradient echo sequence following parameters: echo time (TE) = 4 ms, repetition time (TR) = 9 ms, flip angle = 5°, field of view = 240 x 240 mm², matrix = 240 x 240, 170 sagittal slices, slice thickness = 1 mm, and 0 mm interslice gap, voxel size = 1 x 1 x 1 mm^3. All acquired MRI images were visually inspected for excessive head motion, apparent or aberrant artifacts and excluding subjects with poor data quality.

White matter tract-based spatial statistics (TBSS)

DTI data was preprocessed using FSL's FDT toolbox (http://fsl.fmrib.ox.ac.uk/fsl/fslwiki/FDT, Version 5.0.3). First, brain mask was generated by removing skull and non-brain tissue to extract only brain tissues. Eddy-current distortion and head motion were corrected by aligning all diffusion-weighted images to reference image (b0). Secondly, diffusion tensors were estimated in each voxel of the whole brain, which models the

distribution of the water molecule diffusion. Based on diffusion tensor model, fractional anisotropy (FA), and mean (MD), axial (AD), and radial (RD) diffusivity were computed, as the surrogate measure for white matter microstructural features. Thirdly, Tract-Based Spatial Statistics (Smith et al., 2006), was carried out for voxelwise statistical analysis of white matter microstructure following: (i) nonlinear alignment of each participant's FA image to the standard Montreal Neurological Institute (MNI152) space template; (ii) calculation of the mean of all aligned FA images; (iii) generation of the across-all mean FA skeleton which represents centers of white matter tracts common to all subjects, considered as the group-specific template; (iv) projection of each subject's aligned FA image onto the mean FA skeleton using the threshold (FA > 0.2), to obtain individual maps. Individual mean, axial, and radial diffusivity (MD, AD, and RD) maps were further obtained by using the same mean FA skeleton and *tbss_non_FA* script. Over whole brain white matter, the general linear model and nonparametric inference (5000 random permutations) was adopted to perform statistical analyses on FA as well as MD, AD, and RD between different participant groups by using FSL's *randomize* script (http://fsl.fmrib.ox.ac.uk/fsl/fslwiki/randomise/) (Anderson and Robinson, 2001). By using contrast setting, covariate effects of age and sex were ruled out from group comparisons based on the permutation test. The statistical threshold was set as $P_{FWE} < 0.05$ with multiple comparison correction by threshold-free cluster enhancement (TFCE) (Smith and Nichols, 2009). In addition to group-generated white matter skeleton mask, FSL's standard FA skeleton was employed in validation analysis of between-group differences.

Gray matter voxel-based morphometry (VBM)

As described recently (Meng et al., 2014), we used the VBM8 toolbox

(http://dbm.neuro.uni-jena.de/vbm.html) to analyze brain structure via voxel-based morphometry. T1-weighted images were corrected for bias-field inhomogeneity, registered using linear (12-parameter affine) and nonlinear transformations, and tissue-classified into gray matter, white matter, and cerebrospinal fluid within the same generative model. The segmented and normalized images were modulated to account for structural changes resulting from the normalization process, indicating gray matter volume. Here, we only considered non-linear changes so that further analyses did not have to account for differences in head size. Finally images were smoothed with a Gaussian kernel of 8mm (FWHM).

Correlation analysis

Within MDD group, linear relationships between white matter FA values and variables of interest were investigated in affected white matter tracts of reduced FA, including: (i) the course of recurrent episodes in MDD, indexed by the number of depressive episodes; (ii) the symptom severity of current depressive episode, indexed by HAM-D. To test the specific association with variables of interest independent of each other, partial correlation was utilized. For example, for associations between FA and the number of depressive episodes, the HAM-D score was controlled as the covariate of no interest.

Firstly we adopted voxelwise permutation-based correlation analysis by using the same approach as for group comparisons based on white matter tract skeleton ($P_{FWE} < 0.05$, TFCE corrected). Secondly, we carried out ROI analysis by using 20 anatomically defined tracts according to JHU white matter atlas. Mean FA value of each tract was derived for each patient and correlated with one of variables of interest independent of another one ($P < 0.05$, Bonferroni

correction). Finally we examined the result based on threshold ($P_{uncorred} < 0.005$, with cluster size > 20 voxels).

Results:

Widely distributed changes of WM integrity in MDD patients.

To investigate group differences of white matter integrity between MDD and control groups, major white matter tracts were identified by TBSS analysis, providing a consistent whole brain WM skeleton of 134,152 voxels across all subjects. In this skeleton, MDD patients showed significant extensive FA reduction ($P_{FWE} < 0.05$, TFCE corrected), which included: (1) association tracts such as bilateral superior and inferior longitudinal, inferior fronto-occipital, uncinate fasciculi and cingulum tracts; (2) projection fibers encompassing right corticospinal tracts and bilateral anterior thalamic radiations; (3) commissural fibers including the genu, body and splenium of the corpus callosum (Table 2 and Figure 1). For MD and RD, overlapped and even larger patterns of affected tracts were found with significant increases in MDD group. For AD, no significant group difference was identified (Figure S1).

Depressive symptoms and episodes were differentially associated with affected white matter tracts.

To investigate the relationship between white matter integrity, recurrent episodes, and depressive symptoms, we applied partial correlation analysis of corresponding scores (e.g. FA, number of episodes, HAM-D). To note, HAM-D and the number of depressive episodes were not correlated ($r = 0.041$, $p = 0.844$). In MDD group,

reduced FA was found negatively associated with number of episodes independent of HAM-D in left inferior fronto-occipital fasciculus and right temporal tract ($P < 0.005$, cluster extent > 20 voxels; Table 3 and Figure 2). Furthermore, reduced FA was associated with HAM-D independent of number of episodes, including positive correlation in right anterior thalamic radiation and negative correlation in right temporal tract (Table 3 and Figure 3).

Discussion:

To analyze how white matter integrity is linked with the course of depressive episodes in major depression, we applied DTI and TBSS in patients with recurrent major depression and healthy controls. We found significant FA reductions and MD/RD increases in widespread white matter tracts in MDD group. No significant association was identified between white matter alterations and patients' number of depressive episodes or current depressive symptoms. However, it was hinted at the liberal threshold that FA in affected frontal, occipital, and temporal tracts was linked with patients' number of depressive episodes independent of current depressive symptoms. Our findings suggest potential structural basis linked with depressive relapse risk in major depression.

White matter changes in MDD consistent with other reports

In this study, TBSS was employed to investigate tract-based microstructural changes in MDD compared to healthy controls (Figure 1). Significant FA reductions were identified at the threshold of $P < 0.05$ with TFCE-based multiple comparison correction, referring to corpus callosum and

white matter tracts connecting frontal, parietal, temporal, occipital and limbic regions. These findings were in line with previously reported reduced FA over WM regions associated with the limbic system, prefrontal cortex, thalamic projection fibers, corpus callosum, and other association fibers (Korgaonkar et al., 2011; Henderson et al., 2013). The smaller FA was robustly reported across affective disorders with most reproducible abnormalities in frontal and temporal regions (Sexton et al., 2009). Earlier postmortem studies showed pathological white matter in prefrontal region like decreased oligodendrocyte density and so on (Tham et al., 2011). The frontal-limbic system is critical in affective processing and emotion regulation, which is disrupted underpinning dysfunctional brain in MDD (Clark et al., 2009). Moreover, previous studies using meta-analysis of MDD abnormalities showed smaller FA in the superior longitudinal fasciculus which connects frontal, temporal and parietal regions as well as occipital regions (Murphy and Frodl, 2011; Liao et al., 2013). In addition, other imaging approaches also demonstrated widespread regional changes of gray matter and hyper/hypo-functional connectivity in MDD (Drevets et al., 2008; Lorenzetti et al., 2009).

Despite FA reduction we found significantly increased MD and RD but unchanged AD in MDD by TBSS analysis. The animal models of axonal disease have shown that an increase in RD is sensitive to demyelination (Song et al., 2002). Taken together, in the majority of affected white matter tracts with FA reductions, largely overlapped patterns with increased MD and RD were identified (Table S2). Our data suggest possibly decreased myelination or other degeneration change in extensive white matter tracts in MDD, which is consistent with other reports (Korgaonkar et al., 2011; Mettenburg et al., 2012; Hemanth Kumar et al., 2014).

Associations with number of depressive episodes and HAM-D

Within MDD group, we tested the partial correlations of FA in affected WM tracts with number of depressive episodes and symptom severity of current episode indexed by HAM-D, resulting in no significant results using $P_{TFCE} < 0.05$. The liberal threshold was used to explore potential trend. For patients with recurrent depressive episodes, negative associations ($P_{uncorr} < 0.005$ and cluster extent > 20 voxels) were identified between FA and number of depressive episodes independent of HAM-D in left inferior fronto-occipital fasciculus and right temporal tract (Table 3 and Figure 2). Previously we found in MDD that right striatal functional network topology linked with number of depressive episodes independent of HAM-D (Meng et al., 2014). The subcortical regions like striatum and thalamus constitute a loop with cortical layers to support higher-order function like cognitive and emotional processing which is impaired in MDD (Hamilton et al., 2012). Current findings on WM tracts might imply potential structural basis for the association between disrupted functional network and disorder course of recurrent MDD however the interpretation must be careful due to the weak statistical significance and effect size. As for the partial correlation between FA in affected WM tracts and HAM-D independent of number of depressive episodes, positive association ($P_{uncorr} < 0.005$ and cluster extent > 20 voxels) was identified in right anterior thalamic radiation and negative association in right temporal tract (Table 3 and Figure 3). The anterior thalamic radiation forms thalamic-cortical connections and links to prefrontal lobe, which is dysfunctional in MDD, and probably links with disrupted frontal-limbic-thalamic circuit (Lui et al., 2011). Previous study reported that white matter abnormalities linked with illness severity in MDD (Cole et al., 2012; Henderson et al.,

2013; de Diego-Adelino et al., 2014). Interestingly, our prior work based on the same cohort and resting-state functional connectivity found significant association between HAM-D and network centrality in inferior frontal gyrus and supermarginal gyrus in right hemisphere, which supported current findings in underlying right anterior thalamic radiation and temporal tract (Meng et al., 2014).

Conclusion.

The extensive microstructural WM FA reductions and RD increases are present in recurrent MDD, supporting prior hypothesis of WM demyelination underlying dysfunctional brain in MDD. No significant associations of white matter changes were identified with the course of depressive episodes and current symptoms despite some hints for potential trend of associations.

Acknowledgements:

This work was supported by the Chinese Scholar Council (CSC), File No: 2010604026 (C.M.), the German Federal Ministry of Education and Research (BMBF 01EV0710 to A.M.W., BMBF 01ER0803 to C.S.) and the Kommission für Klinische Forschung, Technische Universität München (KKF 8765162 to C.S). We are grateful to the participants of the study and the staff of the Department of Psychiatry and Neuroradiology for their help in recruitment and data collection.

Financial Disclosures

All authors report no biomedical financial interests or potential conflicts of interest.

References:

Aizenstein HJ, Andreescu C, Edelman KL, Cochran JL, Price J, Butters MA, Karp J, Patel M, Reynolds CF, 3rd (2011) fMRI correlates of white matter hyperintensities in late-life depression. The American journal of psychiatry 168:1075-1082.

American Psychiatric Association (2000) Diagnostic and statistical manual of mental disorders, Ed 4, text revision. Washington, DC: American Psychiatric Association.

Anderson MJ, Robinson J (2001) Permutation tests for linear models. Australian & New Zealand Journal of Statistics 43:75-88.

Clark L, Chamberlain SR, Sahakian BJ (2009) Neurocognitive mechanisms in depression: implications for treatment. Annual review of neuroscience 32:57-74.

Cole J, Chaddock CA, Farmer AE, Aitchison KJ, Simmons A, McGuffin P, Fu CH (2012) White matter abnormalities and illness severity in major depressive disorder. The British journal of psychiatry : the journal of mental science 201:33-39.

de Diego-Adelino J, Pires P, Gomez-Anson B, Serra-Blasco M, Vives-Gilabert Y, Puigdemont D, Martin-Blanco A, Alvarez E, Perez V, Portella MJ (2014) Microstructural white-matter abnormalities associated with treatment resistance, severity and duration of illness in major depression. Psychological medicine 44:1171-1182.

Drevets WC, Price JL, Furey ML (2008) Brain structural and functional abnormalities in mood disorders: implications for neurocircuitry models of depression. Brain structure & function 213:93-118.

Erk S, Mikschl A, Stier S, Ciaramidaro A, Gapp V, Weber B, Walter H (2010) Acute and sustained effects of cognitive emotion regulation in major depression. The Journal of neuroscience : the official journal of the Society for Neuroscience 30:15726-15734.

Farb NA, Anderson AK, Bloch RT, Segal ZV (2011) Mood-linked responses in medial prefrontal cortex predict relapse in patients with recurrent unipolar depression. Biological psychiatry 70:366-372.

Greicius MD, Flores BH, Menon V, Glover GH, Solvason HB, Kenna H, Reiss AL, Schatzberg AF (2007) Resting-state functional connectivity in major depression: abnormally increased contributions from subgenual cingulate cortex and thalamus. Biological psychiatry 62:429-437.

Grieve SM, Korgaonkar MS, Koslow SH, Gordon E, Williams LM (2013) Widespread reductions in gray matter volume in depression. NeuroImage Clinical 3:332-339.

Hamilton JP, Etkin A, Furman DJ, Lemus MG, Johnson RF, Gotlib IH (2012) Functional neuroimaging of major depressive disorder: a meta-analysis and new integration of base line activation and neural response data. The

American journal of psychiatry 169:693-703.
Hamilton M (1960) A rating scale for depression. Journal of neurology, neurosurgery, and psychiatry 23:56-62.
Hardeveld F, Spijker J, De Graaf R, Nolen WA, Beekman AT (2010) Prevalence and predictors of recurrence of major depressive disorder in the adult population. Acta psychiatrica Scandinavica 122:184-191.
Hemanth Kumar BS, Mishra SK, Trivedi R, Singh S, Rana P, Khushu S (2014) Demyelinating evidences in CMS rat model of depression: A DTI study at 7T. Neuroscience 275:12-21.
Henderson SE, Johnson AR, Vallejo AI, Katz L, Wong E, Gabbay V (2013) A preliminary study of white matter in adolescent depression: relationships with illness severity, anhedonia, and irritability. Frontiers in psychiatry 4:152.
Hennings JM et al. (2009) Clinical characteristics and treatment outcome in a representative sample of depressed inpatients - findings from the Munich Antidepressant Response Signature (MARS) project. Journal of psychiatric research 43:215-229.
Kendler KS, Thornton LM, Gardner CO (2001) Genetic risk, number of previous depressive episodes, and stressful life events in predicting onset of major depression. The American journal of psychiatry 158:582-586.
Kessler RC, Berglund P, Demler O, Jin R, Koretz D, Merikangas KR, Rush AJ, Walters EE, Wang PS (2003) The epidemiology of major depressive disorder: results from the National Comorbidity Survey Replication (NCS-R). JAMA : the journal of the American Medical Association 289:3095-3105.
Korgaonkar MS, Grieve SM, Koslow SH, Gabrieli JD, Gordon E, Williams LM (2011) Loss of white matter integrity in major depressive disorder: evidence using tract-based spatial statistical analysis of diffusion tensor imaging. Human brain mapping 32:2161-2171.
Lewis CM et al. (2010) Genome-wide association study of major recurrent depression in the U.K. population. The American journal of psychiatry 167:949-957.
Li B, Liu L, Friston KJ, Shen H, Wang L, Zeng LL, Hu D (2012) A Treatment-Resistant Default Mode Subnetwork in Major Depression. Biological psychiatry.
Liao Y, Huang X, Wu Q, Yang C, Kuang W, Du M, Lui S, Yue Q, Chan RC, Kemp GJ, Gong Q (2013) Is depression a disconnection syndrome? Meta-analysis of diffusion tensor imaging studies in patients with MDD. Journal of psychiatry & neuroscience : JPN 38:49-56.
Lorenzetti V, Allen NB, Fornito A, Yucel M (2009) Structural brain abnormalities in major depressive disorder: a selective review of recent MRI studies. Journal of affective disorders 117:1-17.
Lui S, Wu Q, Qiu L, Yang X, Kuang W, Chan RC, Huang X, Kemp GJ, Mechelli A, Gong Q (2011) Resting-state functional connectivity in treatment-resistant

depression. The American journal of psychiatry 168:642-648.
Meng C, Brandl F, Tahmasian M, Shao J, Manoliu A, Scherr M, Schwerthoffer D, Bauml J, Forstl H, Zimmer C, Wohlschlager AM, Riedl V, Sorg C (2014) Aberrant topology of striatum's connectivity is associated with the number of episodes in depression. Brain : a journal of neurology 137:598-609.
Mettenburg JM, Benzinger TL, Shimony JS, Snyder AZ, Sheline YI (2012) Diminished performance on neuropsychological testing in late life depression is correlated with microstructural white matter abnormalities. NeuroImage 60:2182-2190.
Moylan S, Maes M, Wray NR, Berk M (2012) The neuroprogressive nature of major depressive disorder: pathways to disease evolution and resistance, and therapeutic implications. Molecular psychiatry.
Murphy ML, Frodl T (2011) Meta-analysis of diffusion tensor imaging studies shows altered fractional anisotropy occurring in distinct brain areas in association with depression. Biology of mood & anxiety disorders 1:3.
Mwangi B, Ebmeier KP, Matthews K, Steele JD (2012) Multi-centre diagnostic classification of individual structural neuroimaging scans from patients with major depressive disorder. Brain : a journal of neurology 135:1508-1521.
Savitz J, Drevets WC (2009) Bipolar and major depressive disorder: neuroimaging the developmental-degenerative divide. Neuroscience and biobehavioral reviews 33:699-771.
Sexton CE, Mackay CE, Ebmeier KP (2009) A systematic review of diffusion tensor imaging studies in affective disorders. Biological psychiatry 66:814-823.
Sheline YI, Price JL, Yan Z, Mintun MA (2010) Resting-state functional MRI in depression unmasks increased connectivity between networks via the dorsal nexus. Proceedings of the National Academy of Sciences of the United States of America 107:11020-11025.
Smith SM, Nichols TE (2009) Threshold-free cluster enhancement: addressing problems of smoothing, threshold dependence and localisation in cluster inference. NeuroImage 44:83-98.
Smith SM, Jenkinson M, Johansen-Berg H, Rueckert D, Nichols TE, Mackay CE, Watkins KE, Ciccarelli O, Cader MZ, Matthews PM, Behrens TE (2006) Tract-based spatial statistics: voxelwise analysis of multi-subject diffusion data. NeuroImage 31:1487-1505.
Song SK, Sun SW, Ramsbottom MJ, Chang C, Russell J, Cross AH (2002) Dysmyelination revealed through MRI as increased radial (but unchanged axial) diffusion of water. NeuroImage 17:1429-1436.
Spitzer RL, Williams JB, Gibbon M, First MB (1992) The Structured Clinical Interview for DSM-III-R (SCID). I: History, rationale, and description. Archives of general psychiatry 49:624-629.
Tham MW, Woon PS, Sum MY, Lee TS, Sim K (2011) White matter abnormalities

in major depression: evidence from post-mortem, neuroimaging and genetic studies. Journal of affective disorders 132:26-36.

Whitfield-Gabrieli S, Ford JM (2012) Default mode network activity and connectivity in psychopathology. Annual review of clinical psychology 8:49-76.

Zeng LL, Shen H, Liu L, Wang L, Li B, Fang P, Zhou Z, Li Y, Hu D (2012) Identifying major depression using whole-brain functional connectivity: a multivariate pattern analysis. Brain : a journal of neurology 135:1498-1507.

Zhang J, Wang J, Wu Q, Kuang W, Huang X, He Y, Gong Q (2011) Disrupted brain connectivity networks in drug-naive, first-episode major depressive disorder. Biological psychiatry 70:334-342.

Tables:

Table 1. Demographic and clinical data

Characteristic	**MDD group N = 24**	**Control group N = 25**	***P* value**
Age [year]	48.04 (14.70)	44.08 (14.78)	0.352
Sex, female/male	13/11	14/11	0.897
Number of episodes	5.46 (2.47)	NA	
Duration of major depression [years]	15.96 (9.68)	NA	
Age at onset [year]	32.08 (13.90)	NA	
Current episode			
HAM-D	22.29 (7.16)	0	< 0.001*
GAF	49.33 (10.49)	99.5 (1.1)	< 0.001*
Duration [weeks]	16.54 (6.76)	NA	
Current medication			
Number of medications	1.75 (0.74)	NA	
Types, 1/2/3/4	10/10/4/0	NA	
SSRI/SNRI/NL/Alpha-2	17/7/5/13	NA	

Group comparisons: two-sample t-tests for age, HAM-D, GAF; χ^2-test for sex. Data are presented as mean and standard deviation like mean (SD). MDD Major Depressive Disorder; HAM-D Hamilton Rating Scale for Depression; GAF Global Assessment of Functioning; SSRI Selective serotonin reuptake inhibitor; SNRI Serotonin-norepinephrine reuptake inhibitor; NL neuroleptics; alpha-2 alpha-2 receptor modulator
*Data shown indicate statistical significance ($P < 0.05$)

Table S1 Overall volumetric results revealed by VBM

Measures	**MDD group N = 24**	**Control group N = 25**	***P* value**
TIV (mm3)	1448.69 (124.88)	1398.25 (142.21)	0.194
GMV/TIV	0.44 (0.02)	0.46 (0.02)	0.001*
WMV/TIV	0.37 (0.02)	0.37 (0.02)	0.201
CSFV/TIV	0.19 (0.03)	0.18 (0.02)	0.055

Age and sex were included as covariates for comparisons of whole brain volume and GM, WM, and CSF percentage. MDD Major Depressive Disorder; GM gray matter; WM white matter; CSF cerebrospinal fluid.
*Data shown indicate statistical significance ($P < 0.05$)

Table S2 Overall skeleton-based results revealed by TBSS

Measures	Voxels
Group-generated skeleton	134152
Standard skeleton	137832
Reduced FA in MDD	18545
Increased MD in MDD	42981
Increased RD in MDD	42090
Overlap of results	
FA and MD overlap	11237
FA and RD overlap	16189
RD and MD overlap	31017
All 3 overlap	11196

Table 2. TBSS results: reduced FA, increased MD and RD in MDD

JHU-atlas-defined white matter tracts[a]	FA		MD		RD	
	Voxels (%)[b]	Mean probabilities[c]	Voxels (%)[b]	Mean probabilities[c]	Voxels (%)[b]	Mean probabilities[c]
Anterior thalamic radiation L	1.360	0.724	1.350	0.695	1.450	0.731
Anterior thalamic radiation R	0.440	0.155	0.910	0.441	0.340	0.130
Corticospinal tract L			1.170	0.452	0.970	0.387
Corticospinal tract R	0.870	0.407	0.680	0.290	0.550	0.248
Cingulum (cingulate gyrus) L	0.070	0.021	0.160	0.058	0.020	0.006
Cingulum (cingulate gyrus) R	0.020	0.005	0.080	0.025	0.240	0.082
Cingulum (hippocampus) L					0.010	0.003
Cingulum (hippocampus) R						
Forceps major	0.390	0.132	0.970	0.313	0.950	0.306
Forceps minor	11.300	6.297	5.580	3.015	5.990	3.288
Inferior fronto-occipital fasciculus L	2.340	0.871	2.430	0.908	2.480	0.915
Inferior fronto-occipital fasciculus R	4.260	1.630	2.350	0.891	2.820	1.067
Inferior longitudinal fasciculus L	1.530	0.535	2.800	1.095	2.440	0.946
Inferior longitudinal fasciculus R	3.120	1.254	1.020	0.394	1.670	0.657
Superior longitudinal fasciculus L	2.600	1.439	2.430	1.206	1.870	0.965
Superior longitudinal fasciculus R	1.960	0.978	0.830	0.334	1.050	0.469
Uncinate fasciculus L	0.110	0.033	0.290	0.112	0.280	0.107
Uncinate fasciculus R	0.490	0.173	0.270	0.087	0.310	0.104

Superior longitudinal fasciculus (temporal part) L	1.450	0.565	1.040	0.386	0.930	0.361
Superior longitudinal fasciculus (temporal part) R	0.830	0.299	0.250	0.082	0.480	0.163

Group comparison of skeletonized white matter measures was carried out by nonparametric t-test (5000 permutations) using randomize in FSL, with age and sex as covariates of no interest. Statistical significance was set at $P < 0.05$, FWE (familywise error rate) corrected, by using threshold-free cluster enhancement (TFCE). Resulted group difference map was converted to binary mask in order to locate and identify white matter tracts in the result mask by using atlasquery in FSL. MDD Major Depressive Disorder; FA: fractional anisotropy; MD: mean diffusivity; RD: radial diffusivity.

[a]White matter tracts according to JHU white matter tractography atlas.

[b]Percentage of voxels of the considered tract within the result mask.

[c]Mean probabilities of the considered tract within the result mask.

L/R: left/right.

Table 3. Correspondences with HAM-D and number of episodes in MDD

White matter tracts	Side	Cluster size (voxel)	MNI coordinates of peak voxel (mm)			r	*p*
			X	Y	Z		
Association between FA and number of episodes							
Inferior fronto-occipital fasciculus	L	20	-34	-80	21	-0.821	< 0.001
Superior longitudinal fasciculus (temporal part)	R	12	50	-25	-25		
Association between FA and depressive symptom							
Anterior thalamic radiation	R	38	22	7	18	0.680	< 0.001
		25	19	20	0		
Superior longitudinal fasciculus (temporal part)	R	21	35	-19	-27	- 0.705	< 0.001

The relationships between white matter FA and number of episodes as well as depressive symptom indexed by HAM-D was evaluated by nonparametric t-test (5000 permutations) using randomize in FSL. Positive and negative correlations between FA and number of episodes independently of HAM-D, and between FA and HAM-D independently of number of episodes, were identified (voxelwise $P_{uncorr} < 0.005$, cluster size > 10 voxels). Overall correlation coefficients and p values of mean FA values of resulting clusters were reported. White matter tracts of resulting clusters were reported according to JHU white matter tractography atlas. L/R: left/right; MDD Major Depressive Disorder; FA: fractional anisotropy; HAM-D Hamilton Rating Scale for Depression.

Figure Legends:

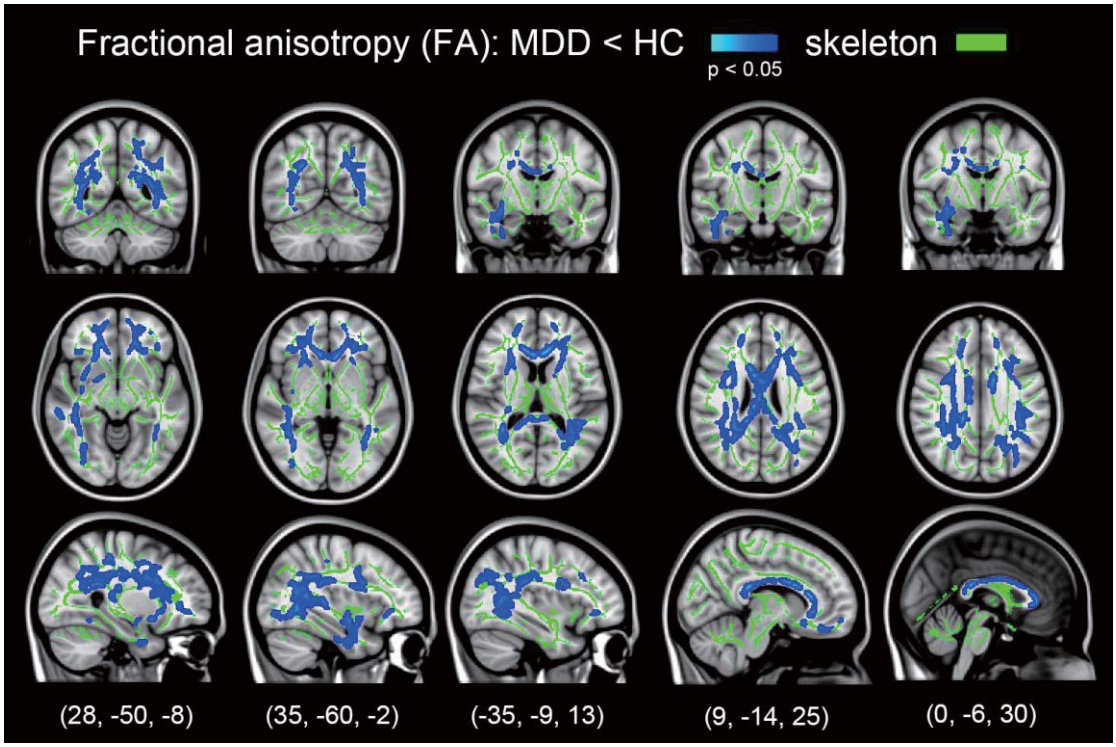

Figure 1. Whole brain white matter changes in MDD. Coronal, axial, and sagittal views illustrated significant group difference of white matter fractional anisotropy (FA) between MDD and control groups, superimposed on the T1-weighted brain image of MNI152 structural standard template and group-generated white matter skeleton. Green color indicated the common skeleton over MDD and control groups. Blue color indicated reduced FA in MDD (permutation test, $P < 0.05$, FWE corrected). Significant between-group difference was displayed using the *tbss_fill* script, which dilates resulted clusters in the white matter skeleton for better visualization. MNI coordinates were provided at the bottom.

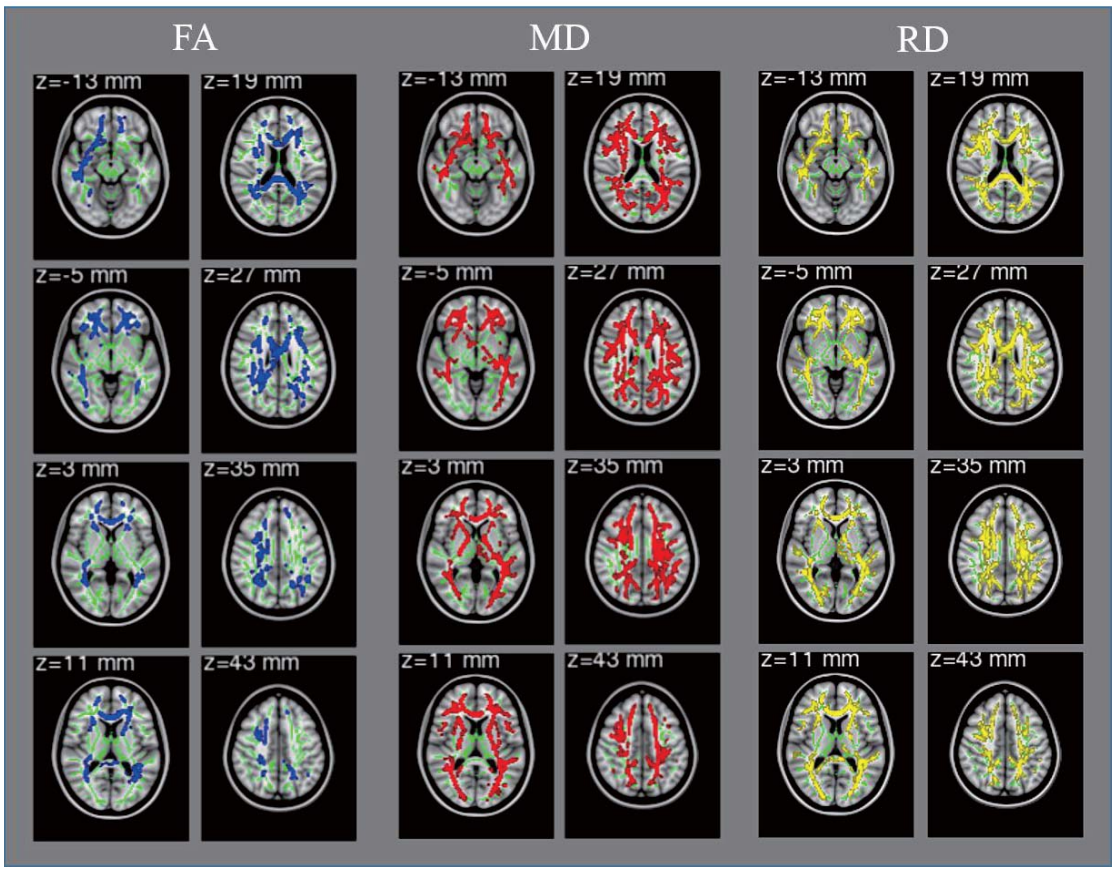

Figure S1. Whole brain white matter changes in MDD. Axial views illustrated significantly reduced fractional anisotropy (FA, colored by blue), increased mean diffusivity (MD, colored by red), and increased radial diffusivity (RD, colored by yellow) in MDD patients (permutation test, $P < 0.05$, FWE corrected). The affected tracts were superimposed on the T1-weighted brain image of MNI152 structural standard template and group-generated white matter skeleton (colored by green). The affected tracts were displayed using the *tbss_fill* script, which dilates resulted clusters in the white matter skeleton for better visualization.

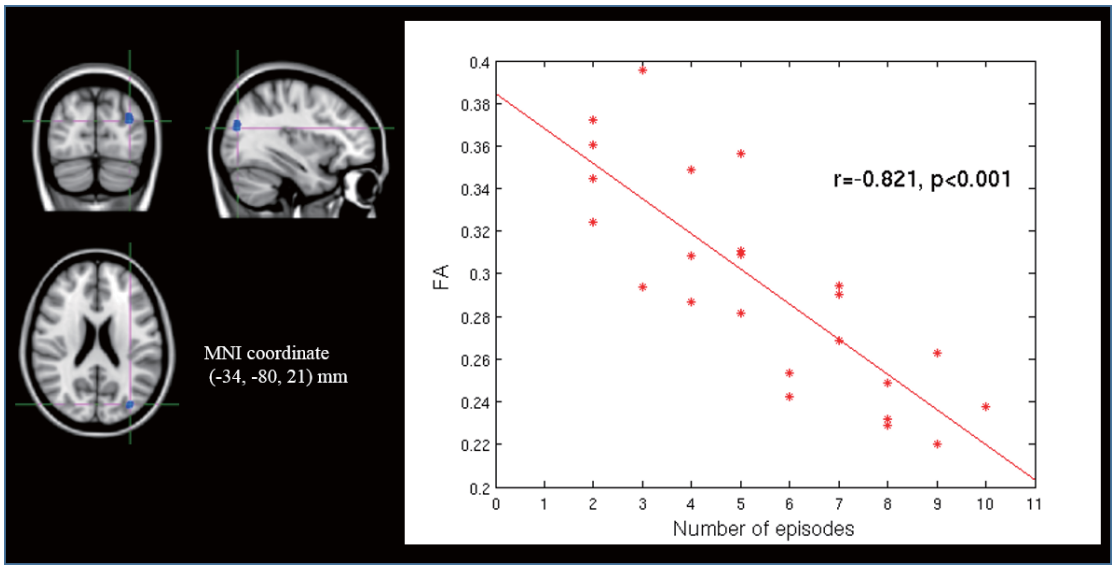

Figure 2. Correspondence between affected white matter and number of episodes in MDD patients. In the left panel, coronal, axial, and sagittal views illustrated significant negative correlation between FA and number of episodes, independently of HAM-D, within MDD group. In the right panel for visualization, number of episodes and averaged FA of related white matter tracts were illustrated in the scatter plot.

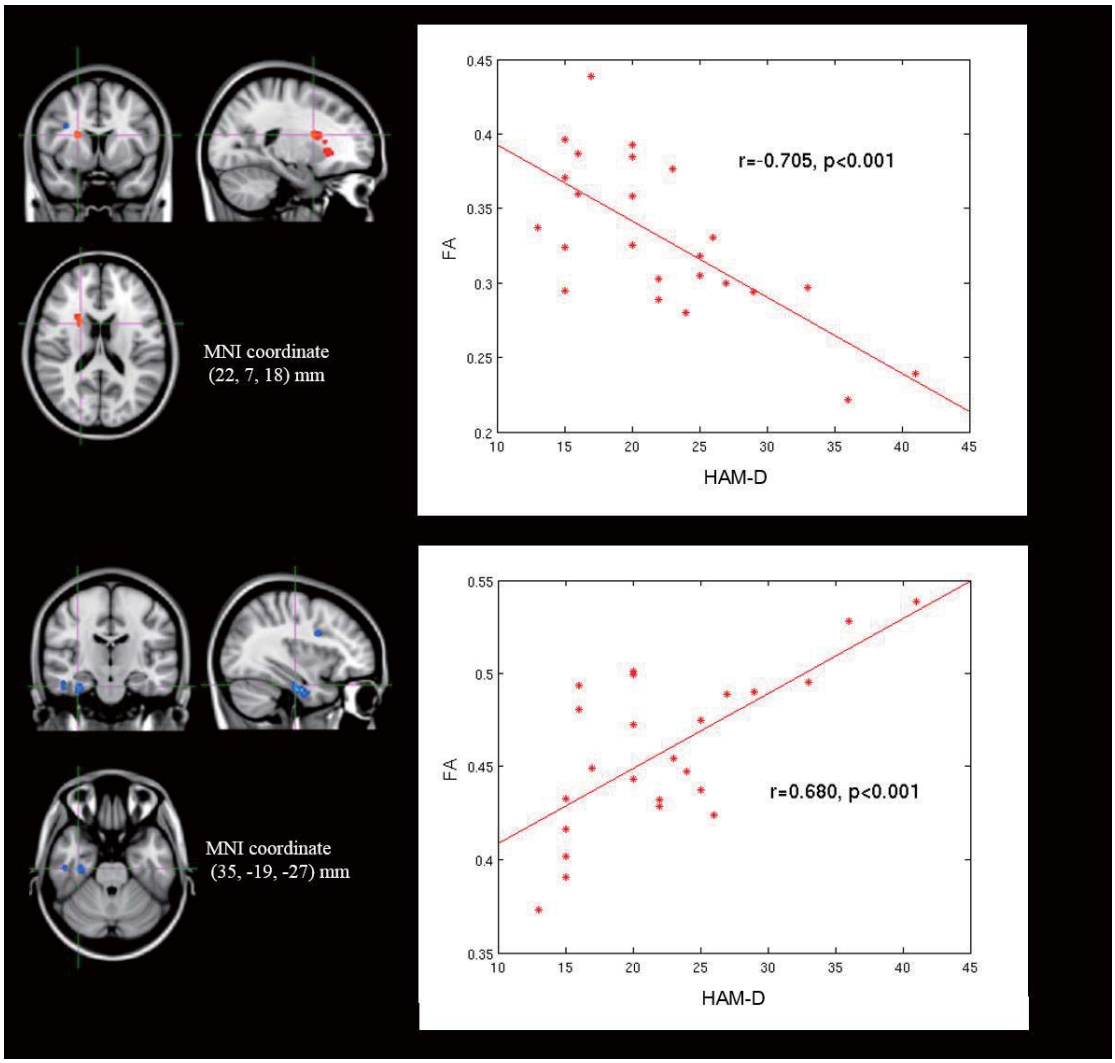

Figure 3. Correspondence between affected white matter and severity of depressive symptom in MDD patients. In the left panel, coronal, axial, and sagittal views illustrated associations between FA and severity of depressive symptom indexed by HAM-D, independently of number of episodes, within MDD group. In the right panel for visualization, HAM-D and averaged FA of related white matter tracts were illustrated in the scatter plot. The upper row displayed positive correlation result while the lower row displayed negative correlation result.

Manuscript 2

Altered functional brain connectome in very preterm born adults (submitted)

Title page:

Title:

Altered functional brain connectome in very preterm born adults

Abbreviated title:

Connectome in preterm born adults

Authors and Affiliations:

Chun Meng[1,4,5], Josef G. Bäuml[1,4], Yong He[7], Xiyao Xie[1,4,6], Julia Jaekel[8,11], Marcel Daamen[9,10], Junming Shao[1,13], Lukas Scheef[9], Barbara Busch[10], Nicole Baumann[11], Peter Bartmann[10], Dieter Wolke[11], Henning Boecker[9], Afra Wohlschläger[1,3,4,5], Christian Sorg[1,2,4]

Departments of [1]Neuroradiology, [2]Psychiatry, [3]Neurology, [4]TUM-Neuroimaging Center of Klinikum rechts der Isar, Technische Universität München TUM, Ismaninger Strasse 22, 81675 Munich, Germany; [5]Graduate School of Systemic Neurosciences GSN, [6]Department of Psychology, Ludwig-Maximilians-Universität LMU, Großhaderner Strasse 2, 82152 Munich, Germany; [7]State Key Laboratory of Cognitive Neuroscience and Learning & IDG/McGovern Institute for Brain Research, Center for Collaboration and Innovation in Brain and Learning Sciences, Beijing Normal University,100875 Beijing, China; [8]Department of Developmental Psychology, Ruhr-University Bochum, 44801 Bochum, Germany; [9]Functional Neuroimaging Group, Department of Radiology, [10]Department of Neonatology, University Hospital Bonn, 53127 Bonn, Germany; [11]Department of Psychology, [12]Warwick Medical School, University of Warwick, Coventry CV4 7AL, United

Kingdom. [13]Institute for computer science and Technology, University of Electronic Science and Technology of China, 611731 Chengdu, China.

Corresponding Author:

Christian Sorg, Department of Psychiatry and Neuroradiology, Klinikum rechts der Isar, Ismaninger Strasse 22, 81675 Munich, Germany, phone: +49 89 4140-7631, fax: -7665, c.sorg@lrz.tu-muenchen.de

Counts:

Number of pages: 42

Number of figures: 4

Number of tables: 4

Number of words for Abstract: 244

Number of words for Introduction: 490

Number of words for Discussion: 1406

Conflict of Interest:

The authors declare no competing financial interests.

Acknowledgements:

We thank all current and former members of the Bavarian Longitudinal Study Group who contributed to general study organization, recruitment, and data collection, management and subsequent analyses, including (in alphabetical order): Stephan Czeschka, Claudia Grünzinger, Christian Koch, Diana Kurze, Sonja Perk, Andrea Schreier, Antje Strasser, Julia Trummer, and Eva van Rossum. We are grateful to the

51 staff of the Department of Neuroradiology in Munich and the Department of
52 Radiology in Bonn for their help in data collection. Most importantly, we thank all our
53 study participants for their efforts to take part in this study.
54 This study was supported by Chinese Scholar Council (CSC, File No: 2010604026 to
55 C.M.), the German Federal Ministry of Education and Science (BMBF 01ER0801 to
56 P.B. and D.W., BMBF 01EV0710 to A. W., BMBF 01ER0803 to C.S.) and the
57 Kommission für Klinische Forschung, Technische Universität München (KKF
58 8765162 to C.S).

Abstract:

Humans are highly susceptible to adverse long-term consequences of very preterm birth (< 32 weeks of gestation), ranging from growth failure to disturbed brain development and compromised cognition. The macroscopic brain connectome in very preterm newborns shows aberrant subcortical connectivity with a relative increase of cortico-cortical connectivity despite largely unchanged overall architecture. Yet little is known about adult connectome after very preterm birth. We hypothesized that altered connectome may persist in very preterm born adults, with differential potentials for compensatory adaption in subcortical and cortical changes. Thus, resting-state fMRI, graph-based network analysis, and cognitive testing were used to investigate the functional brain connectome and general cognitive performance in 64 very preterm and 72 full-term born adults.

While global network metrics such as small-world organization were unchanged in very preterm born adults, local network metrics were altered in cortical and subcortical regions regarding functional integration and segregation. Associated with early prematurity and adulthood cognition, subcortical and primary cortical regions (such as caudate, hippocampus or auditory cortex) showed lesion-like alterations of network topology (e.g. the more caudate nodal efficiency is reduced the worse cognitive performance), whereas associative cortical regions (such as inferior frontal gyrus (IFG) and superior parietal cortex) displayed compensation-like alterations (e.g. the more IFG nodal efficiency is increased the better cognitive performance).

Results provide first evidence for the altered functional brain connectome in very preterm born adults with both lesion-like and compensation-like reorganizations. Data suggest specific developmental trajectory of human connectome after preterm delivery.

Key words:

Preterm born adults, functional connectome, resting-state fMRI, graph analysis, IQ, compensation.

89 **Introduction:**

90 In humans, very preterm birth (< 32 weeks of gestation) is associated with potentially
91 lasting adverse consequences that range from an increased risk for neuropsychiatric
92 disorders to lowered cognitive performance or socio-economic status (Nosarti et al.,
93 2012; D'Onofrio et al., 2013). The current study focuses on potential alterations in
94 macroscopic brain organization in very preterm born adults and their functional
95 relevance.

96 Brain function depends on both specialized local information processing (i.e.
97 functional segregation) and efficient global integration of distributed regions (i.e.
98 functional integration) within a network of neural interactions called the human
99 connectome (Sporns et al., 2005). Graph-based network analysis combined with
100 diffusion-weighted imaging and resting-state fMRI allows for in-vivo characterization
101 of the macroscopic connectome (Bullmore and Bassett, 2011). The macroscopic
102 functional connectome comprises both brain regions (i.e. nodes of the graph) and
103 functional connections of synchronized spontaneous activities (i.e. edges between
104 nodes), which is characterized by network metrics such as local clustering (i.e.
105 segregation of functional modules) and global efficiency (i.e. integration of local
106 modules) (Rubinov and Sporns, 2010).

107 The human macroscopic connectome emerges and gets modified during early
108 brain maturation (Ball et al., 2014; van den Heuvel et al., 2014), development (Collin
109 and van den Heuvel, 2013; Cao et al., 2014), and aging (Filippi et al., 2013).
110 Hallmarks of the adult connectome such as so-called small-world and rich-club
111 organization are already present in very preterm newborns with both increasing
112 capacity of global integration and increasing coupling of structural and functional
113 connectivity during early postnatal development to week 40 (Ball et al., 2014; van den

Heuvel et al., 2014). However, while the fundamental connectome architecture is present in preterm newborns, particularly subcortico-cortical connectivity appears to be altered compared to term-born newborns, with a relative increase of cortico-cortical connectivity and cortical local clustering (Ball et al., 2014). Recently widespread altered functional connectivity has been reported in preterm born adults (White et al., 2014; Bäuml et al., 2014). These findings suggest an altered developmental trajectory for the connectome of preterm born individuals and potentially distinctive functional relevance for subcortico-cortical and cortico-cortical connectivity in such process. For example, subcortical changes of intrinsic functional connectivity in preterm born adults link with persistent subcortical gray matter disruptions in a lesion-like way (i.e. the lower gestational age at birth the stronger connectivity changes) (Bäuml et al., 2014), and cortical processes in preterm born adults appear to show compensatory reorganization during cognitive tasks (Narberhaus et al., 2009).

Therefore, we hypothesized: (i) the basic global organization of human functional connectome may be preserved into adulthood after preterm birth; (ii) divergent regional, specifically cortical and subcortical, topological organization may account for long-term detrimental effect of preterm birth as well as potential compensatory adaption, featured by lesion-like or compensation-like mode of changes in preterm adults. Here we applied connectome analysis combining resting-state fMRI and graph theory to examine the topological organization of functional connectome in very preterm born adults and potential associations with early prematurity and adulthood cognitive ability.

137 **Materials and Methods:**

138 ***Overview.*** Sixty-four very preterm (VPT, defined by the birth with less than 32
139 gestational weeks; 38 males) and 72 full-term (FT, defined by birth after 36
140 gestational weeks; 48 males) born adults at the age of about 26y were assessed by
141 both resting-state functional MRI (rs-fMRI) and cognitive testing to define
142 topological properties of the functional connectome and general cognitive
143 performance. Outcome measures were global and regional network metrics of
144 functional segregation (e.g. local clustering) and functional integration (e.g. path
145 length), prematurity (i.e. gestational age and birth weight), neonatal medical risk, and
146 full-scale intelligence quotient (IQ). For hypothesized lesion-like mode of network
147 changes, it indicates the more the prematurity (or the higher the neonatal medical risk,
148 or the lower the IQ) the more the network changes. Complementarily,
149 compensation-like mode indicates the less the prematurity (or the lower the neonatal
150 medical risk, or the higher the IQ) the more the network changes.

151 **Participants**

152 ***Sample.*** Participants were recruited as part of the prospective Bavarian Longitudinal
153 Study (BLS) (Riegel et al., 1995; Wolke and Meyer, 1999). The BLS investigates a
154 geographically defined whole-population sample of neonatal at-risk children and
155 healthy controls. Born between February 1985 and March 1986 in southern Bavaria,
156 all infants who required admission to neonatal units in 17 children's hospitals within
157 the first ten days of life, comprised the target sample. A total of 7505 infants (10.6%
158 of all live births) were classified neonatal at-risk, including 560 VPT infants (0.8% of
159 all live births). During the same period, 705 healthy FT infants (> 36 weeks gestation;
160 normal postnatal care) born in the same hospital centres were recruited as control
161 infants. Over the following years, subjects of both groups were repeatedly assessed

with neurological and psychological test batteries, and parental interviews to monitor their development. Full eligible sample details of the follow-up are provided elsewhere (Wolke and Meyer, 1999; Gutbrod et al., 2000). At the age of 26, 205 VPT and 229 FT subjects were eligible for a follow-up assessment. Of them, 64 VPT and 72 FT adults (aged 25 to 27 years) underwent MRI assessments (Table 1). MRI was carried out at two different sites: The Department of Neuroradiology, Klinikum Rechts der Isar, Technische Universität München, Germany (N=89), and the Department of Radiology, University Hospital Bonn, Germany (N=47). The study was approved by the local ethics committees of the Klinikum rechts der Isar and University Hospital Bonn. All participants gave written informed consent and received travel expenses and a payment for attendance.

Birth-related variables. Gestational age (GA) was estimated from maternal reports of the last menstrual period and serial ultrasounds during pregnancy. In cases where the two measures differed by more than two weeks, clinical assessment with the Dubowitz method was applied (Dubowitz et al., 1970). Maternal age and birth weight (BW) was obtained from obstetric records. We use the term prematurity to refer both GA and BW. To assess neonatal medical risk, the duration of intensive neonatal treatment Index (DINTI) was computed as the number of days until VPT infants reached a stable clinical state (Gutbrod et al., 2000). Family socio-economic status (SES) at birth was collected through structured parental interviews within 10 days of child birth. It was computed as a weighted composite score based on the profession of the self-identified head of each family together with the highest educational qualification held by either parent (Bauer, 1988).

Cognitive assessment

187 To estimate cognitive functioning in adulthood, participants was assessed at age of 26
188 years by trained psychologists with the Wechsler Adult Intelligence scale-III
189 (WAIS-III) (Von Aster et al., 2006) , which provided full-scale IQ representing
190 general cognitive ability.
191
192 **Imaging data acquisition and preprocessing**
193 ***Acquisition.*** MRI scans were acquired on MR scanners in Munich and Bonn, for
194 which we controlled by the use of covariates of no-interest: 3T Philips Achieva TX (in
195 Munich center coded as [0 0 1]: VPT=40, FT=49, total=89; in Bonn center coded as
196 [1 0 0]: VPT=4, FT=9, total=13) and 3T Philips Ingenia (in Bonn center coded as [0 1
197 0]: VPT=20, FT=14, total=34), with an 8-channel head coil, applying consistent
198 sequences and parameter settings. For co-registration and volumetric analysis,
199 T1-weighted anatomical data were obtained by using a magnetization-prepared rapid
200 acquisition gradient echo sequence (echo time = 3.9 ms, repetition time = 7.6 ms, flip
201 angle = 15°, field of view = 256 x 256 mm^2, matrix = 256 x 256, 180 sagittal slices,
202 slice thickness = 1 mm, and 0 mm interslice gap, voxel size = 1 x 1 x 1 mm^3). For
203 resting-state functional MRI scans, subjects were instructed to keep their eyes closed,
204 lie still and relax, but not to fall asleep, which was verified by the intercom.
205 Functional data were acquired by using a gradient echo EPI sequence (echo time = 35
206 ms, repetition time = 2608 ms, flip angle = 90°, field of view = 230 x 230 mm^2,
207 matrix = 64 x 64, 41 axial slices, slice thickness = 3.6 mm, and 0 mm interslice gap,
208 voxel size = 3.6 x 3.6 x 3.6 mm^3; 255 volumes).
209 ***Preprocessing.*** For each subject, resting-state fMRI data preprocessing was
210 performed by using SPM8 (http://www.fil.ion.ucl.ac.uk/spm/) and AFNI
211 (http://afni.nimh.nih.gov/afni/) comprising following steps. First, the first five

212 volumes were discarded for equivalence of magnetization effect. Second, remained
213 brain images were corrected for head motion by spatially realigning them to the first
214 volume. Moreover, temporal signal-to-noise ratio and point-to-point head motion
215 were estimated to ensure data quality as described in previous studies (Murphy et al.,
216 2007; Van Dijk et al., 2012; Meng et al., 2014). Third, functional images were
217 spatially aligned with individual anatomical image by co-registration, then normalized
218 into MNI standard space (Montreal Neurological Institute; http://www.mni.mcgill.ca/)
219 following segmentation of anatomical image, resulted in isotropic voxel of 3 mm.
220 Fourth, data was spatially smoothed using an isotropic Gaussian kernel with 6 mm
221 FWHM to reduce spatial noise, and temporally despiked via censoring
222 high-motion-contaminated volumes (using 3dDespike for neighboring interpolation)
223 to limit the impact of statistical outliers on signal intensity (Alexander-Bloch et al.,
224 2013; Siegel et al., 2014). Regarding recent findings about biased influence of micro
225 head motion on functional connectivity, average of root-mean-square motion was
226 calculated in VPT group (mean [SD], 0.040 [0.015] mm) and FT group (mean [SD],
227 0.035 [0.018] mm) (Van Dijk et al., 2012). Mean framewise displacement was also
228 calculated in VPT group (mean [SD], 0.151 [0.057] mm) and FT group (mean [SD],
229 0.134 [0.058] mm) (Power et al., 2012). Two-sample t-tests yielded no significant
230 between-group difference regarding evaluated head motions ($p > 0.08$) as well as
231 temporal signal-to-noise ratio ($p > 0.29$).
232 ***Accounting for structural changes.*** In this study, we focused on the functional
233 connectome, which depends on the structural integrity of polysynaptic pathways (Lu
234 et al., 2011). To control for the influence of potential structural variations, we
235 included total gray matter volume as covariate-of-no-interest in functional network
236 analyses based on our recent work (Sorg et al., 2013; Meng et al., 2014). Standard

237 voxel-based morphometry (VBM) analysis was performed on T1-weighted images by
238 the VBM8 toolbox (http://dbm.neuro.uni-jena.de/vbm.html) to analyze brain structure,
239 resulting in macroscopic estimates of gross structural variation including total gray
240 matter, white matter, cerebrospinal fluid, and brain volumes. To note, modulated gray
241 matter images were generated by accounting for non-linear volume changes during
242 normalization process, which ruled out differences of head size (for more details see
243 elsewhere (Meng et al., 2014)).
244
245 **Network construction of the functional connectome**
246 The functional connectome was defined at the macro scale based on whole-brain
247 resting-state functional connectivity networks. Here we describe the analysis pipeline
248 in brief as the methodological details can be found elsewhere (Meng et al., 2014). For
249 each subject, the brain network, with nodes representing brain regions and edges
250 representing between-node connections, was constructed from preprocessed
251 resting-state fMRI data. First, the whole brain was divided into cortical and
252 subcortical nodes (N = 112) by anatomical parcellation according to Harvard-Oxford
253 atlas (FSL, Oxford University). Second, 112 regional mean time series were extracted
254 regarding node-specific functional signal. To account for spurious signal changes
255 attributable to head movements or physiological confounds, each regional mean time
256 series was regressed on six head motion parameters estimated from realignment and
257 three averaged time series derived from whole gray matter, white matter and
258 cerebrospinal fluid according to recent literatures (Craddock et al., 2013; Smith et al.,
259 2013; Power et al., 2014). Third, to identify between-node connection, each regional
260 time series was band-pass filtered into four wavelet scales corresponding to different
261 frequency intervals using the maximal overlap discrete wavelet transform, and

Pearson's correlation of wavelet coefficients (at scale 2 of 0.048–0.096 Hz for low frequency of intrinsic functional connectivity) were computed between each pair of regional time series, resulting in 112 by 112 association matrices based on functional connectivity (Percival and Walden, 2006; Lynall et al., 2010). The sensitive frequency scale was selected according to our prior study (Meng et al., 2014) and recent literature (Giessing et al., 2013). Fourth, absolute correlation coefficients at the low-frequency scale 2 were used to denote the individual functional connectome in line with previous studies (Alexander-Bloch et al., 2012; Meng et al., 2014).

Network analysis of the functional connectome

Analysis of global functional connectivity properties. To analyze simple global properties of functional connectivity, global strength and diversity of functional connectivity were estimated simply as the mean and variance of each individual functional connectivity matrix (Lynall et al., 2010). In addition, performing principal component analysis on each matrix, the global integration was estimated by the ratio of the first eigenvalue to the sum of all other eigenvalues (Tononi et al., 1994; Friston, 1996). Next, graph-based network analysis was performed to characterize network topology of the individual functional connectome.

Analysis of global and local network topology. Binary-graph-based network analysis was conducted using Matlab-based in-house scripts and Brain Connectivity Toolbox (Rubinov and Sporns, 2010). Networks were constructed at 41 different connection densities in the range 5 – 50%, providing sparser or less densely connected adjacency matrices of costs from 0.05 to 0.50 at the interval of 0.01 (Meng et al., 2014). Network cost is defined as the number of edges in the graph as a percentage of the maximum possible number of edges (N*N-N)/2 = 6212. A thresholding algorithm

287 based on minimum spanning tree was used to enable that all regional nodes were
288 connected even at the lowest cost (Alexander-Bloch et al., 2012; Giessing et al., 2013;
289 Meng et al., 2014). For each cost threshold and corresponding graph, key topological
290 measures were calculated for each node and network. More specifically, nodal and
291 global topological properties quantify comprehensively the topology of the functional
292 connectome regarding both functional integration and functional segregation.
293 Functional integration in the brain is the ability of fast information processing and
294 combining over distributed brain regions, and – here - reflected by three nodal
295 centrality metrics (i.e. degree, betweenness, and efficiency) and two global metrics
296 (i.e. characteristic path length and network global efficiency of whole network)
297 (Rubinov and Sporns, 2010). Functional segregation in the brain is the ability of local
298 specialized processing within densely interconnected groups of brain regions, and –
299 here - reflected by one nodal metric (i.e. nodal local efficiency) and two global
300 metrics (i.e. clustering coefficient and network local efficiency of whole network)
301 (Rubinov and Sporns, 2010).
302 ***Nodal properties.*** Concerning nodal functional integration: degree is defined as the
303 number of edges connected with the given node and betweenness-centrality is defined
304 as the fraction of all shortest paths (the smallest number of intermediate edges)
305 between all other nodes that pass through the given node in the network, which both
306 quantify nodal centrality in a network (Rubinov and Sporns, 2010). Efficiency is a
307 measure of the capacity for global parallel information process and transfer, estimated
308 by the inverse of harmonic mean of shortest path lengths between the given node and
309 all other nodes in the network (Latora and Marchiori, 2001). So nodal efficiency is
310 inversely related to the path length and a node featured by higher efficiency will play
311 a more central role in the integrated organization of the network. Concerning nodal

functional segregation: Nodal local efficiency is a measure of the capacity for local information exchange between the nearest neighbors of the given node, defined by averaged efficiency of subgraph comprising neighboring nodes of the given node (Rubinov and Sporns, 2010). It is worth mentioning, nodal local efficiency is highly related to the clustering coefficient, which implys the extent of segregated organization (Watts and Strogatz, 1998). So a node featured by higher local efficency will contribute more to the cliquish organization of the network (Giessing et al., 2013).

Global properties. To assess global functional network topology, global topological properties were computed for the whole network of all nodes across costs, including clustering coefficient, characteristic path length, small-worldness, network global and local efficiency (Rubinov and Sporns, 2010).The characteristic path length of a network is defined as the average shortest path length between all pairs of nodes in the network (Watts and Strogatz, 1998). The clustering coefficient of a node is defined as the fraction of the given node's neighbors that are also neighbors of each other. The clustering coefficient of a network is defined as mean clustering coefficient across all nodes (Watts and Strogatz, 1998). The small-worldness is defined as the ratio of clustering coefficient against characteristic path length of a network compared with random networks with the same number of nodes, edges and degree distribution, describing the small-world property of high local specialization and high global integration (Watts and Strogatz, 1998; Rubinov and Sporns, 2010). In this study, 100 corresponding random networks were generated for each comparison in line with previous studies (Maslov and Sneppen, 2002; Meng et al., 2014). Global efficiency and local efficiency of a network is computed by averaging efficiency and local efficiency of all nodes in the network, which is respectively related to characteristic

path length and clustering coefficient, and frequently evaluated for global network topology (Cao et al., 2013).

Statistical analysis

Group comparisons. Two-sample t-tests and Chi-square tests were used for descriptive group comparisons of neonatal and clinical data. For network metrics, each metric was averaged over the prior defined cost range (5-50%) to avoid multiple comparisons due to the individual density sampling and to reduce the dependency of any significant differences in network topology on the arbitrary choice of a single cost (Ginestet et al., 2011; Giessing et al., 2013; Meng et al., 2014). To identify group differences in network metrics of functional connectome, statistical comparisons were carried out between VPT and FT groups using permutation testing (van den Heuvel et al., 2013). For each network metric (i.e. clustering coefficient, characteristic path length, small-worldness, network global and local efficiency; nodal degree, betweenness, efficiency, and local efficiency), confounding factors of MRI center, gender, and total gray matter volume were firstly ruled out by multiple regression. Then the difference between the two group means was calculated. Next, 100, 000 permutations were employed to generate the null model of the group difference occurring by chance, which finally yielded a p value for the original group difference that reflects the statistical significance. Significance thresholds were set for global topological properties ($p < 0.05$) and nodal topological properties ($p < 0.009$, using False Positive Correction according to the number of nodes, $1/N \sim = 0.009$) in agreement with previous studies on functional brain topology (Lynall et al., 2010; Meng et al., 2014).

Association between network topology, VPT-related variables, adulthood IQ. To analyze the separate relationship of VPT effect and cognitive performance with topological properties of aberrant nodal connectivity in VPT adults, we calculated the partial correlation coefficients of network metrics with birth-related variables (i.e. GA, BW, DINTI) independent of adult cognitive functioning (i.e. full-scale IQ), and vice versa. Additional common covariates (i.e. gender, center, SES, and total gray matter volume) were also controlled in partial correlation analyses. Partial correlation analysis was used because it allows for measuring the degree of association between two interested variables (e.g. network metric and gestational age), with controlling other variables (e.g. cognitive performance reflected by full-scale IQ). Such type of control is relevant, since previous studies demonstrated significant relationships between prematurity level and cognitive performance (Isaacs et al., 2004; Eikenes et al., 2011). In more detail, the partial correlation between the network metric and gestational age given controlling variables $\mathbf{Z}$ = (IQ, gender, center, SES, and total gray matter volume), written as $\rho(\text{METRIC}, \text{GA}; \mathbf{Z})$, is the correlation between the residuals R(METRIC) and R(GA) resulting from the linear regression of METRIC with $\mathbf{Z}$ and of GA with $\mathbf{Z}$, respectively. Therefore, partial correlation analysis allows for testing the relationship between network topology and VPT-related variables independent of adulthood IQ and vice versa.

380 **Results:**

381 ***Cognitive performance and global brain structure in VPT adults***

382 Descriptive results of VPT and FT groups are reported (Table 1). Both groups had a
383 mean age of 26.3 years at scan and were gender-, SES-, and MRI-center-matched ($p >$
384 0.05). The VPT group had significantly lower IQs compared with the FT group ($p <$
385 0.0001).

386 Volumetric analysis revealed significantly smaller total brain volume and white
387 matter volume as well as larger cerebrospinal fluid volume in VPT adults ($p < 0.05$;
388 Table 2), whereas the group difference of total gray matter volume was not significant
389 ($p > 0.05$).

390

391 ***Unchanged global functional connectivity and network topology in VPT adults***

392 Concerning global properties of functional connectome, no significant group
393 differences were found between VPT and FT adults in global functional connectivity
394 (global strength, diversity, and integration) and global network topology
395 (small-worldness, local clustering coefficient, characteristic path length, global and
396 local efficiency) (for all tests $p > 0.05$; Table 2).

397

398 ***Altered nodal functional integration and segregation in VPT adults***

399 Concerning regional properties of network topology (Figure 1 and Table 3), we
400 assessed nodal network metrics by performing permutation tests for nodal functional
401 integration (i.e. degree, betweenness, and efficiency) and nodal functional segregation
402 (i.e. local efficiency). Compared to FT adults, significant changes of nodal network
403 metrics were found in VPT adults across frontal, temporal, parietal, occipital, and
404 subcortical regions (Figure 1 A).

405 Specifically for nodal functional integration (Figure 1 B), the VPT group
406 exhibited increased nodal degree and efficiency primarily in the pars triangularis and
407 opercularis of left inferior frontal gyrus, posterior division of left inferior temporal
408 gyrus, and left amygdala. Decreased degree, betweenness, and efficiency were found
409 primarily in the bilateral supplementary motor cortex, temporoocicipital part of left
410 inferior temporal gyrus, right temporal regions including planum temporale and
411 Heschl's gyrus, left lingual and occipital fusiform gyrus, right caudate and right
412 thalamus ($p < 0.009$; Table 3, Figure 1 B).
413 For nodal functional segregation (Figure 1 C), the VPT group exhibted
414 significantly higher nodal local efficiency primarily in the posterior division of left
415 inferior temporal gyrus, left superior parietal lobule, and right hippocampus, and
416 lower nodal local efficiency primarily in the bilateral supplementary motor cortex,
417 inferior division of left lateral occipital cortex, and right caudate ($p < 0.009$; Table 3,
418 Figure 1 C).
419
420 ***Altered nodal network topology is associated with preterm birth and IQ in a***
421 ***lesion-like way in subcortical and primary cortical regions while in a***
422 ***compensation-like way in associative cortical areas***
423 To uncover the long-term effect of VPT birth on altered network topology with
424 respect to functional relevance, we carried out partial correlation analysis between
425 prematurity and neonatal medical risk scores, IQ, and altered network topology of the
426 functional connectome within the VPT group, by controlling for gender, MRI center,
427 SES, and total gray matter volume ($p < 0.05$; Table 4; Figure 2). In general, we found
428 lesion-like connectome changes in subcortical and primary cortical areas (Figures 2
429 and 3, see non-gray marked panels; Table 4), while compensation-like connectome

changes were present in associative cortical areas (Figures 2 and 3, see gray marked panels; Table 4). In Figure 4, these results are summarized with red and green nodes representing brain regions of lesion- and compensation-like altered network topology.

In more detail, results concerning the relationship between very preterm birth and altered regional functional connectome properties are shown in Figure 2 and Table 4: For altered lesion-like functional integration, right Heschl's gyrus showed positive correlation with gestational age and posterior division of left inferior temporal gyrus showed positive correlation with neonatal medical risk (i.e. DINTI); right planum temporale showed negative correlation with DINTI. For altered compensation-like functional integration, pars triangularis of left inferior frontal gyrus correlated positively with birth weight and negatively with DINTI. For altered lesion-like functional segregation, left supplementary motor cortex showed positive correlation with gestational age. For altered compensation-like functional segregation, left superior parietal lobule was associated with gestational age and DINTI.

Results concerning the relationship between IQ and altered regional functional connectome properties are shown in Figure 3 and Table 4: potential compensation-like result was identified in pars triangularis of left inferior frontal gyrus with positively associated IQ and nodal efficiency. Potential lesion-like associations were found in amygdala, hippocampus, as well as caudate between IQ and nodal functional integration/segregation.

450 **Discussion:**

451 The objective of our study was to test the hypothesis that in very preterm born adults,
452 global functional connectome properties are preserved while regional connectome
453 properties are changed with a differential potential for compensatory adaption in
454 subcortical and cortical connectivity patterns. 64 VPT and 72 FT adults of age 26
455 years were assessed by cognitive testing and resting-state fMRI combined with
456 graph-based network analysis. While global connectome properties such as
457 small-worldness and global efficiency were preserved in the VPT group, subcortical
458 and cortical regions showed altered functional segregation and integration.
459 Particularly, subcortical and primary cortical connectome changes displayed a
460 lesion-like association with early prematurity and adulthood IQ (e.g. the more caudate
461 nodal efficiency was reduced the worse cognitive performance), while changes in
462 associative cortical regions such as the inferior frontal gyrus (IFG) had a
463 compensation-like pattern (e.g. the more IFG nodal efficiency was increased the better
464 cognitive performance). Results provide first evidence for an altered functional
465 connectome in VPT adults with some hints for compensation-like cortical
466 connectivity changes. Data suggest that preterm birth modifies the developmental
467 trajectory of human connectome in a lasting and adaptive way.
468

469 **After preterm birth, basic global properties of the adult connectome are**
470 **preserved but nodal connectivity is altered in subcortical and cortical regions.**
471 In VPT adults, we found preserved small-world organization, clustering coefficient,
472 and global efficiency of the functional connectome (Table 2), while nodal
473 connectivity was changed regarding both functional segregation and integration
474 properties in subcortical and cortical areas (Table 3; Figure 1). For example, thalamus'

475 degree and caudate's degree and efficiency were reduced in VTP born adults
476 compared with FT adults, suggesting less optimal functional integration of
477 information processing in these subcortical regions in VPT adults. On the other hand,
478 nodal degree, betweenness-centrality, and efficiency of the inferior frontal gyrus were
479 consistently increased in VPT adults, suggesting increased functional integration
480 capacity for this cortical region. Such complex pattern of both increased and reduced
481 properties of functional connectivity topology matches our previous finding about
482 increased and reduced functional connectivity in intrinsic brain networks of preterm
483 born adults (Bäuml et al., 2014); particularly, we found altered connectivity in
484 thalamus and caudate that was associated with lasting gray matter disruptions and the
485 degree of prematurity. Recent studies reported optimal small-world architecture was
486 preserved in the structural connectome of preterm newborns while subcortical-cortical
487 connectivity was disrupted with a relative increase of cortico-cortical connectivity
488 (Ball et al., 2014; van den Heuvel et al., 2014). Together with current evidences that
489 demonstrate widespread lasting effects of preterm birth in brain structure and function
490 of infants (Fischi-Gomez et al., 2014), children (Constable 2008), adolescents
491 (Gimenez et al., 2006; Nosarti et al., 2008; Gozzo et al., 2009; Mullen et al., 2011; de
492 Kieviet et al., 2012; Nosarti, 2013), and adults (Eikenes et al., 2011; Bäuml et al.,
493 2014; White et al., 2014), our findings further suggest that preterm birth induce a
494 specific developmental trajectory for the human connectome with a complex pattern
495 of regional connectivity changes.
496
497 **Lesion-like connectome changes in subcortical and primary cortical areas versus**
498 **compensation-like changes in associative cortical areas.**
499 With respect to the complexity of regional connectivity changes in the VPT group, we

found lesion-like connectome changes primarily in subcortical and primary cortical areas (Table 4; Figure 2 and 3). For example, the lower the gestational age of VPT adults, the lower the nodal degree of the Heschl's gyrus, which was reduced in VPT; the lower the local efficiency of the caudate, which was reduced in VPT, the more IQ is reduced. Concerning subcortical areas, Ball and colleagues demonstrated explicitly subcortical-cortical connectivity disruptions for preterm newborns and infants (Ball et al., 2012; Ball et al., 2013; Pandit et al., 2013b; Ball et al., 2014). Subcortical white and gray matter, which underlies subcortical-cortical connectivity, is known to be prominently affected by preterm birth (Inder et al., 2005; Srinivasan et al., 2007; Zubiaurre-Elorza et al., 2011; Ball et al., 2012; Ball et al., 2013; Pandit et al., 2013a). Since these changes persist at least partly into adolescence (Nosarti et al., 2008; Northam et al., 2012), subcortical gray and white matter changes likely represent lasting brain lesions of preterm birth, being in line with our findings. For primary cortical areas, auditory, motor, or visual cortices show specifically higher levels of adult-like connectivity organization than associative cortical areas at birth, which reach an adult-like connectivity pattern later in the brain development (Fransson et al., 2011; Gao et al., 2011). Moreover high degree of connectivity is present between primary cortical and subcortical areas such as thalamus. So our finding of lesion-like changes specifically in subcortical and primary cortical areas in VPT adults may suggest adverse subcortical and primary cortical connectome changes after very preterm delivery endure along development.

On the other hand, we found compensation-like connectome changes in VPT adults in associative cortical areas (Table 4; Figure 2 and 3). For example, the higher IFG nodal efficiency and degree, which were abnormally increased in preterm born adults, the higher IQ; the lower gestational age and the more neonatal medical risk the

525 lower the local efficiency of the superior parietal lobule, which was abnormally
526 increased in VPT adults. Inferior frontal gyrus and superior parietal lobule (SPL) are
527 key regions of the salience and central executive network (Seeley et al., 2007).
528 Salience and central executive network are both essentially involved in cognitive
529 control processes (Dosenbach et al., 2007; Fair et al., 2007). In contrast to primary
530 cortical networks such as the sensorimotor network, connectivity of these networks
531 reaches an adult-like connectivity pattern at later stage of neurodevelopment,
532 suggesting longer flexible development trajectories (Dosenbach et al., 2010; Fransson
533 et al., 2011; Collin and van den Heuvel, 2013). Due to both cognitive control function
534 and longer developmental trajectory of salience and executive control network, IFG
535 and SPL might be candidates for potential compensatory adaptions during
536 development in response to birth-related lesions. This argument is in line with
537 relatively increased cortico-cortical and reduced subcortico-cortical connectivity in
538 preterm newborns, suggesting distinctive developmental trajectories for subcortical
539 and cortical connectome (Ball et al., 2014). Our finding of compensation-like
540 connectome changes in IFG and SPL in very preterm born adults may indicate such
541 distinct developmental trajectory with compensatory cortical adaptions after preterm
542 delivery.

543 Taken together our data show different developmental outcomes for the
544 subcortical and cortical connectome with distinctive functional relevance: while
545 subcortical connectivity may represent a more lasting lesion-like pattern induced by
546 preterm birth, cortical connectivity may represent a more resilient pattern, which has
547 some potential to adapt in a compensatory way. Interestingly, cortical upper layers 1-3
548 subserve mainly cortico-cortical connectivity, while lower layers 4-6 subserve
549 cortico-subcortical connectivity (Swanson, 2000; Douglas and Martin, 2004). One

might speculate that upper and lower layer connectivity patterns may follow distinct developmental trajectories with respect to functional relevance in terms of lesion and compensation potential. While previous data support aberrant cortical microstructure due to preterm birth in general (Ball et al., 2013; Dean et al., 2013; Vinall et al., 2013), to the best of our knowledge no data about layer specific development changes after preterm birth are available at current stage. Future study with new technologies (e.g. high-tesla MRI to map cortical layers) might address such open issues.

Methodological issues.

Some points should be taken into account when interpreting our results. First, the current sample consisted of VPT adults with lower neonatal complications and higher IQ. Individuals with more complications or severe impairments in the initial BLS sample were more likely to be excluded in initial screening for MRI or reject MRI scanning. Thus here reported differences in the functional connectome between VPT and FT adults are conservative estimates of true differences. Second, current sample size is large (n=64), enhancing the generalizability power of our findings. Third, our findings were not confounded by brain structural variance since we controlled total gray matter volume. Given potential gender effect on long-term neurodevelopmental outcome (Mayoral et al., 2009), we also controlled for gender in this study. Family SES at birth was also ruled out to limit potential confounding influence on brain development affected by preterm birth (Wong and Edwards, 2013). Fourth, in this study, we used Harvard-Oxford-atlas-based brain parcellation and undirected binary graph approach, which is substantially valid framework for brain connectome analysis and largely comparable with other human connectome studies (Bullmore and Bassett, 2011; Sporns, 2014).

Conclusion.

Results demonstrate an altered functional connectome in very preterm born adults, with both lesion-like connectivity changes in subcortical and primary cortical regions and compensation-like changes in associative cortices.

References:

Alexander-Bloch A, Raznahan A, Bullmore E, Giedd J (2013) The convergence of maturational change and structural covariance in human cortical networks. The Journal of neuroscience : the official journal of the Society for Neuroscience 33:2889-2899.

Alexander-Bloch A, Lambiotte R, Roberts B, Giedd J, Gogtay N, Bullmore E (2012) The discovery of population differences in network community structure: new methods and applications to brain functional networks in schizophrenia. NeuroImage 59:3889-3900.

Bäuml JG, Daamen M, Meng C, Neitzel J, Scheef L, Jaekel J, Busch B, Baumann N, Bartmann P, Wolke D, Boecker H, Wohlschlager AM, Sorg C (2014) Correspondence Between Aberrant Intrinsic Network Connectivity and Gray-Matter Volume in the Ventral Brain of Preterm Born Adults. Cerebral cortex (New York, NY : 1991) Advance online publication. doi: 10.1093/cercor/bhu133.

Ball G, Srinivasan L, Aljabar P, Counsell SJ, Durighel G, Hajnal JV, Rutherford MA, Edwards AD (2013) Development of cortical microstructure in the preterm human brain. Proceedings of the National Academy of Sciences of the United States of America 110:9541-9546.

Ball G, Boardman JP, Rueckert D, Aljabar P, Arichi T, Merchant N, Gousias IS,

601 Edwards AD, Counsell SJ (2012) The effect of preterm birth on thalamic and
602 cortical development. Cerebral cortex (New York, NY : 1991) 22:1016-1024.
603 Ball G, Aljabar P, Zebari S, Tusor N, Arichi T, Merchant N, Robinson EC, Ogundipe
604 E, Rueckert D, Edwards AD, Counsell SJ (2014) Rich-club organization of the
605 newborn human brain. Proceedings of the National Academy of Sciences of the
606 United States of America 111:7456-7461.
607 Bauer A (1988) Ein Verfahren zur Messung des für das Bildungsverhalten relevanten
608 Sozial Status (BRSS) - überarbeitete Fassng. Frankfurt (Germany): Deutsches
609 Institut für Internationale Pädagogische Forschung.
610 Bullmore ET, Bassett DS (2011) Brain graphs: graphical models of the human brain
611 connectome. Annual review of clinical psychology 7:113-140.
612 Cao M, Wang JH, Dai ZJ, Cao XY, Jiang LL, Fan FM, Song XW, Xia MR, Shu N,
613 Dong Q, Milham MP, Castellanos FX, Zuo XN, He Y (2014) Topological
614 organization of the human brain functional connectome across the lifespan.
615 Developmental cognitive neuroscience 7:76-93.
616 Cao Q, Shu N, An L, Wang P, Sun L, Xia MR, Wang JH, Gong GL, Zang YF, Wang
617 YF, He Y (2013) Probabilistic diffusion tractography and graph theory analysis
618 reveal abnormal white matter structural connectivity networks in drug-naive
619 boys with attention deficit/hyperactivity disorder. The Journal of neuroscience :
620 the official journal of the Society for Neuroscience 33:10676-10687.
621 Collin G, van den Heuvel MP (2013) The ontogeny of the human connectome:
622 development and dynamic changes of brain connectivity across the life span.
623 The Neuroscientist : a review journal bringing neurobiology, neurology and
624 psychiatry 19:616-628.
625 Craddock RC, Jbabdi S, Yan CG, Vogelstein JT, Castellanos FX, Di Martino A, Kelly

626 C, Heberlein K, Colcombe S, Milham MP (2013) Imaging human connectomes
627 at the macroscale. Nature methods 10:524-539.
628 D'Onofrio BM, Class QA, Rickert ME, Larsson H, Langstrom N, Lichtenstein P
629 (2013) Preterm birth and mortality and morbidity: a population-based
630 quasi-experimental study. JAMA psychiatry 70:1231-1240.
631 de Kieviet JF, Zoetebier L, van Elburg RM, Vermeulen RJ, Oosterlaan J (2012) Brain
632 development of very preterm and very low-birthweight children in childhood
633 and adolescence: a meta-analysis. Developmental medicine and child neurology
634 54:313-323.
635 Dean JM, McClendon E, Hansen K, Azimi-Zonooz A, Chen K, Riddle A, Gong X,
636 Sharifnia E, Hagen M, Ahmad T, Leigland LA, Hohimer AR, Kroenke CD,
637 Back SA (2013) Prenatal cerebral ischemia disrupts MRI-defined cortical
638 microstructure through disturbances in neuronal arborization. Science
639 translational medicine 5:168ra167.
640 Dosenbach NU, Fair DA, Miezin FM, Cohen AL, Wenger KK, Dosenbach RA, Fox
641 MD, Snyder AZ, Vincent JL, Raichle ME, Schlaggar BL, Petersen SE (2007)
642 Distinct brain networks for adaptive and stable task control in humans.
643 Proceedings of the National Academy of Sciences of the United States of
644 America 104:11073-11078.
645 Dosenbach NU, Nardos B, Cohen AL, Fair DA, Power JD, Church JA, Nelson SM,
646 Wig GS, Vogel AC, Lessov-Schlaggar CN, Barnes KA, Dubis JW, Feczko E,
647 Coalson RS, Pruett JR, Jr., Barch DM, Petersen SE, Schlaggar BL (2010)
648 Prediction of individual brain maturity using fMRI. Science (New York, NY)
649 329:1358-1361.
650 Douglas RJ, Martin KA (2004) Neuronal circuits of the neocortex. Annual review of

651 neuroscience 27:419-451.
652 Dubowitz LM, Dubowitz V, Goldberg C (1970) Clinical assessment of gestational age
653 in the newborn infant. The Journal of pediatrics 77:1-10.
654 Eikenes L, Lohaugen GC, Brubakk AM, Skranes J, Haberg AK (2011) Young adults
655 born preterm with very low birth weight demonstrate widespread white matter
656 alterations on brain DTI. NeuroImage 54:1774-1785.
657 Fair DA, Dosenbach NU, Church JA, Cohen AL, Brahmbhatt S, Miezin FM, Barch
658 DM, Raichle ME, Petersen SE, Schlaggar BL (2007) Development of distinct
659 control networks through segregation and integration. Proceedings of the
660 National Academy of Sciences of the United States of America
661 104:13507-13512.
662 Filippi M, van den Heuvel MP, Fornito A, He Y, Hulshoff Pol HE, Agosta F, Comi G,
663 Rocca MA (2013) Assessment of system dysfunction in the brain through
664 MRI-based connectomics. Lancet neurology 12:1189-1199.
665 Fischi-Gomez E, Vasung L, Meskaldji DE, Lazeyras F, Borradori-Tolsa C, Hagmann P,
666 Barisnikov K, Thiran JP, Huppi PS (2014) Structural Brain Connectivity in
667 School-Age Preterm Infants Provides Evidence for Impaired Networks Relevant
668 for Higher Order Cognitive Skills and Social Cognition. Cerebral cortex (New
669 York, NY : 1991) Advance online publication. doi: 10.1093/cercor/bhu073.
670 Fransson P, Aden U, Blennow M, Lagercrantz H (2011) The functional architecture of
671 the infant brain as revealed by resting-state fMRI. Cerebral cortex (New York,
672 NY : 1991) 21:145-154.
673 Friston KJ (1996) Theoretical neurobiology and schizophrenia. British medical
674 bulletin 52:644-655.
675 Gao W, Gilmore JH, Giovanello KS, Smith JK, Shen D, Zhu H, Lin W (2011)

676 Temporal and spatial evolution of brain network topology during the first two
677 years of life. PloS one 6:e25278.
678 Giessing C, Thiel CM, Alexander-Bloch AF, Patel AX, Bullmore ET (2013) Human
679 brain functional network changes associated with enhanced and impaired
680 attentional task performance. The Journal of neuroscience : the official journal
681 of the Society for Neuroscience 33:5903-5914.
682 Gimenez M, Junque C, Narberhaus A, Bargallo N, Botet F, Mercader JM (2006)
683 White matter volume and concentration reductions in adolescents with history
684 of very preterm birth: a voxel-based morphometry study. NeuroImage
685 32:1485-1498.
686 Ginestet CE, Nichols TE, Bullmore ET, Simmons A (2011) Brain network analysis:
687 separating cost from topology using cost-integration. PloS one 6:e21570.
688 Gozzo Y, Vohr B, Lacadie C, Hampson M, Katz KH, Maller-Kesselman J, Schneider
689 KC, Peterson BS, Rajeevan N, Makuch RW, Constable RT, Ment LR (2009)
690 Alterations in neural connectivity in preterm children at school age.
691 NeuroImage 48:458-463.
692 Gutbrod T, Wolke D, Soehne B, Ohrt B, Riegel K (2000) Effects of gestation and birth
693 weight on the growth and development of very low birthweight small for
694 gestational age infants: a matched group comparison. Archives of disease in
695 childhood Fetal and neonatal edition 82:F208-214.
696 Inder TE, Warfield SK, Wang H, Huppi PS, Volpe JJ (2005) Abnormal cerebral
697 structure is present at term in premature infants. Pediatrics 115:286-294.
698 Isaacs EB, Edmonds CJ, Chong WK, Lucas A, Morley R, Gadian DG (2004) Brain
699 morphometry and IQ measurements in preterm children. Brain : a journal of
700 neurology 127:2595-2607.

701 Latora V, Marchiori M (2001) Efficient behavior of small-world networks. Physical
702 review letters 87:198701.
703 Lu J, Liu H, Zhang M, Wang D, Cao Y, Ma Q, Rong D, Wang X, Buckner RL, Li K
704 (2011) Focal pontine lesions provide evidence that intrinsic functional
705 connectivity reflects polysynaptic anatomical pathways. The Journal of
706 neuroscience : the official journal of the Society for Neuroscience
707 31:15065-15071.
708 Lynall ME, Bassett DS, Kerwin R, McKenna PJ, Kitzbichler M, Muller U, Bullmore
709 E (2010) Functional connectivity and brain networks in schizophrenia. The
710 Journal of neuroscience : the official journal of the Society for Neuroscience
711 30:9477-9487.
712 Maslov S, Sneppen K (2002) Specificity and stability in topology of protein networks.
713 Science (New York, NY) 296:910-913.
714 Mayoral SR, Omar G, Penn AA (2009) Sex differences in a hypoxia model of preterm
715 brain damage. Pediatric research 66:248-253.
716 Meng C, Brandl F, Tahmasian M, Shao J, Manoliu A, Scherr M, Schwerthoffer D,
717 Bauml J, Forstl H, Zimmer C, Wohlschlager AM, Riedl V, Sorg C (2014)
718 Aberrant topology of striatum's connectivity is associated with the number of
719 episodes in depression. Brain : a journal of neurology 137:598-609.
720 Mullen KM, Vohr BR, Katz KH, Schneider KC, Lacadie C, Hampson M, Makuch RW,
721 Reiss AL, Constable RT, Ment LR (2011) Preterm birth results in alterations in
722 neural connectivity at age 16 years. NeuroImage 54:2563-2570.
723 Murphy K, Bodurka J, Bandettini PA (2007) How long to scan? The relationship
724 between fMRI temporal signal to noise ratio and necessary scan duration.
725 NeuroImage 34:565-574.

726 Narberhaus A, Lawrence E, Allin MP, Walshe M, McGuire P, Rifkin L, Murray R,
727 Nosarti C (2009) Neural substrates of visual paired associates in young adults
728 with a history of very preterm birth: alterations in fronto-parieto-occipital
729 networks and caudate nucleus. NeuroImage 47:1884-1893.
730 Northam GB, Liegeois F, Tournier JD, Croft LJ, Johns PN, Chong WK, Wyatt JS,
731 Baldeweg T (2012) Interhemispheric temporal lobe connectivity predicts
732 language impairment in adolescents born preterm. Brain : a journal of neurology
733 135:3781-3798.
734 Nosarti C (2013) Structural and functional brain correlates of behavioral outcomes
735 during adolescence. Early human development 89:221-227.
736 Nosarti C, Giouroukou E, Healy E, Rifkin L, Walshe M, Reichenberg A, Chitnis X,
737 Williams SC, Murray RM (2008) Grey and white matter distribution in very
738 preterm adolescents mediates neurodevelopmental outcome. Brain : a journal of
739 neurology 131:205-217.
740 Nosarti C, Reichenberg A, Murray RM, Cnattingius S, Lambe MP, Yin L, MacCabe J,
741 Rifkin L, Hultman CM (2012) Preterm birth and psychiatric disorders in young
742 adult life. Archives of general psychiatry 69:E1-8.
743 Pandit AS, Ball G, Edwards AD, Counsell SJ (2013a) Diffusion magnetic resonance
744 imaging in preterm brain injury. Neuroradiology 55 Suppl 2:65-95.
745 Pandit AS, Robinson E, Aljabar P, Ball G, Gousias IS, Wang Z, Hajnal JV, Rueckert D,
746 Counsell SJ, Montana G, Edwards AD (2013b) Whole-Brain Mapping of
747 Structural Connectivity in Infants Reveals Altered Connection Strength
748 Associated with Growth and Preterm Birth. Cerebral cortex (New York, NY :
749 1991) Advance online publication. doi: 10.1093/cercor/bht086.
750 Percival DB, Walden AT (2006) Wavelet methods for time series analysis: Cambridge

751 University Press.
752 Power JD, Barnes KA, Snyder AZ, Schlaggar BL, Petersen SE (2012) Spurious but
753 systematic correlations in functional connectivity MRI networks arise from
754 subject motion. NeuroImage 59:2142-2154.
755 Power JD, Mitra A, Laumann TO, Snyder AZ, Schlaggar BL, Petersen SE (2014)
756 Methods to detect, characterize, and remove motion artifact in resting state
757 fMRI. NeuroImage 84:320-341.
758 Riegel K, Orth B, Wolke D, Osterlund K (1995) Die Entwicklung gefährdet geborener
759 Kinder bis zum 5 Lebensjahr. Stuttgart (Germany): Thieme.
760 Rubinov M, Sporns O (2010) Complex network measures of brain connectivity: uses
761 and interpretations. NeuroImage 52:1059-1069.
762 Seeley WW, Menon V, Schatzberg AF, Keller J, Glover GH, Kenna H, Reiss AL,
763 Greicius MD (2007) Dissociable intrinsic connectivity networks for salience
764 processing and executive control. The Journal of neuroscience : the official
765 journal of the Society for Neuroscience 27:2349-2356.
766 Siegel JS, Power JD, Dubis JW, Vogel AC, Church JA, Schlaggar BL, Petersen SE
767 (2014) Statistical improvements in functional magnetic resonance imaging
768 analyses produced by censoring high-motion data points. Human brain mapping
769 35:1981-1996.
770 Smith SM, Vidaurre D, Beckmann CF, Glasser MF, Jenkinson M, Miller KL, Nichols
771 TE, Robinson EC, Salimi-Khorshidi G, Woolrich MW, Barch DM, Ugurbil K,
772 Van Essen DC (2013) Functional connectomics from resting-state fMRI. Trends
773 in cognitive sciences 17:666-682.
774 Sorg C, Manoliu A, Neufang S, Myers N, Peters H, Schwerthoffer D, Scherr M,
775 Muhlau M, Zimmer C, Drzezga A, Forstl H, Bauml J, Eichele T, Wohlschlager

776 AM, Riedl V (2013) Increased intrinsic brain activity in the striatum reflects
777 symptom dimensions in schizophrenia. Schizophrenia bulletin 39:387-395.
778 Sporns O (2014) Contributions and challenges for network models in cognitive
779 neuroscience. Nature neuroscience 17:652-660.
780 Sporns O, Tononi G, Kotter R (2005) The human connectome: A structural
781 description of the human brain. PLoS computational biology 1:e42.
782 Srinivasan L, Dutta R, Counsell SJ, Allsop JM, Boardman JP, Rutherford MA,
783 Edwards AD (2007) Quantification of deep gray matter in preterm infants at
784 term-equivalent age using manual volumetry of 3-tesla magnetic resonance
785 images. Pediatrics 119:759-765.
786 Swanson LW (2000) Cerebral hemisphere regulation of motivated behavior. Brain
787 research 886:113-164.
788 Tononi G, Sporns O, Edelman GM (1994) A measure for brain complexity: relating
789 functional segregation and integration in the nervous system. Proceedings of the
790 National Academy of Sciences of the United States of America 91:5033-5037.
791 van den Heuvel MP, Kersbergen KJ, de Reus MA, Keunen K, Kahn RS, Groenendaal
792 F, de Vries LS, Benders MJ (2014) The Neonatal Connectome During Preterm
793 Brain Development. Cerebral cortex (New York, NY : 1991) Advance online
794 publication. doi: 10.1093/cercor/bhu095.
795 van den Heuvel MP, Sporns O, Collin G, Scheewe T, Mandl RC, Cahn W, Goni J,
796 Hulshoff Pol HE, Kahn RS (2013) Abnormal rich club organization and
797 functional brain dynamics in schizophrenia. JAMA psychiatry 70:783-792.
798 Van Dijk KR, Sabuncu MR, Buckner RL (2012) The influence of head motion on
799 intrinsic functional connectivity MRI. NeuroImage 59:431-438.
800 Vinall J, Grunau RE, Brant R, Chau V, Poskitt KJ, Synnes AR, Miller SP (2013)

801 Slower postnatal growth is associated with delayed cerebral cortical maturation
802 in preterm newborns. Science translational medicine 5:168ra168.
803 Von Aster M, Neubauer A, Horn R (2006) Wechsler Intelligenztest für Erwachsene
804 (WIE). Deutschsprachige Bearbeitung und Adaptation des WAIS-III von David
805 Wechsler. Frankfurt/Main (Germany): Harcourt Test Services.
806 Watts DJ, Strogatz SH (1998) Collective dynamics of 'small-world' networks. Nature
807 393:440-442.
808 White TP, Symington I, Castellanos NP, Brittain PJ, Froudist Walsh S, Nam KW, Sato
809 JR, Allin MP, Shergill SS, Murray RM, Williams SC, Nosarti C (2014)
810 Dysconnectivity of neurocognitive networks at rest in very-preterm born adults.
811 NeuroImage Clinical 4:352-365.
812 Wolke D, Meyer R (1999) Cognitive status, language attainment, and prereading
813 skills of 6-year-old very preterm children and their peers: the Bavarian
814 Longitudinal Study. Developmental medicine and child neurology 41:94-109.
815 Wong HS, Edwards P (2013) Nature or nurture: a systematic review of the effect of
816 socio-economic status on the developmental and cognitive outcomes of children
817 born preterm. Maternal and child health journal 17:1689-1700.
818 Zubiaurre-Elorza L, Soria-Pastor S, Junque C, Segarra D, Bargallo N, Mayolas N,
819 Romano-Berindoague C, Macaya A (2011) Gray matter volume decrements in
820 preterm children with periventricular leukomalacia. Pediatric research
821 69:554-560.
822

823 **Tables:**

824 ***Table 1. Birth-related and adult neuropsychological data.***

	Very preterm (VPT) N=64	Full-term (FT) N=72	*p*-value
Neonatal characteristics at birth			
Gender (m/f)	38/26	48/24	0.379
Gestational age (week)	29.64 ± 1.26 (26 - 31)	40.00 ± 0.77 (39 - 42)	< 0.0001*
Birth weight (gram)	1294.53 ± 349.93 (630 - 2070)	3440.68 ± 491.48 (1950 - 4200)	< 0.0001*
Neonatal medical risk (DINTI)	59.10 ± 29.85 (11 - 149)	Not applicable	
Family socioeconomic status (SES)	1.98 ± 0.75 (1 - 3)	1.97 ± 0.73 (1- 3)	0.924
Adulthood characteristics at scan			
Age (year)	26.34 ± 0.52 (25.51 - 27.55)	26.35 ± 0.42 (25.56 - 27.69)	0.890
Full-scale IQ	92.94 ± 13.03 (64 - 131)	102.54 ± 12.72 (77 - 130)	< 0.0001*
Location (MUC/BN)	40/24	49/23	0.497
MRI center			
MUC	40	49	0.497
BN1	4	9	0.216
BN2	20	14	0.1125

825 Group comparisons: two-sample t-tests for gestational age, birth weight, DINTI, socioeconomic status,
826 term age, and IQ; χ^2-test for gender, location and detailed MRI centers. Data are presented as mean ±
827 standard deviation as well as the range (in brackets). VPT very preterm group; FT full-term group;
828 DINTI Duration of Intensive Neonatal Treatment Index; MUC Munich, referring to the MRI scanner in
829 Munich; BN Bonn; BN1 referring to 1st scanner in Bonn and BN2 referring to 2nd scanner in Bonn. To
830 note, one VPT (MUC) had no recording for IQ and another VPT (BN) for DINTI. IQ, intelligence
831 quotient.
832

833 ***Table 2. Global structural, functional connectivity and network topology.***
834

Measures	VP	FT	*p*-value
Global structural volume			
Gray matter	0.440 ± 0.023	0.443 ± 0.019	0.1754
White matter	0.403 ± 0.018	0.411 ± 0.017	0.0153*
Cerebrospinal fluid	0.157 ± 0.021	0.146 ± 0.013	0.0005*
Total brain	1369.703 ± 130.009	1467.757 ± 145.723	< 0.0001*
Global functional connectivity			
Global strength	0.218 ± 0.047	0.209 ± 0.036	0.3244
Global diversity	0.025 ± 0.007	0.024 ± 0.005	0.3082
Global integration	0.221 ± 0.050	0.214 ± 0.041	0.4288
Global functional network topology			
Characteristic path length	2.103 ± 0.139	2.080 ± 0.114	0.3269
Clustering coefficient	0.513 ± 0.043	0.508 ± 0.033	0.4217
Small-worldness	1.426 ± 0.232	1.437 ± 0.208	0.4066
Global efficiency	0.593 ± 0.012	0.595 ± 0.010	0.3495
Local efficiency	0.706 ± 0.018	0.706 ± 0.018	0.3982

835 Data are presented as mean ± standard deviation. Total gray matter, white matter, and cerebrospinal
836 fluid volumes were corrected for individual variability of brain size by dividing total brain volume.
837 Network topology metrics were averaged over whole range of costs (0.05-0.5). Group comparisons of
838 global measures were carried out by permutation tests with 100,000 iterations. For global structural
839 changes, covariates of gender and MRI center were ruled out from group comparisons of global
840 structural volumes. For global functional changes, covariates of gender, MRI center, and total gray
841 matter volume were controlled for group comparisons of global functional connectivity and network
842 topology. * denotes significant group difference ($p < 0.05$). Abbreviations: VP very preterm group; FT
843 full-term group.
844

845 ***Table 3. Group differences of nodal network topology between VP and FT.***
846

Lobe	Region	Side	Topological measure	VP	FT	*p*-value
Functional integration						
VP > FT						
Frontal	IFG, pars triangularis	L	Deg	27.89 ± 11.00	22.81 ± 7. 17	0.0008
			E_{nodal}	0.58 ± 0.07	0.56 ± 0.05	0.002
	IFG, pars opercularis	L	Deg	31.12 ± 9.75	27.44 ± 8.99	0.004
			BC	142.24 ± 98.05	108.86 ± 67.89	0.005
			E_{nodal}	0.60 ± 0.06	0.58 ± 0.06	0.003
Temporal	ITG, posterior division	L	Deg	25.69 ± 16.22	18.03 ± 12.89	0.003
			E_{nodal}	0.56 ± 0.10	0.51 ± 0.08	0.002
Subcortical	Amygdala	L	Deg	29.18 ± 12.03	24.79 ± 9.51	0.006
			E_{nodal}	0.58 ± 0.07	0.56 ± 0.06	0.006
VP < FT						
Frontal	SMA	L	Deg	27.38 ± 12.50	32.63 ± 9.49	0.006
			E_{nodal}	0.57 ± 0.09	0.61 ± 0.06	0.005
		R	Deg	27.05 ± 13.49	33.75 ± 10.09	0.002
			E_{nodal}	0.57 ± 0.09	0.62 ± 0.06	0.001
Temporal	ITG, temporo-occi pital part	L	BC	84.19 ± 65.31	121.97 ± 100.16	0.002
	Heschl's Gyrus (includes H1 and H2)	R	Deg	29.62 ± 9.79	34.64 ± 7.75	0.001
			BC	63.25 ± 53.68	87.27 ± 62.28	0.005
			E_{nodal}	0.59 ± 0.07	0.62 ± 0.04	0.001
	Planum Temporale	R	Deg	35.87 ± 9.67	39.60 ± 8.98	0.005
			E_{nodal}	0.63 ± 0.06	0.65 ± 0.05	0.004
Occipital	Lingual Gyrus	L	E_{nodal}	0.61 ± 0.07	0.64 ± 0.05	0.004
	Occipital Fusiform Gyrus	L	Deg	33.02 ± 9.67	37.56 ± 9.87	0.003
			BC	125.85 ± 83.53	185.20 ± 143.91	0.002
			E_{nodal}	0.61 ± 0.06	0.64 ± 0.06	0.004
Subcortical	Caudate	R	Deg	18.24 ± 9.34	23.32 ± 10.89	0.004
			E_{nodal}	0.51± 0.08	0.55 ± 0.08	0.004
	Thalamus	R	Deg	22.49 ± 10.61	27.13 ± 12.04	0.008
			BC	82.25 ± 66.73	116.60 ± 99.24	0.007
Functional segregation						
VP > FT						
Temporal	ITG, posterior division	L	$E_{nodalloc}$	0.66 ± 0.16	0.57 ± 0.18	0.002
Parietal	SPL	L	$E_{nodalloc}$	0.71 ± 0.12	0.66 ± 0.10	0.002
Subcortical	Hippocampus	R	$E_{nodalloc}$	0.71 ± 0.10	0.67 ± 0.13	0.003

VP < FT						
Frontal	SMA	L	$E_{nodalloc}$	0.70 ± 0.12	0.77 ± 0.08	< 0.0001
		R	$E_{nodalloc}$	0.69 ± 0.13	0.76 ± 0.07	< 0.0001
Occipital	LOC, inferior division	L	$E_{nodalloc}$	0.72 ± 0.10	0.76 ± 0.06	0.003
Subcortical	Caudate	R	$E_{nodalloc}$	0.59 ± 0.17	0.67 ± 0.12	0.005

Permutation tests with 100,000 iterations were used for group comparison of nodal network topology. Reported group differences of functional integration and segregation were significant for $p<0.009$ based on False Positive Correction for multiple comparison. Group comparisons were controlled for gender, MRI center, and total gray matter volume. Nodal network scores were averaged over cost range 0.05-0.50 and reported as mean ± SD. VP very preterm group; FT full-term group; R right; L left; Functional integration was reflected by nodal betweenness-centrality (BC), nodal degree (Deg), and nodal efficiency (E_{nodal}). Functional segregation was reflected by nodal local efficiency ($E_{nodalloc}$). Inferior Frontal Gyrus (IFG), Inferior Temporal Gyrus (ITG), Supplementary Motor Cortex (SMA), Superior Parietal Lobule (SPL), Lateral Occipital Cortex (LOC)

858 ***Table 4. Altered nodal network topology separately associated with preterm birth***
859 ***and cognitive outcome in adulthood.***

Lobe	Region/node	Side	Topological measure	Parameters	r	*p*-value
Association with preterm birth						
Frontal	IFG, pars triangularis	L	Deg	Birth weight	0.3939	0.0024
				DINTI	-0.3162	0.0176
			E_{nodal}	Birth weight	0.3902	0.0027
				DINTI	-0.3382	0.0108
	SMA	L	$E_{nodalloc}$	Gestational age	0.3027	0.0221
Temporal	Heschl's Gyrus (includes H1 and H2)	R	Deg	Gestational age	0.2843	0.0321
	Planum Temporale	R	Deg	DINTI	-0.3552	0.0072
			E_{nodal}	DINTI	-0.3254	0.0144
	ITG, posterior division	L	E_{nodal}	DINTI	0.2667	0.0469
Parietal	SPL	L	$E_{nodalloc}$	Gestational age	0.3056	0.0208
				DINTI	-0.2994	0.025
Association with cognitive outcome in adulthood						
Frontal	IFG, pars triangularis	L	Deg	IQ	0.2497	*0.0587*
			E_{nodal}	IQ	0.2879	0.0299
Subcortical	Amygdala	L	Deg	IQ	-0.4086	0.0016
			E_{nodal}	IQ	-0.397	0.0022
	Hippocampus	R	$E_{nodalloc}$	IQ	-0.3675	0.0049
	Caudate	R	$E_{nodalloc}$	IQ	0.2673	0.0464

860
861 Partial correlation analyses were applied within very preterm group between altered nodal topological
862 measures, neonatal variables (i.e. gestational age, birth weight, and neonatal medical risk), and IQ in
863 adulthood. Confounding influence of covariates was ruled out, including gender, imaging center, total
864 gray matter volume, socioeconomic status. P values of significant linear dependence were in bold when
865 $p < 0.05$. Gray colored results refer to compensation-like mode of network metric change. R right; L
866 left; Deg nodal Degree; E_{nodal} nodal efficiency; $E_{nodalloc}$ nodal local efficiency; DINTI Duration of
867 Neonatal Treatment Index. Inferior Frontal Gyrus (IFG), Inferior Temporal Gyrus (ITG),
868 Supplementary Motor Cortex (SMA), Superior Parietal Lobule (SPL).
869

870 **Figures and legends:**

871

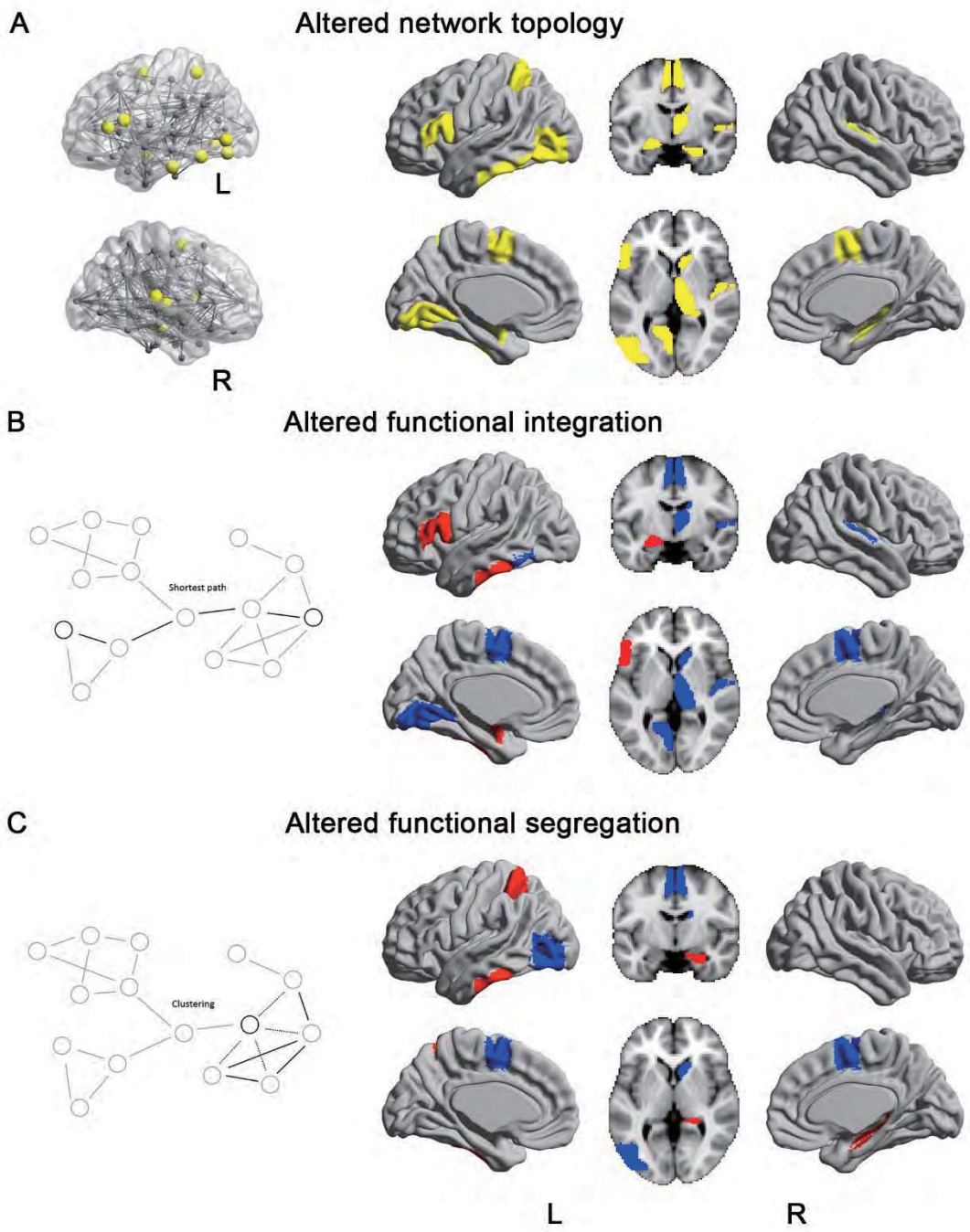

872

873

874 **Figure 1. Altered nodal network topology in VPT adults.** (A) Group comparisons
875 between VPT and FT adults were performed for each node and each network
876 topology metric reflecting functional integration and segregation by the use of

permutation tests (n=100,000) controlling for gender, center, SES, and total gray matter volume ($p<0.009$ based on False Positive Correction for multiple comparisons). Brain regions of significant group difference were colored in yellow and visually illustrated on both node-edge view and surface view by using *BrainNet Viewer* and on axial slice view with MNI standard structural image from *fslview*. (B, C) Group differences of functional integration (i.e. degree, betweenness, and efficiency) and segregation (i.e. nodal local efficiency) were shown separately. Blue/red colors indicate decreased/increased nodal network metrics in VPT adults.

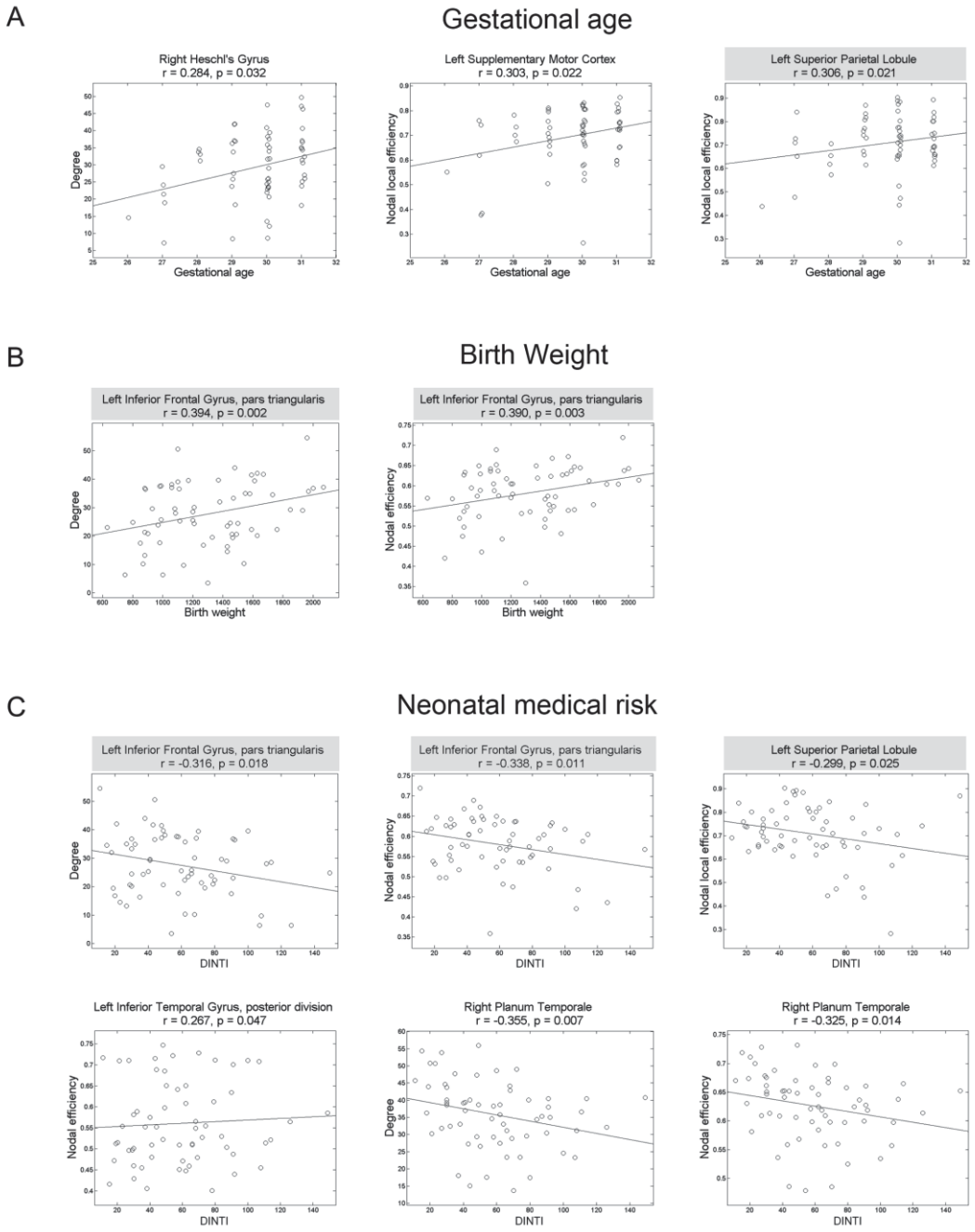

Figure 2. Correlation between altered nodal network metrics and birth-related parameters in VPT adults. Within VPT adults, linear relationships between altered nodal network metrics and birth-related variables were studied by the use of partial correlation analysis ($p < 0.05$), specifically for gestational age (A), birth weight (B), and neonatal medical risk (C). Analysis was controlled for gender, MRI center, total

gray matter volume, SES, and IQ. For visualization, scatter plots show data of the VPT group (circles slightly jittered according to x axis for better visualization), and fitting lines illustrate positive or negative correlations between nodal network metrics and birth-related parameters. Gray-colored headlines indicate a compensation-like mode of network metric change.

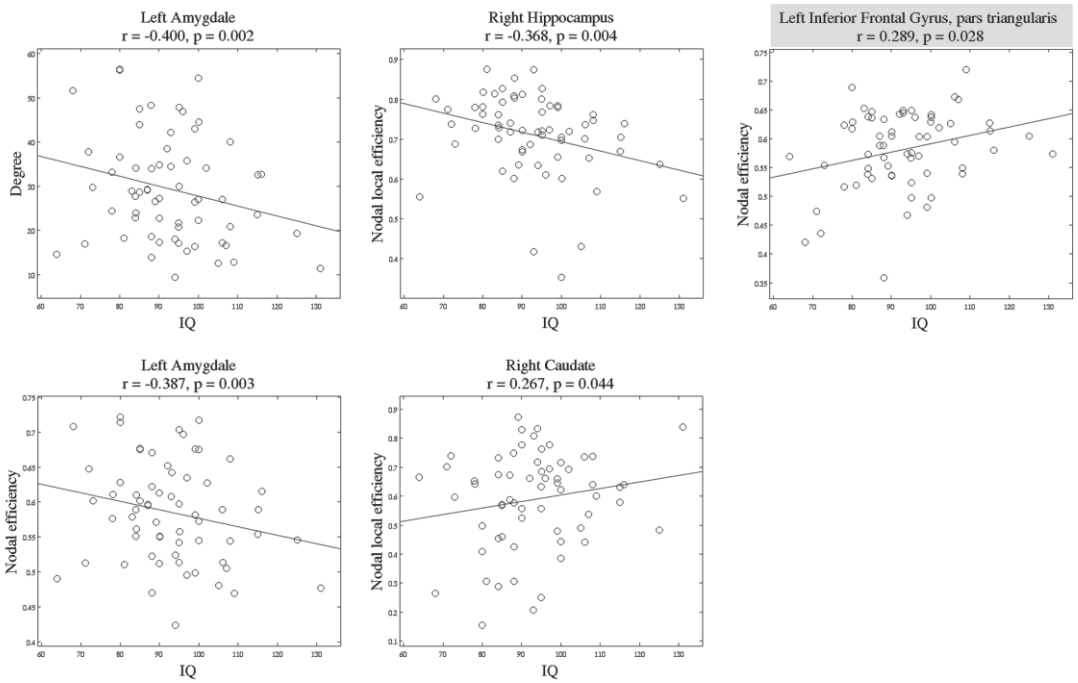

Figure 3. Correlation between altered nodal network metrics and general cognitive performance in VPT adults. Within VPT adults, linear relationships between altered nodal network metrics and IQ were studied by the use of partial correlation analysis ($p < 0.05$). Analysis was controlled for gender, MRI center, total gray matter volume, SES, and birth-related parameters. For visualization, scatter plots show data of the VPT group (circles slightly jittered according to x axis for better visualization), and fitting lines illustrate positive or negative correlations between

nodal network metrics and IQ. Gray-colored headlines indicate a compensation-like mode of network metric change.

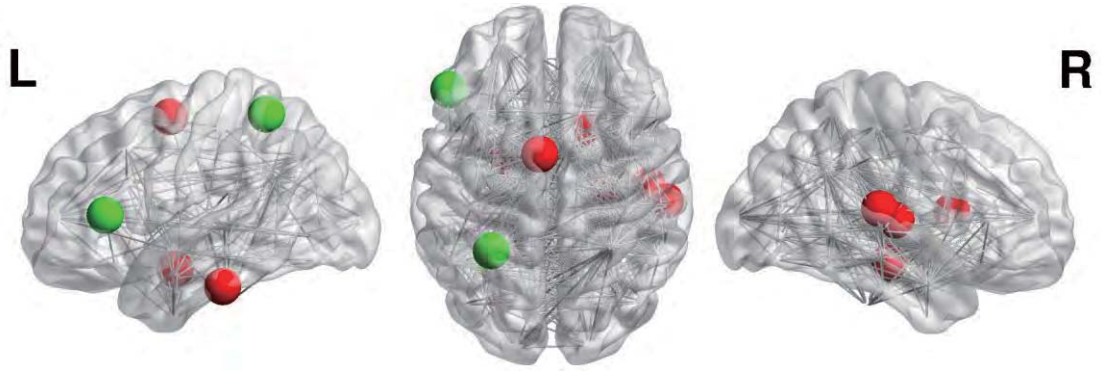

Figure 4. Nodes of the functional connectome with lesion- or compensation-like altered network metric in VPT adults. Summary figure for results of Figures 2 and 3 with respect to lesion-like (in red) and compensation-like (in green) mode of altered network metric. For increased network metrics in VPT adults in comparison with FT adults, a lesion-like mode of network change was proposed when the more the network metric is increased the more prematurity (or the more neonatal medical risk or the less IQ). Complementary, for increased network metrics a compensation-like mode of change was proposed when the more the metric is increased the less prematurity (or the less neonatal medical risk or the higher IQ). For decreased network metrics, lesion- and compensation-like mode of change were analogously specified but with inverse relationships between metric decrease and prematurity (or neonatal medical risk, or IQ).

Manuscript 3

Extensive and interrelated subcortical white and gray matter alterations in preterm born adults (submitted)

Title page

Title:

Extensive and interrelated subcortical white and gray matter alterations in preterm born adults

Authors and Affiliations:

Meng, C.[1,4,5], Bäuml, JG.[1,4], Daamen, M.[6,7], Jaekel, J.[8,10], Neitzel, J.[1,4,5], Scheef, L.[6], Busch, B.[7], Baumann, N.[8], Boecker, H.[6], Zimmer, C.[1], Bartmann, P.[7], Wolke, D.[8,9], Wohlschläger, A. M.[1,3,4,5], Sorg, C.[1,2,4]

Departments of [1]Neuroradiology, [2]Psychiatry, [3]Neurology, [4]TUM-Neuroimaging Center of Klinikum rechts der Isar, Technische Universität München TUM, Ismaninger Strasse 22, 81675 Munich, Germany; [5]Graduate School of Systemic Neurosciences GSN, Ludwig-Maximilians-Universität, Biocenter, Großhaderner Strasse 2, 82152 Munich, Germany; [6]Functional Neuroimaging Group, Department of Radiology, University Hospital Bonn, Germany; [7]Department of Neonatology, University Hospital Bonn, Germany; [8]Department of Psychology, University of Warwick, Coventry, United Kingdom; [9]Warwick Medical School, University of Warwick, Coventry, United Kingdom; [10]Department of Developmental Psychology, Ruhr-University Bochum, Bochum, Germany.

Corresponding Author

Christian Sorg, Department of Psychiatry and Neuroradiology, Klinikum rechts der

Isar, Ismaninger Strasse 22, 81675 Munich, Germany, phone: +49 89 4140-7631, fax: -7665, c.sorg@lrz.tu-muenchen.de

Number of words: Abstract 248; main text 4683

Number of figures: 5

Number of tables: 1

Number of Supplementary material: 1

Abstract:

Preterm birth is a leading cause for impaired neurocognitive development with an increased risk for persistent cognitive deficits in adulthood. In newborns, preterm birth is associated with interrelated white matter (WM) alterations and deep gray (GM) matter loss; however, little is known about persistence and relevance of these subcortical brain changes. We tested the hypothesis that the pattern of correspondent subcortical WM and GM changes is present in preterm born adults and has a lesion-like nature i.e. it predicts lowered general cognitive performance.

Eighty-five preterm and 69 matched term born adults were assessed by diffusion- and T1-weighted MRI and cognitive testing. Main outcome measures were fractional anisotropy of water diffusion to map WM integrity, GM volume to map GM integrity, and full-scale total IQ to measure cognitive performance.

In preterm born adults reduced fractional anisotropy was widely distributed ranging from cerebellum to brainstem to hemispheres. GM volume was reduced in the thalamus, striatum, temporal cortices, and increased in the cingulate cortices. Fractional anisotropy reductions were associated with GM loss in thalamus and striatum, with correlation patterns for both regions extensively overlapping in the white matter of brainstem and hemispheres. For overlap regions, fractional anisotropy was positively related with both gestational age and total IQ.

Results provide evidence for extensive, interrelated, and adverse white and gray matter subcortical changes in preterm born adults. Data suggest persistent lesion-like changes of subcortical-cortical connectivity after preterm delivery, which may reflect

the specifically altered developmental trajectory of brain organization in preterm born persons.

Key words:

Preterm born adults, diffusion MRI, white matter, voxel-based morphometry, gray matter, IQ

Introduction

Preterm birth is defined by delivery before 37 weeks of gestation are completed. The global prevalence of preterm birth is more than 10% (i.e. about 15 million preterm newborns per year), with increasing rates in almost all countries due to medical progress, the increased number of births to mothers over 35y and other factors (Blencowe et al. 2012). Preterm born individuals have an increased risk for growth failure, higher levels of morbidity, impaired neurocognitive development, and adverse psychiatric, cognitive, academic, and socio-economic outcomes, featured by increasing deficits with lower gestational age (D'Onofrio et al. 2013; Jaekel et al. 2013; Katz et al. 2013; Milligan 2010; Nosarti et al. 2012). Therefore, it is highly important to better understand mechanistic effects of premature birth on the brain, their developmental trajectories and outcomes, in order to specify focused prevention and treatment. Since subcortical brain changes stand out in preterm born newborns (Ball et al. 2013a; Ball et al. 2012; Boardman et al. 2010; Inder et al. 2005; Pierson et al. 2007; Srinivasan et al. 2007; Zubiaurre-Elorza et al. 2011), the current study focuses on the potential persistence of such subcortical changes into adulthood, and asks for their functional relevance.

According to neurobiological research in animal models, premature birth leads to disturbed brain maturation primarily by both impaired maturation of GABAergic interneurons and aberrant development of oligodendro- and astrocytes, with the latter being critical for white matter myelination (Dean et al. 2013; Komitova et al. 2013; Ritter et al. 2013) (for the review see (Deng 2010; Salmaso et al. 2014)).

Neuropathological and in-vivo imaging studies in preterm newborns have demonstrated that most prominent changes concern distributed white matter (WM) alterations that – when strong enough - coincide with gray matter (GM) alterations in the ventral brain, particularly in subcortical structures such as thalamus and striatum, following the pattern "the more WM changes the more GM changes" (Ball et al. 2013a; Ball et al. 2012; Boardman et al. 2010; Inder et al. 2005; Pierson et al. 2007; Srinivasan et al. 2007; Zubiaurre-Elorza et al. 2011). For example, studies using immunocytochemical approaches revealed specific impairments in white matter axons and subplate neurons that guide thalamo-cortical neuronal development (Haynes et al. 2008; Kinney et al. 2012; Robinson et al. 2006), while studies using in-vivo T1- and diffusion-weighted MRI found thalamus volume reductions being linked with impaired WM microstructure (Ball et al. 2013a; Ball et al. 2012).

These findings indicate a substantial effect of preterm birth on the subcortical brain and therefore on subcortical-cortical connectivity, i.e. the connectivity pattern among deep brain subcortical nuclei and the isocortex with strong focus on lower cortical layers 4-6, which realize cortical in- and output functions (Douglas and Martin 2004; Swanson 2000). While the evidence for a specific impact of preterm birth on the subcortical brain in newborns is definitive, less is known about the long-term trajectory of these subcortical changes and their functional relevance in terms of general cognitive outcome. The current study hypothesized that the pattern of correspondent subcortical white and gray matter changes, which reflects the general impact of preterm delivery on subcortical-cortical connectivity, persists into adulthood

and has a lesion-like nature i.e. it is associated with lowered general cognitive performance. Initial support for this hypothesis is given by separate findings of either subcortical white or gray matter alterations in preterm born children (Constable et al. 2008; Counsell et al. 2008; Fischi-Gomez et al. 2014), adolescents (Mullen et al. 2011; Northam et al. 2012; Nosarti et al. 2008; Skranes et al. 2007), and young adults (Allin et al. 2011; Eikenes et al. 2011).

To test our hypothesis of correspondent, persistent, and adverse WM and GM alterations after preterm birth, we used diffusion- and T1-weighted MRI and cognitive testing in a sample of 85 preterm and 69 matched term-born adults at the age of 26. To estimate white matter microstructural integrity, fractional anisotropy (FA) of water diffusion was investigated by tract-based spatial statistics; to estimate gray matter integrity, gray matter volume (GMV) was examined by voxel-based morphometry. Regional GMV, prematurity at birth, and full-scale IQ representing general cognitive capabilities were explored in relation to white matter FA values.

Materials and methods

Participants

Participants were recruited as part of the prospective Bavarian Longitudinal Study (BLS) (Riegel et al. 1995; Wolke and Meyer 1999). The BLS investigates a geographically defined whole-population sample of neonatal at-risk children and healthy term controls. All live-birth infants that were born between January 1985 and March 1986 in southern Bavaria and required admission to neonatal units in 17 children's hospitals within the first ten days of life, comprised the target sample (Wolke and Meyer 1999). A total of 7505 children (10.6% of all live births) were classified as neonatal at-risk children, whereupon 2759 children were born before 37 weeks of gestation (Riegel et al. 1995). During the same period, 916 healthy term infants (>36 weeks gestation; normal postnatal care) born in the same hospitals were recruited as control infants. Over the following years, subjects of both groups were repeatedly assessed with neurological and psychological test batteries, and parental interviews to monitor development. Full eligible sample details of the follow-up are provided elsewhere (Gutbrod et al. 2000; Wolke and Meyer 1999). At 26 years of age and based on the study design of preterm population versus reference population, 435 preterm born and 329 control subjects were invited for a follow-up assessment, selected to be similar regarding the overall distribution of gender, family socioeconomic status (SES), and maternal age. Of this sample, 183 subjects underwent structural T1- and Diffusion-weighted MRI before May 2012. MRI assessments were carried out at two different sites: The Department of

Neuroradiology, Klinikum Rechts der Isar, Technische Universität München, Germany (N=96), and the Department of Radiology, University Hospital Bonn, Germany (N=58). The study was approved by the local ethics committees of the Klinikum rechts der Isar and University Hospital Bonn. All study participants gave written informed consent and received travel expenses and a payment for attendance. Only participants free from medication and from psychiatric or neurological diseases at the assessment or qualitative signs of brain injury (such as vetriculomegaly or polymicrogyria) were included in the study. Individual MRI images were carefully examined by visual inspection to exclude subjects with apparent or aberrant artifacts. Finally, 85 preterm subjects (PT; born before 37 week of gestation) and 69 term-born subjects (FT; aged 25 to 27 years) entered the following analysis. For more details, see Table 1.

Birth-related variables. Gestational age (GA) was estimated from maternal reports of the last menstrual period and serial ultrasounds during pregnancy. In cases where the two measures differed by more than two weeks, clinical assessment with the Dubowitz method was applied (Dubowitz et al. 1970). Maternal age and birth weight (BW) was obtained from obstetric records. Neonatal medical complications were assessed with a standardized optimality scoring system (OPTN, neonatal optimality) including 21 items (e.g. ventilation or intubation, sepsis, neonatal seizures, cerebral haemorrhage) (Prechtl 1967; Wolke and Meyer 1999). Items were coded as 1 (non-optimal) or 0 (optimal) with the higher value being less optimal, and summarized.

Cognitive assessment

Cognitive assessment was carried out by independent trained psychologists using the German version of the Wechsler Adult Intelligence scale-III (WAIS-III) (Von Aster et al. 2006). The assessors were blind to group membership. Three preterm participants who had missing IQ data were not included in IQ-related analysis. In this study, full-scale IQ was utilized in the following analysis to represent global cognitive functioning at the average age of 26 years.

Imaging data acquisition

Whole brain T1- and diffusion-weighted imaging data were acquired on 3T Philips scanners in Munich and Bonn with standard 8 channel head coils by using consistent sequences and parameter settings across scanners. To account for different scanners in data analyses, additional covariates, namely MRI center, were defined for across subject analysis: (i) Achieva TX in Munich center, coded as MUC = [0 0 1]; (ii) Achieva TX in Bonn center, coded as BN1 = [1 0 0]; (iii) Ingenia in Bonn center, coded as BN2 = [0 1 0]. Diffusion images were acquired using a single-shot spin-echo echo-planar imaging sequence, resulting in one non-diffusion weighted image (b = 0 s/mm^2) and 32 diffusion weighted images (b = 1000 s/mm^2, 32 non-colinear gradient directions) covering whole brain with: echo time (TE) = 47 ms, repetition time (TR) = 20150 ms, flip angle = 90°, field of view = 224 x 224 mm², matrix = 112 x 112, 75 transverse slices, slice thickness = 2 mm, and 0 mm interslice gap, voxel size = 2 x 2 x 2 mm^3. A whole-head, high-resolution T1-weighted image was acquired using a

magnetization-prepared rapid acquisition gradient echo sequence following parameters: echo time (TE) = 3.9 ms, repetition time (TR) = 7.7 ms, flip angle = 15°, field of view = 256 x 256 mm^2, matrix = 256 x 256, 180 sagittal slices, slice thickness = 1 mm, and 0 mm interslice gap, voxel size = 1 x 1 x 1 mm^3. All acquired MRI images were visually inspected for excessive head motion, apparent or aberrant artifacts and excluding subjects with poor data quality. In addition, T2 images were examined to exclude potential lesions and white matter abnormalities by experienced radiologists.

White matter tract-based spatial statistics (TBSS)

Diffusion data was preprocessed using FSL's FDT toolbox (http://fsl.fmrib.ox.ac.uk/fsl/fslwiki/FDT, Version 5.0.3). First, brain-tissue extraction was carried out by removing skull and non-brain tissue. Eddy-current distortion and head motion were corrected by coregistrating all diffusion-weighted images to b0 image. Secondly, after voxel-by-voxel diffusion tensors were estimated, fractional anisotropy (FA), which is a measure of the directional coherence for white matter tracts was calculated for each voxel of the whole brain. Thirdly, Tract-Based Spatial Statistics (Smith et al. 2006), was carried out for voxelwise statistical analysis of white matter microstructure following: (i) nonlinear alignment of each participant's FA image to the standard Montreal Neurological Institute (MNI152) space template; (ii) calculation of the mean of all aligned FA images; (iii) generation of the across-all mean FA skeleton which represents centers of white matter tracts common to all

subjects, considered as the group-specific template; (iv) projection of each subject's aligned FA image onto the mean FA skeleton using the threshold (FA > 0.2), to obtain individual maps. Individual mean, axial, and radical diffusivity (MD, AD, and RD) maps were further obtained by using the same mean FA skeleton and *tbss_non_FA* script. Over whole brain white matter, the general linear model and nonparametric inference (5000 random permutations) was adopted to perform statistical analyses on FA as well as MD, AD, and RD between different participant groups by using FSL's *randomize* script (http://fsl.fmrib.ox.ac.uk/fsl/fslwiki/randomise/) (Anderson and Robinson 2001). By using contrast setting, covariate effects of gender and MRI center were ruled out from group comparisons based on the permutation test. The statistical threshold was set as $P_{FWE} < 0.05$ with multiple comparison correction by threshold-free cluster enhancement (TFCE) (Smith and Nichols 2009). In addition to group-generated white matter skeleton mask, FSL's standard FA skeleton was employed in validation analysis of between-group differences.

Gray matter voxel-based morphometry (VBM)

As described recently (Meng et al. 2013), we used the VBM8 toolbox (http://dbm.neuro.uni-jena.de/vbm.html) to analyze brain structure via voxel-based morphometry. T1-weighted images were corrected for bias-field inhomogeneity, registered using linear (12-parameter affine) and nonlinear transformations, and tissue-classified into gray matter, white matter, and cerebrospinal fluid within the same generative model. The segmented and normalized images were modulated to

account for structural changes resulting from the normalization process, indicating gray matter volume. Here, we only considered non-linear changes so that further analyses did not have to account for differences in head size. Finally images were smoothed with a Gaussian kernel of 8mm (FWHM). For group comparisons, voxel-wise two-sample t-tests were performed ($p < 0.05$ FWE-corrected, cluster extent 30) controlling for gender and MRI center. Group comparisons resulted in discrete clusters of gray matter locating in different anatomical structures, which were used as regions-of-interest (ROI) for following correlation analysis (for details see Tab. S2).

Correlation analysis

Across preterm born adults only, linear relationships between white matter FA values and variables of interest were investigated in affected white matter tracts of reduced FA (see Fig. 1) based on voxelwise correlation analysis. Three types of variables of interest were analyzed respectively in correlation analysis: (i) mean gray matter volumes of affected gray matter areas derived from volumetric analysis (see Fig. 2 and Tab. S2), in order to test the hypothesis of correspondent subcortical white and gray matter changes in preterm born adults; (ii) variables representing the degree of prematurity, indexed by gestational age, birth weight, and OPTN, in order to link directly observed FA changes, which were linked with subcortical gray matter changes, with preterm birth; (iii) general cognitive performance, indexed by full-scale IQ, in order to test for the lesion-like nature of white matter changes that were linked with subcortical gray matter changes. The last correlation analysis was controlled for

gestational age to be independent of confounding effects of prematurity on cognitive performance and white matter integrity. The statistical significance was tested by permutation tests using the same approach as for group comparisons based on white matter tract skeleton ($P_{FWE} < 0.05$, TFCE corrected). The influence of gender and MRI center was always ruled out as covariates of no interest in correlation analysis.

Results:

Lowered general cognitive performance in preterm born adults.

To investigate general cognitive outcomes after preterm birth in adulthood, 85 preterm born adults and 69 term born controls, who were matched for age, gender, maternal age, and family socio-economic status, were assessed by full-scale IQ testing (Table 1). Significantly reduced IQ was found in preterm born adults ($P < 0.005$).

Widely distributed changes of WM integrity in preterm born adults.

To investigate white matter integrity after preterm birth, TBSS analysis of diffusion-weighted MRI data was performed in preterm and term born adults. The analysis revealed a consistent whole brain WM skeleton of 133,223 voxels across all subjects. In this skeleton, preterm born adults had widely distributed FA reduction ($P_{FWE} < 0.05$, TFCE corrected), regarding 34.01% of skeleton voxels and all main white matter tracts due to FSL's JHU white matter tractography atlas (Fig. 1; Tab. S1A). Reduced FA was identified in a large contiguous cluster (45192 voxels, maxima at -26, -79, 0 mm of MNI coordinates) and a smaller cluster (112 voxels, maxima at -7, 22, -6 mm of MNI coordinates), which included: (1) association tracts such as bilateral cingulum bundles, superior and inferior longitudinal, inferior fronto-occipital and uncinate fasciculi; (2) projection fibers encompassing bilateral corticospinal tracts and anterior thalamic radiations; (3) commissural fibers including the genu, body and splenium of the corpus callosum.

To test whether FA changes reflect consistent impairments in WM integrity in preterm born adults, further aspects of diffusivity were analyzed. We found widespread changes in mean, axial, and radial diffusivity that were consistent with the pattern of reduced FA, indicating substantial WM integrity reductions in preterm born adults (Tab. S1B). More specifically, widespread changes of MD, AD, and RD were identified largely overlapping with altered FA, with affected voxels in 20.33%, 16.84%, and 26.38%, respectively, of the whole WM skeleton (Tab. S1B). Results of the validation analysis employing standard skeleton mask from FSL toolbox indicated consistent WM tract changes in preterm born adults.

Aberrant subcortical and cortical GM volume in preterm born adults.

To investigate global and regional brain volumes including GM volumes, VBM of T1-weighted MRI was used. Concerning global brain volumes of different brain tissues, we found for preterm//term born adults the following measurements: mean total intracranial volume (TIV) [SD], 1385[145] //1464 [146] mm^3; mean WM/TIV-ratio [SD], 0.40 [0.02] // 0.41 [0.02]; mean CSF/TIV-ratio [SD], 0.15 [0.02] // 0.15 [0.01]; mean GM/TIV-ratio [SD], 0.44 [0.02] // 0.44 [0.02]. Concerning group differences, TIV and WM/TIV-ratio were reduced, CSF/TIV-ratio was increased (two-sample t-test, $P < 0.05$, Bonferroni corrected), and GM/TIV-ratio was unchanged ($P_{uncorr} > 0.6$) in preterm born adults.

Concerning regional gray matter volumes, preterm born adults had decreased GM volume in bilateral thalamus, striatum (putamen and caudate), middle temporal gyrus

extending to superior and inferior temporal gyrus, right superior occipital gyrus, fusiform gyrus, and hippocampus ($P_{FWE} < 0.05$ and cluster size over 30 voxels). Increased GM volume was found in bilateral posterior and anterior cingulate, left temporal pole and right lower fusiform gyrus (Fig. 2; Tab. S2).

One should note that these clusters of aberrant GM volume were used to define GM ROIs for further voxelwise correlation analysis between GM volume changes and FA changes in preterm born adults. Homologue clusters next to brain midline (for example thalamus or cingulate cortex) were integrated within one ROI, respectively, while lateral cortical clusters were used to define separate ROIs. Correlation analyses for thalamus and striatum GMV were used to test the study's hypothesis, while correlation analyses for cortical GMVs were used to test specificity of interrelated aberrant subcortical GM and WM integrity.

Interrelated impaired WM and GM integrity in the subcortical brain of preterm born adults.

In preterm born adults, widely distributed FA reductions were positively correlated with GM volume reductions for subcortical gray matter regions (i.e. largely overlapping correlation patterns for both thalamus and striatum GMV) ($P_{FWE} < 0.05$, TFCE corrected) (Fig. 3; Tab. S3). In detail, 35.05% of FA alterations were linked with mean GM volume of bilateral thalamus in preterm born adults, specifically in white matter tracts of the right inferior fronto-occipital fasciculus, bilateral anterior thalamic radiation, right corticospinal tract, and the body and splenium of the corpus

callosum. Similarly, 44.55% of FA alterations were correlated with mean GM volume of bilateral striatum in preterm born adults, specifically in the left inferior fronto-occipital fasciculus, right inferior fronto-occipital fasciculus, bilateral anterior thalamic radiation and right corticospinal tract, and the body and splenium of the corpus callosum (Fig. 3; Tab. S3). For other cortical regions with altered GM volume, reduced GMV of temporal cortices was linked with reduced FA in the corpus callosum and thalamus radiation (Fig. S3)

To test whether FA reductions in preterm born adults, which were significantly associated with thalamus and striatum GMV reductions, were directly linked with preterm birth, voxelwise correlation analyses between FA and prematurity indices were performed but limited to those WM tracts that were associated with deep gray matter nuclei in preterm adults. Specifically we tested whether observed WM integrity changes were linked with gestational age, birth weight, and OPTN. In preterm born adults, reduced FA was positively correlated with lower gestational age ranging from 25 to 36 weeks ($P_{FWE} < 0.05$, TFCE corrected), in tracts of the inferior fronto-occipital fasciculus, anterior thalamic radiation and the corpus callosum (Fig. 4; Tab. S4). Birth weight was positively correlated with FA in left anterior thalamic radiation, right inferior fronto-occipital, inferior longitudinal, and uncinate fasciculi (Fig. S1; Tab. S4). Concerning neonatal medical complications, OPTN was significantly negatively correlated with FA in tracts of the inferior fronto-occipital fasciculus, anterior thalamic radiation and the corpus callosum (Fig. S2; Tab. S4).

Correspondent subcortical WM impairments were associated with lowered general cognitive performance in preterm born adults.

Next we tested whether WM changes, which were linked with subcortical GM volume reductions, have a lesion-like nature. We found that in preterm born adults, impaired white matter integrity, which was interrelated with striatal and thalamus GM volume reduction, was positively correlated with lowered adult general cognitive performance (i.e. full-scale IQ) controlled for gestational age; such positive correlation was present in the right inferior fronto-occipital, inferior longitudinal and uncinate fasciculi, right anterior thalamic radiation and corticospinal tract ($P_{FWE} < 0.05$, TFCE corrected; Fig. 5; Tab. S5).

Discussion:

To test the hypothesis of interrelated and lesion-like subcortical white and gray matter changes in preterm born adults, we assessed 85 pre- and 69 term born adults of about 26 years with diffusion- and T1-weighted MRI and cognitive testing. Extensive reduced WM integrity in cerebellum, brainstem, and both hemispheres was found in preterm born adults, which was significantly related with reduced striatal and thalamic GM volume. The degree of reduced tract integrity of correspondent WM changes was associated with lowered full-scale IQ of preterm born adults, confirming a lesion-like nature of correspondent subcortical changes. Data provide first evidence for extensive, interrelated and adverse white and gray matter subcortical changes in preterm born adults. Results suggest lasting impairments of subcortical-cortical connectivity after preterm delivery.

Extensive and interrelated subcortical WM and GM impairments in preterm born adults.

In preterm born adults, we found positive correlations between FA and GM volume reductions, particularly for the striatum and thalamus (Fig. 3; Tab. S3). More specifically, reduced FA was found in large parts of WM in cerebellum, brainstem, and both hemispheres (Fig. 1; Tab. S1), in line with findings in preterm newborns (Anjari et al. 2007), children (Constable et al. 2008), adolescents (Skranes et al. 2007), and young adults (i.e. 19y) (Allin et al. 2011; Eikenes et al. 2011). Aberrant GM volume was found in subcortical thalamus and striatum and in temporal and cingulate cortex (Fig. 2; Tab. S2), in line with findings in preterm newborns (Padilla

et al. 2014; Srinivasan et al. 2007), children (Peterson et al. 2000), and adolescents (Nagy et al. 2009; Nosarti et al. 2008), and young adults (i.e. 19y) (Nosarti et al. 2009). Interrelated reduced FA and reduced GMV for both thalamus and striatum covered large parts of hemispheric WM (Fig. 3). Most of these FA changes overlapped with changes in other aspects of diffusivity such as mean diffusivity (Tab. S1), demonstrating impaired WM tract integrity. Variance of reduced FA in WM regions, whose tract integrity was related to reduced subcortical GM volume, was linearly associated with gestational age and neonatal medical complications (Fig. 4, S2; Tab. S4), demonstrating that the observed effect of correspondent subcortical changes is likely due to preterm birth. Notably, patterns of positive FA-GMV correlation for both striatum and thalamus overlapped extensively in the two hemispheres and the brainstem. The significant link between subcortical WM and GM changes indicates that a large part of WM changes is systematically linked to subcortical GM changes, suggesting that subcortical-cortical connectivity (i.e. the striato/thalamo-cortical connectivity system) is substantially and persistently affected by preterm birth. This finding is complementary to our previous finding in preterm born adults of correspondently altered GM intrinsic functional connectivity and structural integrity specifically for thalamus and striatum (Bäuml et al. 2014). It matches findings in preterm newborns of impaired structural connectivity between thalamus and several cortical regions (Ball et al. 2013a; Ball et al. 2012; Pandit et al. 2013). In summary, our result provides evidence that extensive and interrelated disruptions of subcortical white and gray matter are present in preterm born adults,

suggesting that observed changes of the thalamo/striato-cortical system in preterm newborns are of lasting nature.

From a cellular point of view, translational research in animal models of preterm birth suggests that prematurity affects primarily GABAergic interneurons and myelination based on oligodendrocytes and astroglia (for review (Salmaso et al. 2014)). Both regulating interneurons and WM myelination is critical for development and functioning of fine-tuned connectivity (Bartos et al. 2007; Huang et al. 2007), and both are impaired after preterm birth (Kinney et al. 2012; Salmaso et al. 2014). In particular, our data suggest that impaired myelination of WM tracts supporting subcortical-cortical connectivity is persistently impaired after preterm birth (Fig. 3, 4). Furthermore, since mainly cortical layers 4 - 6 realize cortical in- and output from or to subcortical structures (i.e. layer 4 receives most thalamic input while in layers 5 and 6, larger pyramidal output cells are located) (Douglas and Martin 2004; Swanson 2000), we speculate that correspondently altered WM changes are linked with altered organization of lower cortical layers (Ball et al. 2013b; Dean et al. 2013).

On the other hand, our finding does not exclude effects of preterm birth on cortical development of all cortical layers. For example, Dean and colleagues found aberrant dendritic arborization and synaptic density for whole cortical columns due to ischemia after preterm birth (Dean et al. 2013); in-vivo imaging of cortical diffusivity in newborns suggests that microstructure of the whole cortical system strongly depends on gestational age less than 38 weeks and is related with neurodevelopmental outcomes at age of 2y (Ball et al. 2013b). Our result adds to these findings by

demonstrating that some part of these microstructural cortical changes might link specifically and persistently with altered subcortical-cortical connectivity. Future studies (maybe e.g. applying advanced high-tesla MRI to reveal cortical layers) are necessary to test a potential link between correspondent subcortical WM/GM changes and lower layer cortical microstructure alterations after preterm birth. In particular, it would be of interest to test whether upper and lower cortical layer connectivity might have different developmental trajectories after preterm birth, possibly with different adaptive or compensatory potentials for cortical-cortical and cortical-subcortical connectivity.

Correspondent subcortical WM/GM changes after preterm birth have a lesion-like nature.

We found that reduced integrity of WM, which is correspondent with subcortical GM changes, is associated with lower full-scale IQ scores in preterm born adults, independent of gestational age (Fig. 5; Tab. S5). According to the neural basis of normal human intelligence, white matter integrity and general cognitive ability have been shown to be related with each other (Deary et al. 2006; Deary et al. 2010). Premature gestational age is well known to affect general cognitive abilities (Poulsen et al. 2013; Serenius et al. 2013), and recent study showed that reduced FA is positively correlated with IQ in young preterm adults of about 19 years, in line with our finding (Allin et al. 2011; Eikenes et al. 2011). Our result of the more WM integrity is reduced in regions, whose integrity is linked with subcortical GM

integrity, the less general cognitive performance, indicates the lesion-like nature of correspondent subcortical white and gray matter changes after preterm birth. Accounting for similar interrelated GM-WM changes in preterm newborns (Ball et al. 2013a; Ball et al. 2012; Boardman et al. 2010; Inder et al. 2005; Pierson et al. 2007; Srinivasan et al. 2007; Zubiaurre-Elorza et al. 2011), we suggest that particularly subcortical connectivity changes after preterm birth may contribute to the individual risk for adverse neurodevelopmental outcomes. This idea has two implications. On the one hand, subcortical changes after preterm delivery may serve as marker for at-risk cognitive outcomes. On the other hand and in line with the finding that in preterm newborns, cortical-subcortical connectivity is reduced compared to term-born infants while cortical-cortical connectivity is relatively increased (Ball et al. 2014), cortical-cortical connectivity may have a differential developmental trajectory in comparison with subcortical connectivity with some potential for compensatory adaption. Future longitudinal studies are necessary to test both suggestions.

Methodological issues.

First, the current sample that participated in this MRI study consisted of preterm born adults with lower neonatal complications and higher IQ. Individuals with more complications or severe impairments in the initial BLS sample were more likely to be excluded in initial screening for MRI or declined to participate in MRI scanning. Thus the reported differences compared to term born controls are conservative estimates of the true differences in subcortical WM integrity in preterm born adults. Second, the

current sample size is large (n = 154), covers a wide range of gestational ages in preterm and term born adults (25 – 36 and 37 – 42 weeks), and has a long follow-up period, which may enhance the generalization power and robustness of our findings. Third, other evidence for correspondent WM/GM changes after preterm birth, e.g. using direct region-to-region connectivity, is missing in the present study. Such spatially more focused approach is based on tractography and was beyond the current study's aim. Fourth, we chose general cognitive performance assessed by full-scale IQ as the measure for general cognitive outcome. The integrative nature of such general cognitive outcome measure prevents detailed analysis of more specific cognitive long-term effects of preterm birth and its subcortical correlates. However, full-scale IQ shows high ecological validity for predicting life time academic and economic success.

Conclusion

The current study provides evidence for the persistence of extensive and interrelated subcortical white and gray matter disruptions in preterm born adults that predict lower general cognitive outcome. Data implicate that primarily subcortical indices at birth may help to evaluate the extent of adverse consequences of preterm birth.

Acknowledgements:

We thank all current and former members of the Bavarian Longitudinal Study Group who contributed to general study organization, recruitment, and data collection, management and subsequent analyses, including (in alphabetical order): Stephan Czeschka, Claudia Grünzinger, Christian Koch, Diana Kurze, Sonja Perk, Andrea Schreier, Antje Strasser, Julia Trummer, and Eva van Rossum. We are grateful to the staff of the Department of Neuroradiology in Munich and the Department of Radiology in Bonn for their help in data collection. Most importantly, we thank all our study participants and their families for their efforts to take part in this study.

This study was supported by Chinese Scholar Council (CSC, File No: 2010604026 to C.M.), German Federal Ministry of Education and Science (BMBF 01ER0801 to P.B. and D.W., BMBF 01EV0710 to A.M.W., BMBF 01ER0803 to C.S.) and the Kommission für Klinische Forschung, Technische Universität München (KKF 8765162 to C.S).

Conflict of Interest

All authors report no biomedical financial interests or potential conflicts of interest.

References:

Allin MP et al. (2011) White matter and cognition in adults who were born preterm PloS one 6:e24525 doi:10.1371/journal.pone.0024525

Anderson MJ, Robinson J (2001) Permutation tests for linear models Australian & New Zealand Journal of Statistics 43:75-88

Anjari M, Srinivasan L, Allsop JM, Hajnal JV, Rutherford MA, Edwards AD, Counsell SJ (2007) Diffusion tensor imaging with tract-based spatial statistics reveals local white matter abnormalities in preterm infants NeuroImage 35:1021-1027 doi:10.1016/j.neuroimage.2007.01.035

Bäuml JG et al. (2014) Correspondence Between Aberrant Intrinsic Network Connectivity and Gray-Matter Volume in the Ventral Brain of Preterm Born Adults Cerebral cortex (New York, NY : 1991) doi:10.1093/cercor/bhu133

Ball G et al. (2014) Rich-club organization of the newborn human brain Proceedings of the National Academy of Sciences of the United States of America 111:7456-7461 doi:10.1073/pnas.1324118111

Ball G et al. (2013a) The influence of preterm birth on the developing thalamocortical connectome Cortex; a journal devoted to the study of the nervous system and behavior 49:1711-1721 doi:10.1016/j.cortex.2012.07.006

Ball G et al. (2012) The effect of preterm birth on thalamic and cortical development Cerebral cortex (New York, NY : 1991) 22:1016-1024 doi:10.1093/cercor/bhr176

Ball G et al. (2013b) Development of cortical microstructure in the preterm human brain Proceedings of the National Academy of Sciences of the United States of America 110:9541-9546 doi:10.1073/pnas.1301652110

Bartos M, Vida I, Jonas P (2007) Synaptic mechanisms of synchronized gamma oscillations in inhibitory interneuron networks Nature reviews Neuroscience 8:45-56 doi:10.1038/nrn2044

Blencowe H et al. (2012) National, regional, and worldwide estimates of preterm birth rates in the year 2010 with time trends since 1990 for selected countries: a systematic analysis and implications Lancet 379:2162-2172 doi:10.1016/s0140-6736(12)60820-4

Boardman JP et al. (2010) A common neonatal image phenotype predicts adverse neurodevelopmental outcome in children born preterm NeuroImage 52:409-414 doi:10.1016/j.neuroimage.2010.04.261

Constable RT et al. (2008) Prematurely born children demonstrate white matter microstructural differences at 12 years of age, relative to term control subjects: an investigation of group and gender effects Pediatrics 121:306-316 doi:10.1542/peds.2007-0414

Counsell SJ et al. (2008) Specific relations between neurodevelopmental abilities and white matter microstructure in children born preterm Brain : a journal of neurology 131:3201-3208 doi:10.1093/brain/awn268

D'Onofrio BM, Class QA, Rickert ME, Larsson H, Langstrom N, Lichtenstein P (2013) Preterm birth and mortality and morbidity: a population-based quasi-experimental study JAMA psychiatry 70:1231-1240 doi:10.1001/jamapsychiatry.2013.2107

Dean JM et al. (2013) Prenatal cerebral ischemia disrupts MRI-defined cortical microstructure through disturbances in neuronal arborization Science translational medicine 5:168ra167 doi:10.1126/scitranslmed.3004669

Deary IJ, Bastin ME, Pattie A, Clayden JD, Whalley LJ, Starr JM, Wardlaw JM (2006) White matter integrity and cognition in childhood and old age Neurology 66:505-512 doi:10.1212/01.wnl.0000199954.81900.e2

Deary IJ, Penke L, Johnson W (2010) The neuroscience of human intelligence differences Nature reviews Neuroscience 11:201-211 doi:10.1038/nrn2793

Deng W (2010) Neurobiology of injury to the developing brain Nature reviews Neurology 6:328-336 doi:10.1038/nrneurol.2010.53

Douglas RJ, Martin KA (2004) Neuronal circuits of the neocortex Annual review of neuroscience 27:419-451 doi:10.1146/annurev.neuro.27.070203.144152

Dubowitz LM, Dubowitz V, Goldberg C (1970) Clinical assessment of gestational age in the newborn infant The Journal of pediatrics 77:1-10

Eikenes L, Lohaugen GC, Brubakk AM, Skranes J, Haberg AK (2011) Young adults born preterm with very low birth weight demonstrate widespread white matter alterations on brain DTI NeuroImage 54:1774-1785 doi:10.1016/j.neuroimage.2010.10.037

Fischi-Gomez E et al. (2014) Structural Brain Connectivity in School-Age Preterm Infants Provides Evidence for Impaired Networks Relevant for Higher Order Cognitive Skills and Social Cognition Cerebral cortex (New York, NY : 1991) doi:10.1093/cercor/bhu073

Gutbrod T, Wolke D, Soehne B, Ohrt B, Riegel K (2000) Effects of gestation and birth weight on the growth and development of very low birthweight small for gestational age infants: a matched group comparison Archives of disease in childhood Fetal and neonatal edition 82:F208-214

Haynes RL, Billiards SS, Borenstein NS, Volpe JJ, Kinney HC (2008) Diffuse axonal injury in periventricular leukomalacia as determined by apoptotic marker fractin Pediatric research 63:656-661 doi:10.1203/PDR.0b013e31816c825c

Huang ZJ, Di Cristo G, Ango F (2007) Development of GABA innervation in the cerebral and cerebellar cortices Nature reviews Neuroscience 8:673-686

doi:10.1038/nrn2188

Inder TE, Warfield SK, Wang H, Huppi PS, Volpe JJ (2005) Abnormal cerebral structure is present at term in premature infants Pediatrics 115:286-294 doi:10.1542/peds.2004-0326

Jaekel J, Baumann N, Wolke D (2013) Effects of gestational age at birth on cognitive performance: a function of cognitive workload demands PloS one 8:e65219 doi:10.1371/journal.pone.0065219

Katz J et al. (2013) Mortality risk in preterm and small-for-gestational-age infants in low-income and middle-income countries: a pooled country analysis Lancet 382:417-425 doi:10.1016/S0140-6736(13)60993-9

Kinney HC, Haynes RL, Xu G, Andiman SE, Folkerth RD, Sleeper LA, Volpe JJ (2012) Neuron deficit in the white matter and subplate in periventricular leukomalacia Annals of neurology 71:397-406 doi:10.1002/ana.22612

Komitova M et al. (2013) Hypoxia-induced developmental delays of inhibitory interneurons are reversed by environmental enrichment in the postnatal mouse forebrain The Journal of neuroscience : the official journal of the Society for Neuroscience 33:13375-13387 doi:10.1523/jneurosci.5286-12.2013

Meng C et al. (2013) Aberrant topology of striatum's connectivity is associated with the number of episodes in depression Brain : a journal of neurology doi:10.1093/brain/awt290

Milligan DW (2010) Outcomes of children born very preterm in Europe Archives of disease in childhood Fetal and neonatal edition 95:F234-240 doi:10.1136/adc.2008.143685

Mullen KM et al. (2011) Preterm birth results in alterations in neural connectivity at age 16 years NeuroImage 54:2563-2570 doi:10.1016/j.neuroimage.2010.11.019

Nagy Z et al. (2009) Structural correlates of preterm birth in the adolescent brain Pediatrics 124:e964-972 doi:10.1542/peds.2008-3801

Northam GB et al. (2012) Interhemispheric temporal lobe connectivity predicts language impairment in adolescents born preterm Brain : a journal of neurology 135:3781-3798 doi:10.1093/brain/aws276

Nosarti C et al. (2008) Grey and white matter distribution in very preterm adolescents mediates neurodevelopmental outcome Brain : a journal of neurology 131:205-217 doi:10.1093/brain/awm282

Nosarti C et al. (2012) Preterm birth and psychiatric disorders in young adult life Archives of general psychiatry 69:E1-8 doi:10.1001/archgenpsychiatry.2011.1374

Nosarti C, Shergill SS, Allin MP, Walshe M, Rifkin L, Murray RM, McGuire PK (2009) Neural substrates of letter fluency processing in young adults who were born very preterm: alterations in frontal and striatal regions NeuroImage 47:1904-1913 doi:10.1016/j.neuroimage.2009.04.041

Padilla N, Alexandrou G, Blennow M, Lagercrantz H, Aden U (2014) Brain Growth Gains and Losses in Extremely Preterm Infants at Term Cerebral cortex (New York, NY : 1991) doi:10.1093/cercor/bht431

Pandit AS et al. (2013) Whole-Brain Mapping of Structural Connectivity in Infants Reveals Altered Connection Strength Associated with Growth and Preterm Birth Cerebral cortex (New York, NY : 1991) doi:10.1093/cercor/bht086

Peterson BS et al. (2000) Regional brain volume abnormalities and long-term cognitive outcome in preterm infants JAMA : the journal of the American Medical Association 284:1939-1947

Pierson CR, Folkerth RD, Billiards SS, Trachtenberg FL, Drinkwater ME, Volpe JJ, Kinney HC (2007) Gray matter injury associated with periventricular leukomalacia in the premature infant Acta neuropathologica 114:619-631 doi:10.1007/s00401-007-0295-5

Poulsen G, Wolke D, Kurinczuk JJ, Boyle EM, Field D, Alfirevic Z, Quigley MA (2013) Gestational age and cognitive ability in early childhood: a population-based cohort study Paediatric and perinatal epidemiology 27:371-379 doi:10.1111/ppe.12058

Prechtl HF (1967) Neurological sequelae of prenatal and perinatal complications British medical journal 4:763-767

Riegel K, Orth B, Wolke D, Osterlund K (1995) Die Entwicklung gefährdet geborener Kinder bis zum 5 Lebensjahr. Stuttgart (Germany): Thieme.

Ritter J, Schmitz T, Chew LJ, Buhrer C, Mobius W, Zonouzi M, Gallo V (2013) Neonatal hyperoxia exposure disrupts axon-oligodendrocyte integrity in the subcortical white matter The Journal of neuroscience : the official journal of the Society for Neuroscience 33:8990-9002 doi:10.1523/jneurosci.5528-12.2013

Robinson S, Li Q, Dechant A, Cohen ML (2006) Neonatal loss of gamma-aminobutyric acid pathway expression after human perinatal brain injury Journal of neurosurgery 104:396-408 doi:10.3171/ped.2006.104.6.396

Salmaso N, Jablonska B, Scafidi J, Vaccarino FM, Gallo V (2014) Neurobiology of premature brain injury Nature neuroscience 17:341-346 doi:10.1038/nn.3604

Serenius F et al. (2013) Neurodevelopmental outcome in extremely preterm infants at 2.5 years after active perinatal care in Sweden JAMA : the journal of the American Medical Association 309:1810-1820 doi:10.1001/jama.2013.3786

Skranes J et al. (2007) Clinical findings and white matter abnormalities seen on diffusion tensor imaging in adolescents with very low birth weight Brain : a journal of neurology 130:654-666 doi:10.1093/brain/awm001

Smith SM et al. (2006) Tract-based spatial statistics: voxelwise analysis of multi-subject diffusion data NeuroImage 31:1487-1505 doi:10.1016/j.neuroimage.2006.02.024

Smith SM, Nichols TE (2009) Threshold-free cluster enhancement: addressing problems of smoothing, threshold dependence and localisation in cluster inference NeuroImage 44:83-98 doi:10.1016/j.neuroimage.2008.03.061

Srinivasan L, Dutta R, Counsell SJ, Allsop JM, Boardman JP, Rutherford MA, Edwards AD (2007) Quantification of deep gray matter in preterm infants at term-equivalent age using manual volumetry of 3-tesla magnetic resonance images Pediatrics 119:759-765 doi:10.1542/peds.2006-2508

Swanson LW (2000) Cerebral hemisphere regulation of motivated behavior Brain research 886:113-164

Von Aster M, Neubauer A, Horn R (2006) Wechsler Intelligenztest für Erwachsene (WIE). Deutschsprachige Bearbeitung und Adaptation des WAIS-III von David Wechsler. Frankfurt/Main (Germany): Harcourt Test Services.

Wolke D, Meyer R (1999) Cognitive status, language attainment, and prereading skills of 6-year-old very preterm children and their peers: the Bavarian Longitudinal Study Developmental medicine and child neurology 41:94-109

Zubiaurre-Elorza L et al. (2011) Gray matter volume decrements in preterm children with periventricular leukomalacia Pediatric research 69:554-560 doi:10.1203/PDR.0b013e3182182366

Tables:

Table 1. Neonatal and adulthood data.

	Adults born preterm (PT) N=85	**Adults born term (FT) N=69**	***p*-value**
Age (year)	26.45 ± 0.53 (25.55 – 27.57)	26.35 ± 0.43 (25.56 – 27.69)	0.186
Gender (m/f)	47/38	44/25	0.288
Maternal age at birth	29.73 ± 4.67 (16 - 41)	29.30 ± 5.02 (18 - 42)	0.588
Family SES	1.99 ± 0.75	1.91 ± 0.72	0.765
Gestational age (week)	30.67 ± 2.44 (25 - 36)	39.77 ± 0.96 (37 - 42)	< 0.0001*
Birth weight (gram)	1355.76 ± 378.29 (630 - 2700)	3402.01 ± 465.37 (1950 - 4200)	< 0.0001*
OPTN	8.84 ± 2.44 (4 - 14)	0.42 ± 0.86 (0 - 5)	< 0.0001*
Full-scale IQ	95.34 ± 13.87 (64 – 132)	102.54 ± 12.08 (77 – 130)	< 0.002*
Performance IQ	90.50 ± 13.73 (61 – 118)	98.93 ± 10.20 (70 – 123)	< 0.0001*
Verbal IQ	100.17 ± 14.99 (62 – 141)	106.00 ± 14.81 (77 – 136)	0.03*
MRI Center			
MUC	50	46	0.318
BN1	4	10	0.036*
BN2	31	13	0.016*

Group comparisons: two-sample t-tests for age, maternal age, family SES, gestational age, birth weight, OPTN, and IQ; χ^2-test for gender and MRI centers (first and second MRI scanner in Bonn as well as the scanner in Munich, respectively coded as BN1, BN2, MUC). Data are presented as mean ± standard deviation as well as the range (in brackets). For data missing, 3 PT and 1 FT were not able to join IQ assessment. SES: socioeconomic status; OPTN: neonatal optimality score; IQ: intelligence quotient. *indicates significant group differences

Figures and legends:

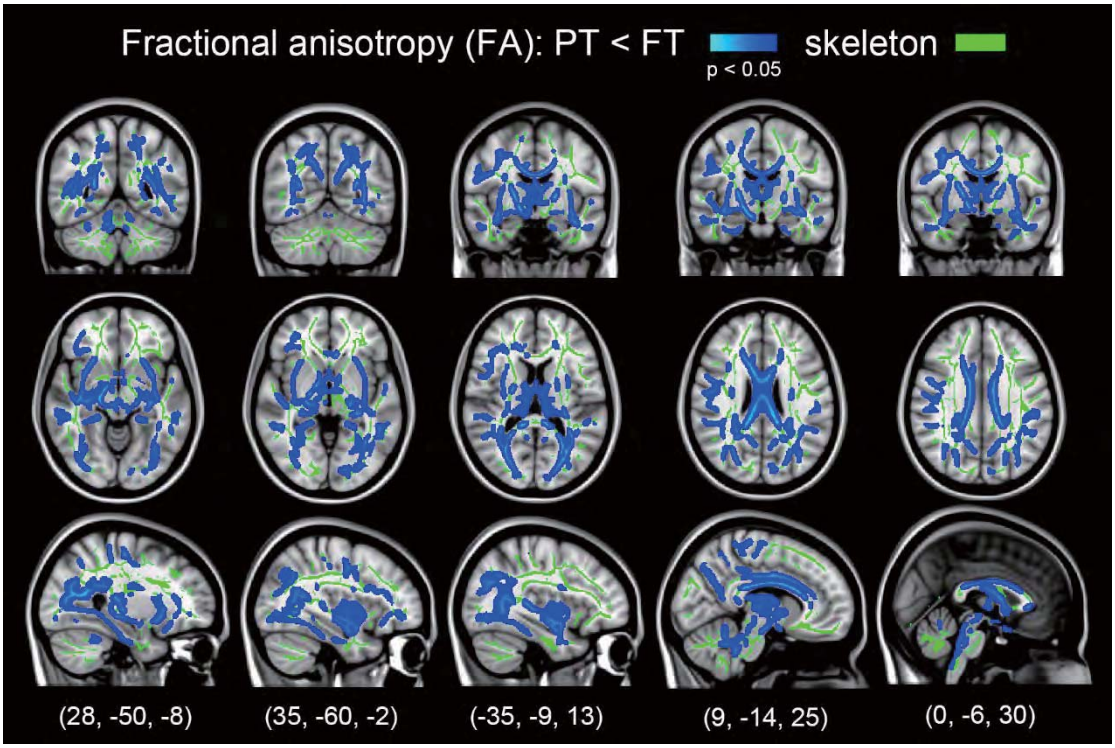

Figure 1. Whole brain white matter changes in preterm born adults. Coronal, axial, and sagittal views illustrated significant group difference of white matter fractional anisotropy (FA) between groups of preterm (PT) and term (FT) born adults, superimposed on the T1-weighted brain image of MNI152 structural standard template and group-generated white matter skeleton. Green color indicated the common skeleton over PT and FT groups. Blue color indicated reduced FA in preterm born adults (permutation test, $P < 0.05$, FWE corrected). Significant between-group difference was displayed using the *tbss_fill* script, which dilates resulted clusters in the white matter skeleton for better visualization. MNI coordinates were provided at the bottom.

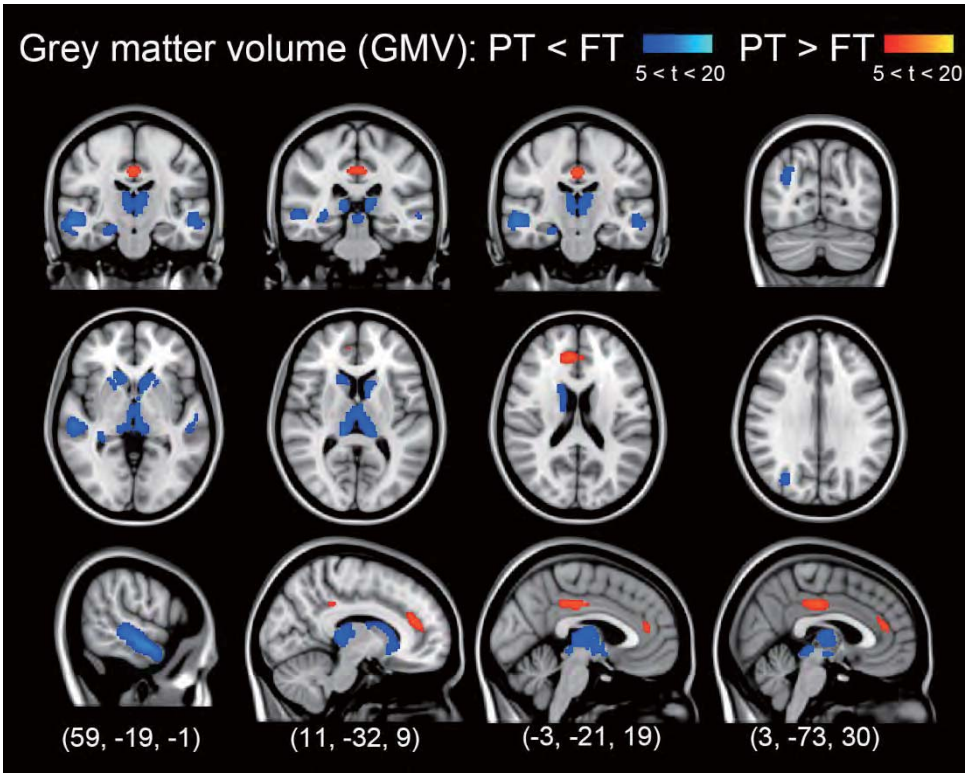

Figure 2. Whole brain gray matter changes in preterm born adults. Coronal, axial, and sagittal views illustrated significant group difference of gray matter volume (GMV) between groups of preterm (PT) and term (FT) born adults, superimposed on the T1-wegihted brain image of MNI152 structural standard template. Red-to-yellow color indicated increased GMV while blue-to-light-blue indicated reduced decreased GMV in preterm born adults (two-sample t-test, $P < 0.05$, FWE corrected). MNI coordinates were provided at the bottom.

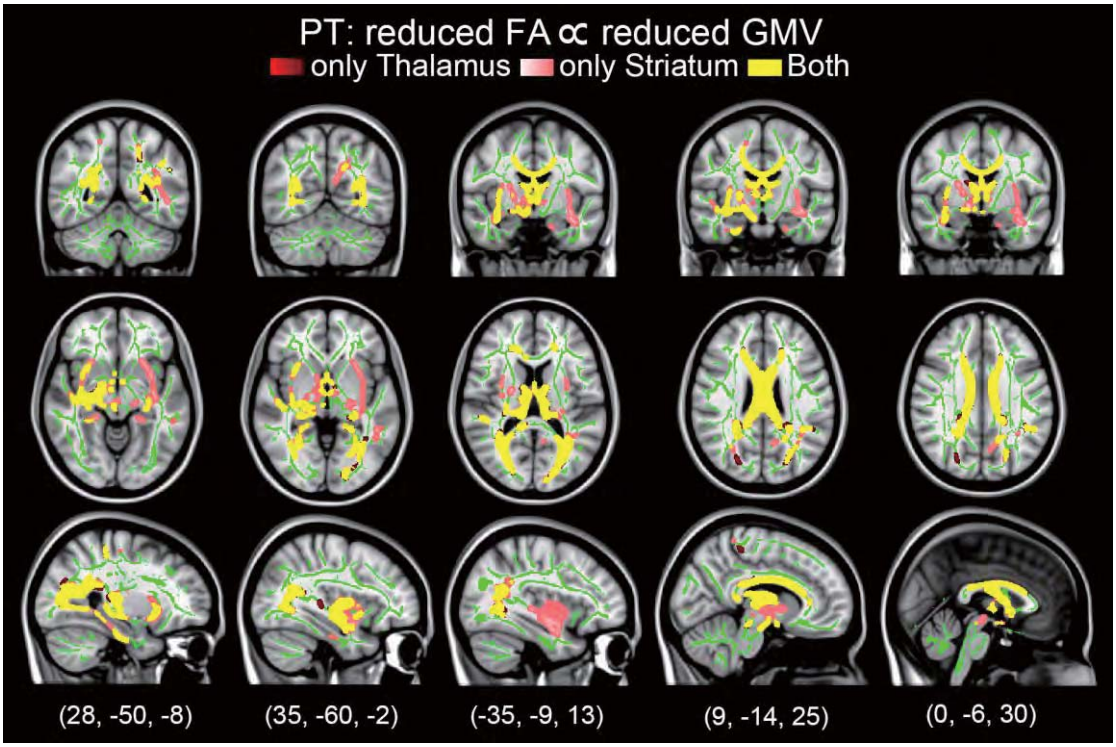

Figure 3. Correspondence between white matter changes and gray matter changes within preterm born adults. Coronal, axial, and sagittal views illustrated affected white matter tracts, in which decreasing fractional anisotropy (FA) was positively correlated with decreasing gray matter volume (GMV) in thalamus (and/or striatum) across preterm born adults (PT). Significant white matter results were dilated for better visualization and superimposed on the T1-wegihted brain image of MNI152 structural standard template. Green color indicated the common skeleton over preterm (PT) and term groups. Yellow color showed the common white matter tracts significantly associated with both thalamic and striatal GMV (permutation test, $P < 0.05$, FWE corrected). Red and pink color illustrated distinct white matter tracts significantly associated with thalamic and striatal GMV respectively. MNI coordinates were provided at the bottom.

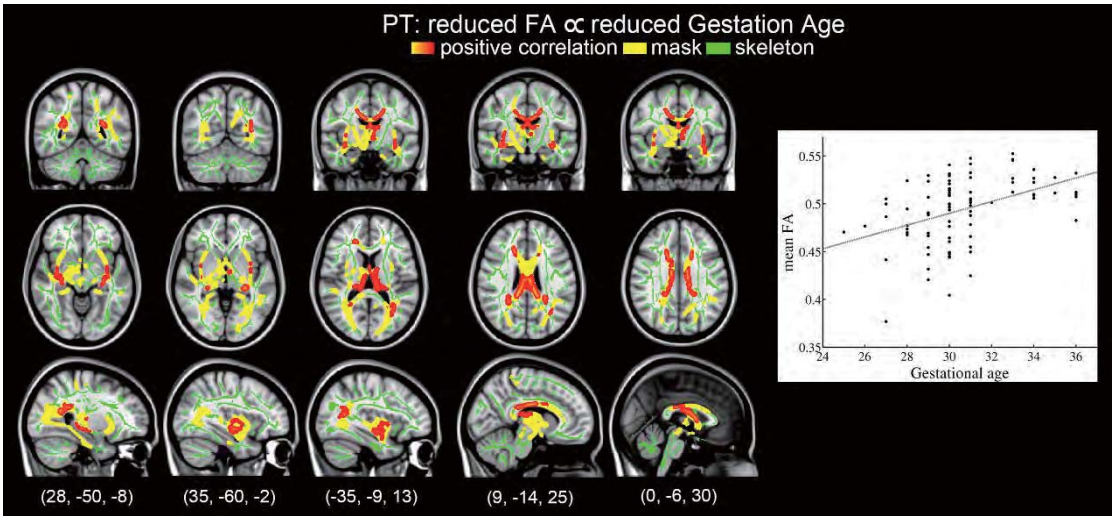

Figure 4. Correspondence between white matter changes and gestational age within preterm born adults. In the left panel, coronal, axial, and sagittal views illustrated significant positive correlation between decreasing fractional anisotropy (FA) and decreasing gestational age. Green color indicated the common skeleton over preterm (PT) and term groups. Yellow color showed affected white matter tracts with significantly reduced FA in PT group (permutation test, $P < 0.05$, FWE corrected). Red illustrated related white matter tracts where gestational age predicted FA in preterm born adults. MNI coordinates were provided at the bottom. In the right panel for visualization, in preterm born adults, gestational age and averaged FA of related white matter tracts were illustrated in the scatter plot.

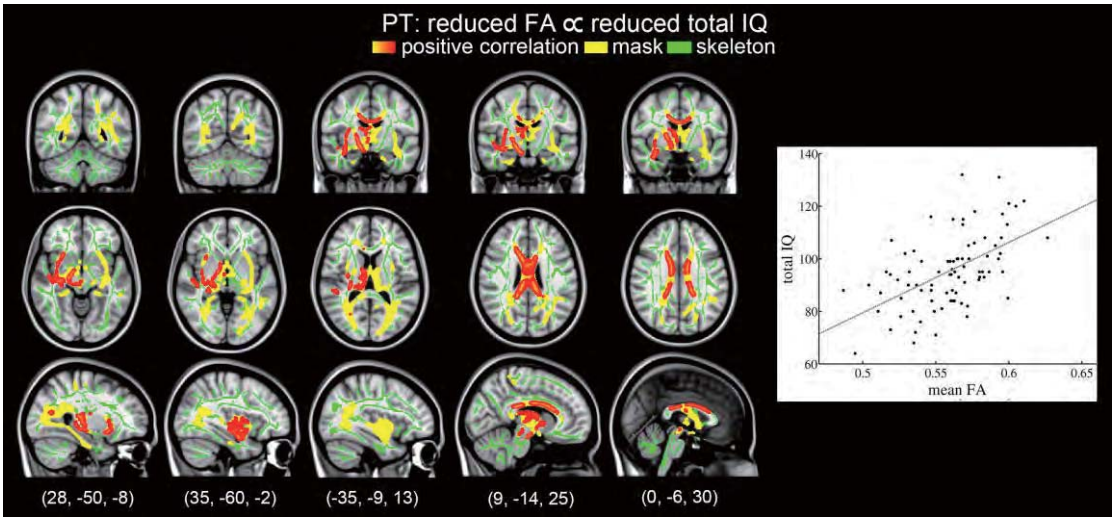

Figure 5. Correspondence between white matter changes and full-scale IQ within preterm born adults. In the left panel, coronal, axial, and sagittal views illustrated significant positive correlation between fractional anisotropy (FA) and full-scale IQ independent of gestational age. Green color indicated the common skeleton over preterm (PT) and term groups. Yellow color showed affected white matter tracts with significantly reduced FA in PT group (permutation test, $P < 0.05$, FWE corrected). Red illustrated related white matter tracts where decreasing FA was significantly positively correlated with decreasing full-scale IQ in preterm born adults controlled for gestational age. MNI coordinates were provided at the bottom. In the right panel for visualization, in preterm born adults, full-scale IQ and averaged FA of related white matter tracts were illustrated in scatter plot.

Supplementary Material for

***"Extensive and interrelated subcortical white and gray matter alterations in preterm born adults"*,**

by Meng, C. et al.

Content:

Supplementary Tables:

- *Table S1A. TBSS results: reduced FA in preterm born adults*
- *Table S1B. TBSS results: reduced FA, increased MD, aberrant AD, and increased RD in preterm born adults*
- *Table S2. VBM results: altered gray matter volumes in preterm born adults*
- *Table S3. Reduced FA associated with subcortical GMV in preterm born adults*
- *Table S4. Reduced FA associated with the degree of prematurity in preterm born adults*
- *Table S5. Reduced FA associated with total IQ in preterm born adults*

Suplementary Figures:

- *Figure S1. Correspondence between white matter changes and birth weight in preterm born adults.*
- *Figure S2. Correspondence between white matter changes and neonatal medical complications in preterm born adults.*
- *Figure S3. Correspondence between white matter changes and cortical gray matter changes in preterm born adults.*

Supplementary Tables:

Table S1A. TBSS results: reduced FA in preterm born adults

Index	JHU-atlas-defined white matter tracts[a]	Voxels (%)[b]	Mean probabilities[c]
1	Anterior thalamic radiation L	8.01	1.1070
2	Anterior thalamic radiation R	8.26	1.3571
3	Corticospinal tract L	2.29	0.3353
4	Corticospinal tract R	5.35	0.8485
5	Cingulum (cingulate gyrus) L	2.70	0.1264
6	Cingulum (cingulate gyrus) R	2.27	0.2662
7	Cingulum (hippocampus) L	1.90	0.2366
8	Cingulum (hippocampus) R	2.31	0.3008
9	Forceps major	9.14	1.3491
10	Forceps minor	1.95	0.5493
11	Inferior fronto-occipital fasciculus L	9.98	1.4036
12	Inferior fronto-occipital fasciculus R	11.42	1.6211
13	Inferior longitudinal fasciculus L	10.90	1.1801
14	Inferior longitudinal fasciculus R	8.62	0.7870
15	Superior longitudinal fasciculus L	8.39	0.7737
16	Superior longitudinal fasciculus R	11.33	1.1276
17	Uncinate fasciculus L	2.76	0.4613
18	Uncinate fasciculus R	2.07	0.2704
19	Superior longitudinal fasciculus (temporal part) L	4.60	0.3782
20	Superior longitudinal fasciculus (temporal part) R	5.90	0.4542

Group comparison of skeletonized white matter measures was carried out by nonparametric t-test (5000 permutations) using randomize in FSL, with gender and MRI center as covariates of no interest. Statistical significance was set at $P < 0.05$, FWE (familywise error rate) corrected, by using threshold-free cluster enhancement (TFCE). Resulted group difference map was converted to binary mask in order to locate and identify white matter tracts in the result mask by using atlasquery in FSL.

[a]White matter tracts according to JHU white matter tractography atlas.

[b]Percentage of voxels of the considered tract within the result mask.

[c]Mean probabilities of the considered tract within the result mask.

L/R: left/right.

Table S1B. TBSS results: reduced FA, increased MD, aberrant AD, and increased RD in preterm born adults

Tract index[a]	FA: PT < FT		MD: PT > FT		AD: PT < FT		AD: PT > FT		RD: PT > FT	
	(%)[b]	Mean P[c]	(%)[b]	Mean P[c]	(%)[b]	Mean P[c]	(%)[b]	Mean P[c]	(%)[b]	Mean P[c]
1	8.01	1.107	6.79	0.8926	9.09	0.2987	12.93	2.2759	7.80	1.0444
2	8.26	1.3571	7.60	0.7705			10.31	0.9656	7.92	1.1424
3	2.29	0.3353	3.38	0.6673			4.82	1.0458	1.42	0.2356
4	5.35	0.8485	7.41	1.3238			5.46	1.1386	6.28	1.1888
5	2.70	0.1264	2.99	0.2329			3.65	0.227	3.91	0.5827
6	2.27	0.2662	1.92	0.092			1.56	0.0699	3.45	0.3921
7	1.90	0.2366	1.28	0.0755			0.23	0.0069	1.64	0.1497
8	2.31	0.3008	2.58	0.1811			1.94	0.089	3.01	0.3472
9	9.14	1.3491	11.50	1.9212	1.82	0.0545	4.92	0.7417	11.11	1.7031
10	1.95	0.5493	6.87	3.0127			9.66	4.3052	4.21	1.581
11	9.98	1.4036	8.99	1.3432	34.29	6.3403	6.34	0.9175	10.62	1.6066
12	11.42	1.6211	14.53	2.4849			13.24	2.2963	12.77	2.0291
13	10.90	1.1801	5.50	0.52	38.96	7.9688	1.88	0.1807	8.64	0.9563
14	8.62	0.787	8.14	0.7688			6.71	1.1087	9.54	0.8971
15	8.39	0.7737	6.61	0.9918	96.88	17.9584	10.22	2.2875	4.44	0.2534
16	11.33	1.1276	12.11	1.6956			12.74	2.7437	9.94	0.8137
17	2.76	0.4613	3.77	0.584			4.51	0.5215	3.12	0.5442
18	2.07	0.2704	2.98	0.2912			4.25	0.3051	2.38	0.3298
19	4.60	0.3782	3.19	0.4044	95.58	15.5506	5.06	0.9632	2.20	0.106
20	5.90	0.4542	6.41	0.5659			6.41	0.8985	5.20	0.2963

Group comparison of skeletonized white matter measures was carried out by nonparametric t-test (5000 permutations) using randomize in FSL, with gender and MRI center as covariates of no interest. Statistical significance was set at $P < 0.05$, FWE (familywise error rate) corrected, by using threshold-free cluster enhancement (TFCE). Resulted group difference map was converted to binary mask in order to locate and identify white matter tracts in the result mask by using atlasquery in FSL. PT: preterm born adults; FT: full-term born adults; FA: fractional anisotropy; AD: axial diffusivity; RD: radial diffusivity.

[a]White matter tracts according to JHU white matter tractography atlas.

[b]Percentage of voxels of the considered tract within the result mask.

[c]Mean probabilities of the considered tract within the result mask.

Table S2. VBM results: altered gray matter volumes in preterm born adults

Side	Gray matter area	Cluster size (voxel)	BA	MNI coordinates of peak voxel				
				X	Y	Z	T value	*p*-value
PT < FT								
L/R	Thalamus	3927	NA	-13.5	-31.5	15	8.09	0
R	Striatum[a]	604	NA	19.5	19.5	-4.5	5.77	0.001
L		246	NA	-18	22.5	-10.5	5.22	0.009
R	Middle Temporal Gyrus	3840	20, 21, 22	57	-7.5	-18	9.69	0
L		889	21	-55.5	-6	-16.5	6.84	0
L	Superior Temporal Gyrus	45	21	-46.5	-28.5	0	5.74	0.001
R	Hippocampus	72	35	22.5	-19.5	-15	5.37	0.005
R	Superior Occipital Gyrus	358	19	27	-66	24	5.88	0.001
R	Fusiform Gyrus	270	37	49.5	-49.5	-12	6.14	0
PT > FT								
L/R	PCC	143	23	3	-22.5	37.5	5.42	0.004
L/R	ACC	136	32	6	42	16.5	6.08	0
L	Temporal_Pole	58	38	-31.5	21	-33	5.27	0.007
R	Fusiform Gyrus	38	37	36	-51	-19.5	5.04	0.018

Group comparison of regional gray matter volume was carried out by independent two-sample t-test using SPM8. Mean gray matter image (threshold > 0.2) was applied as explicit mask and potential confounding factors of gender and MRI center was controlled using covariates in GLM model estimation. For multiple comparison correction, significance level was set at $P_{FWE} < 0.05$ and cluster size K > 30. NA: not applicable; L/R: left/right; MNI: Montreal Neurological Institute; PCC: posterior cingulate cortex; ACC: anterior cingulate cortex; PT: preterm born adults; FT: full-term born adults.
[a]Striatum areas comprising putamen and caudate.

Table S3. Reduced FA associated with subcortical GMV in preterm born adults

Index	JHU-atlas-defined white matter tracts[a]	Striatum		Thalamus	
		Voxels (%)[b]	Mean probabilities[c]	Voxels (%)[b]	Mean probabilities[c]
1	Anterior thalamic radiation L	10.02	1.5302	10.25	1.6767
2	Anterior thalamic radiation R	10.59	2.0611	11.24	1.9411
3	Corticospinal tract L	1.21	0.2884	0.40	0.0194
4	Corticospinal tract R	7.47	1.5001	7.58	1.5776
5	Cingulum (cingulate gyrus) L	3.25	0.1633	3.05	0.1615
6	Cingulum (cingulate gyrus) R	0.52	0.0216	0.77	0.0308
7	Cingulum (hippocampus) L	2.68	0.4082	1.72	0.1452
8	Cingulum (hippocampus) R	3.40	0.5164	3.42	0.3881
9	Forceps major	14.06	2.3014	19.74	3.219
10	Forceps minor	3.19	1.0142	3.96	1.2966
11	Inferior fronto-occipital fasciculus L	13.18	2.1593	10.81	1.417
12	Inferior fronto-occipital fasciculus R	13.45	2.4599	15.40	2.7984
13	Inferior longitudinal fasciculus L	9.30	1.0203	10.55	1.3103
14	Inferior longitudinal fasciculus R	10.08	1.0157	11.97	1.1486
15	Superior longitudinal fasciculus L	7.61	0.7733	5.60	0.5093
16	Superior longitudinal fasciculus R	4.05	0.2013	4.16	0.2039
17	Uncinate fasciculus L	4.86	0.8666	0.02	0.0006
18	Uncinate fasciculus R	3.26	0.5247	1.59	0.2066
19	Superior longitudinal fasciculus (temporal part) L	4.19	0.3686	2.46	0.1706
20	Superior longitudinal fasciculus (temporal part) R	1.74	0.0773	1.48	0.0706

Statistical dependent relationship between white matter FA and gray matter volume in striatum and thalamus was evaluated by nonparametric t-test (5000 permutations) using randomize in FSL, with gender and MRI center as covariates of no interest. Statistical significance was set at $P < 0.05$, FWE (familywise error rate) corrected, by using threshold-free cluster enhancement (TFCE). Significantly correlation map was converted to binary mask in order to locate and identify white matter tracts in the result mask by using atlasquery in FSL. L/R: left/right.

[a]White matter tracts according to JHU white matter tractography atlas.

[b]Percentage of voxels of the considered tract within the result mask.

[c]Mean probabilities of the considered tract within the result mask.

Table S4. Reduced FA associated with the degree of prematurity in preterm born adults

Index	JHU-atlas-defined white matter tracts[a]	FA ∝ GA		FA ∝ BW		FA ∝ Non-OPTN	
		(%)[b]	Mean P[c]	(%)[b]	Mean P[c]	(%)[b]	Mean P[c]
1	Anterior thalamic radiation L	24.79	4.3398	64.89	5.7713	15.10	2.1121
2	Anterior thalamic radiation R	14.33	1.3113	1.06	0.0319	12.05	1.8771
3	Corticospinal tract L	0.28	0.0106			0.39	0.0228
4	Corticospinal tract R	0.06	0.0018			2.93	0.905
5	Cingulum (cingulate gyrus) L	0.94	0.0303			5.45	0.2507
6	Cingulum (cingulate gyrus) R	0.62	0.0187			0.90	0.0269
7	Cingulum (hippocampus) L	0.22	0.0066			0.15	0.0045
8	Cingulum (hippocampus) R	1.12	0.0337			1.22	0.0366
9	Forceps major	6.04	0.5761	12.77	2.2553	11.57	1.7574
10	Forceps minor	4.36	1.3543			4.07	1.4901
11	Inferior fronto-occipital fasciculus L	9.01	1.3495	0.53	0.016	12.18	1.8431
12	Inferior fronto-occipital fasciculus R	8.79	1.4841	18.62	2.016	9.86	1.0945
13	Inferior longitudinal fasciculus L	5.88	0.7509	4.26	0.1915	6.82	0.4547
14	Inferior longitudinal fasciculus R	3.59	0.1433	13.83	0.5585	4.85	0.1974
15	Superior longitudinal fasciculus L	5.80	0.447			4.83	0.3243
16	Superior longitudinal fasciculus R	2.79	0.1046	4.26	0.1277	2.86	0.0973
17	Uncinate fasciculus L	2.49	0.3661			5.35	1.0081
18	Uncinate fasciculus R	0.24	0.0134	10.11	0.5904	0.12	0.0096
19	Superior longitudinal fasciculus (temporal part) L	3.89	0.2206			2.36	0.1303
20	Superior longitudinal fasciculus (temporal part) R	1.53	0.05	0.53	0.016	0.72	0.022

Statistical dependent relationship between white matter FA and the prematurity degree at birth was evaluated by nonparametric t-test (5000 permutations) using randomize in FSL, with gender and MRI center as covariates of no interest. Non-OPTN is defined by OPTN x (-1). Statistical significance was set at $P < 0.05$, FWE (familywise error rate) corrected, by using threshold-free cluster enhancement (TFCE). Significantly correlation map was converted to binary mask in order to locate and identify white matter tracts in the result mask by using atlasquery in FSL. L/R: left/right; FA: fractional anisotropy; GA: gestational age; BW: birth weight; OPTN: neonatal optimality.

[a]White matter tracts according to JHU white matter tractography atlas.

[b]Percentage of voxels of the considered tract within the result mask.

[c]Mean probabilities of the considered tract within the result mask.

Table S5. Reduced FA associated with total IQ in preterm born adults

		IQ	
Index	JHU-atlas-defined white matter tracts[a]	Voxels (%)[b]	Mean probabilities[c]
1	Anterior thalamic radiation L	1.50	0.0469
2	Anterior thalamic radiation R	19.95	4.5223
3	Corticospinal tract L	1.20	0.0512
4	Corticospinal tract R	10.89	2.8377
5	Cingulum (cingulate gyrus) L	1.41	0.0497
6	Cingulum (cingulate gyrus) R	0.77	0.0237
7	Cingulum (hippocampus) L		
8	Cingulum (hippocampus) R	0.12	0.0036
9	Forceps major	0.67	0.088
10	Forceps minor	2.55	0.2203
11	Inferior fronto-occipital fasciculus L		
12	Inferior fronto-occipital fasciculus R	13.69	2.539
13	Inferior longitudinal fasciculus L		
14	Inferior longitudinal fasciculus R	8.07	0.7114
15	Superior longitudinal fasciculus L	0.12	0.0036
16	Superior longitudinal fasciculus R	4.37	0.2645
17	Uncinate fasciculus L		
18	Uncinate fasciculus R	6.31	1.0695
19	Superior longitudinal fasciculus (temporal part) L	0.05	0.0015
20	Superior longitudinal fasciculus (temporal part) R	2.91	0.1231

Statistical dependent relationship between white matter FA and total IQ in adulthood was evaluated by nonparametric t-test (5000 permutations) using randomize in FSL, with gestational age, gender and MRI center as covariates of no interest. Statistical significance was set at $P < 0.05$, FWE (familywise error rate) corrected, by using threshold-free cluster enhancement (TFCE). Significantly correlation map was converted to binary mask in order to locate and identify white matter tracts in the result mask by using atlasquery in FSL. L/R: left/right; FA: fractional anisotropy; IQ: Intelligence Quotient.

[a]White matter tracts according to JHU white matter tractography atlas.

[b]Percentage of voxels of the considered tract within the result mask.

[c]Mean probabilities of the considered tract within the result mask.

Supplemental Figures:

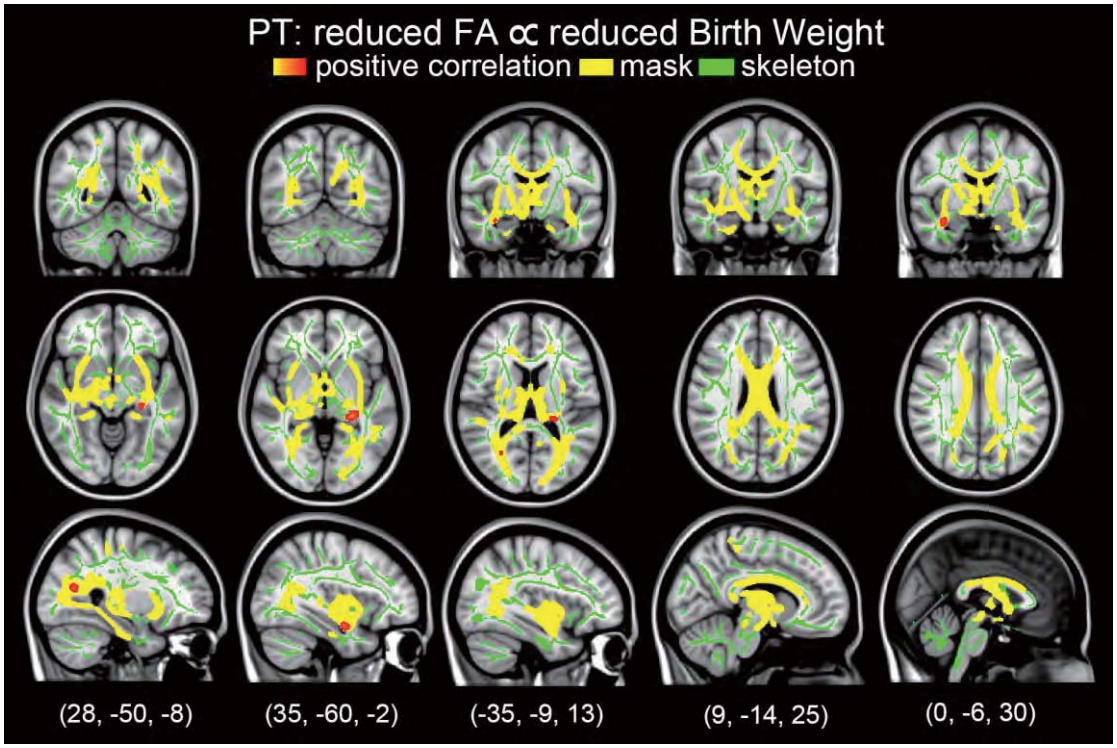

Figure S1. Correspondence between white matter changes and birth weight within preterm born adults. Coronal, axial, and sagittal views illustrated significant positive correlation between decreasing fractional (FA) and decreasing birth weight in preterm born adults (PT). Green color indicated the common skeleton over PT and term born adults. Yellow color showed affected white matter tracts with significantly reduced FA in PT group (permutation test, $P < 0.05$, FWE corrected). Red illustrated related white matter tracts where birth weight predicted FA in preterm born adults. MNI coordinates were provided at the bottom. For more details see Table S4.

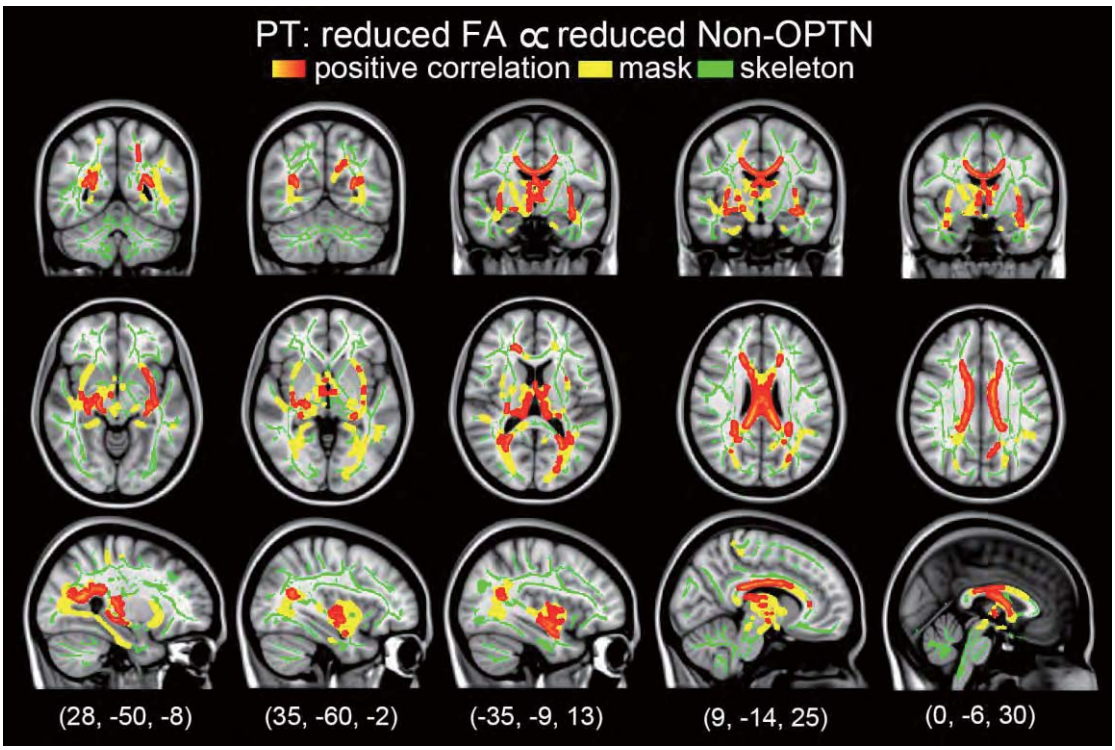

Figure S2. Correspondence between white matter changes and neonatal medical complications within preterm born adults. Coronal, axial, and sagittal views illustrated significant positive correlation between reduced fractional anisotropy (FA) and lower score of Non-OPTN. OPTN reflects neonatal medical complications. Non-OPTN is defined by OPTN x (-1), with the lower Non-OPTN the worse neonatal medical complications. Green color indicated the common skeleton over PT and term born adults. Yellow color showed affected white matter tracts with significantly reduced FA in PT group (permutation test, $P < 0.05$, FWE corrected). Red illustrated related white matter tracts where Non-OPTN predicted FA in preterm born adults. MNI coordinates were provided at the bottom. For more details see Table S4.

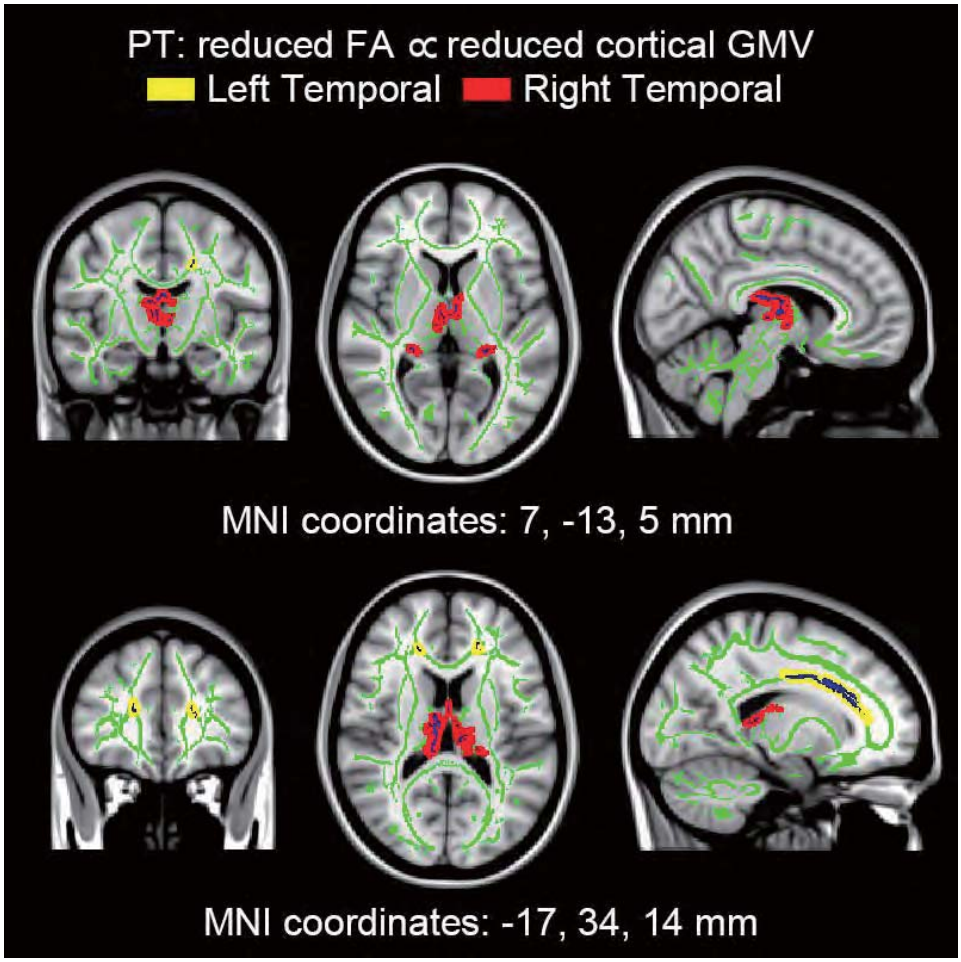

Figure S3. Correspondence between white matter changes and temporal gray matter changes within preterm born adults. Coronal, axial, and sagittal views illustrated affected white matter tracts in preterm born adult (PT) group, where decreasing fractional anisotropy (FA) was positively correlated with decreasing gray matter volume (GMV) in bilateral middle temporal areas across preterm born adults, colored by blue (permutation test, $P < 0.05$, FWE corrected). For better visualization, significant white matter results were dilated and superimposed on the T1-wegihted brain image of MNI152 structural standard template. Yellow color indicated results that left middle temporal gray matter volume was correlated with the body and genu of bilateral corpus callosum. Red color indicated results that right middle temporal gray matter volume was correlated with bilateral anterior thalamic radiation. For the common skeleton over PT and term born adults, it was colored by green. MNI coordinates were provided at the bottom.

Summary and discussion

To address my research questions including whether aberrant functional connectome that was presented in patients with major depressive disorder can predict the course of recurrent depressive episodes, whether aberrant white matter micro-structural integrity was presented in the same patients underlying the disrupted functional connectome, whether aberrant functional connectome was presented in preterm born adults who were at risk for depression together with underlying aberrant white matter microstructural integrity, I have conducted rs-fMRI and DTI studies in patients with major depression and preterm born adults at risk for depression, and provided relevant answers.

Brain connectome is altered in MDD, linked with depressive episodes and symptom severity

MDD patients demonstrate aberrant functional brain connectome featured by impaired efficiency and centrality in functional integration compared with healthy controls. Altered brain connectome was associated with symptom severity of current episode in MDD patients. More importantly, MDD-related abnormalities, specifically striatal network topology, is linked with the number of depressive episode independently of symptom severity of current episode in MDD patients, which might suggest a predictor for disorder course and relapse risk of MDD.

White matter fiber connections constitute the structural basis underlying brain connectome, providing biological communication pathways. The structural basis

indexed by white matter integrity of FA and RD exhibit significant impairments of white matter tracts in MDD. FA-based association with number of episodes provided some hints for the disorder course prediction.

As revealed by the two studies in this thesis, human brain connectome is important for understanding MDD as significant predictor for disorder severity and relapse risk. Current work contributes to biomarker identification and intermediate phenotype in MDD.

Brain connectome is altered in preterm born adults, linked with lesion and compensation

It is a basic challenge in neuroscience to uncover developmental trajectory of human brain as well as disturbed brain development such as affected by preterm birth. Given emerging evidence about reconfigured brain organization in preterm newborns and early development, it becomes important to figure out later outcomes. The 3rd and 4th studies in this thesis provide new evidence about aberrant functional brain connectome and underlying gray and white matter features in preterm born adults.

The optimal small-world organization is preserved in preterm born adults due to comparable global topological properties between preterm and term groups. However, regional alterations of network topology are present in the preterm's brain and linked with the preterm's gestational age, birth weight, neonatal risk factor, and adulthood IQ. Very interestingly, subcortical and primary cortical regions like caudate, hippocampus and auditory cortex, have potentially adverse alterations of network topology which link with higher prematurity at birth and/or lower IQ in adulthood, whereas associative

cortical regions in frontal and parietal cortex display potentially beneficial changes linked with lower prematurity at birth and higher/or IQ in adulthood. As for the white matter, extensive FA reductions are present in preterm born adults. White matter changes keeps the same pace with subcortical gray matter changes like thalamus and striatum. Similar patterns of associations with prematurity and IQ are identified in FA of affected white matter tracts.

These findings suggest that, subcortical brain impairments like thalamus and white matter injury found in infants can persist into adulthood, but during the long-term development, some adaptive reconfigurations in response to early lesion and adverse impact may somehow compete with brain dysfunction.

MDD and preterm born adults show overlap in subcortical regions

By applying the same approach, aberrant functional brain connectome and underlying white matter microstructure are identified in both major depression and preterm born adults at risk for depression. Not surprisingly, brain connetome approach shows more significant results than tract-based approach, for example, altered network topology predicts MDD course and the preterm's risk factor (e.g. gestational age), whereas altered white matter FA predicts the preterm's risk factor but not for MDD course. It may be because brain connectome is an important intermediate phenotype for brain organization (Bullmore and Sporns, 2009; Filippi et al., 2013).

As for the aberrant patterns, both MDD and preterm born adults show disrupted subcortical network topology like thalamus and striatum. The subcortico-cortical loop

is critical for brain functions like motivation, emotion processing and its regulation and executive control (Hamilton et al., 2012). Thalamus, striatum, and primary cortical connectivity seems to be "earlier" developed compared to multimodal associative neocortex (Collin and van den Heuvel, 2013) and vulnerable for prematurity-dependent injuries like hypoxia and inflammation (Salmaso et al., 2014). In brain organization, striatum and thalamus has been found as important hub connectors in rich club organization (van den Heuvel and Sporns, 2011). Therefore, disorganization of these regions' connectivity linked with preterm birth and MDD might hint how preterm birth may link with an increased risk for MDD.

From the view of white matter's connectivity, white matter tracts play an important role in brain connectome as the structural basis. Similar pattern of extensively reduced FA and increased RD are present in both MDD and preterm born adults. The FA reduction and RD increases with unchanged AD is usually associated with demyelination/degeneration in white matter fibers which leads to disconnectivity. Therefore extensive structural alterations provide another overlap between major depression and preterm born adults. In the future, DTI-based structural connectome can be examined and compared with rs-fMRI-based functional connectome, in order to explore structure-function-combined mechanistic link between MDD and preterm born individuals.

To interpret the preterm born individuals at risk for depression as the transient state of preclinical major depression, two lines must be drawn. Firstly, epidemic evidence highlights that preterm birth has been found significantly associated with increased risk

of psychiatric hospitalization in adulthood in a monotonic manner across a range of psychiatric disorders including MDD (Nosarti et al., 2012). Some of emerged brain abnormalities in preterm born adults may be shared by MDD, which can contribute to better understanding the etiology of MDD. Secondly, recent development of Gene-by-Environment interactions studies highlight that interacted genes and experience play important roles in the development of depression. In line with this, evidence based on animal models indicates that perinatal stress like preterm birth is an important trigger for major depression (Meyer et al., 2001; Schmitz et al., 2002; Nabeshima and Kim, 2013; Stepanichev et al., 2014). Future longitudinal study may be needed to track preterm born individuals before and after psychiatric diagnosis in order to refine the biomarker identification.

Overall conclusion

Our findings about aberrant functional connectome and reshaped structural basis in recureent major depression and preterm birth can shed new light on neurobiological pathway of major depressive disorder, particularly with respect to disorder course and potential link between major depressive disorder and adverse consequences of preterm birth as a risk factor for depression. Moreover, human brain organization at the macro scale still shows the nature of complex network. The MRI-based macroscopic brain connectome provide a fundamental and powerful framework to explore organizational principles in human brain. Brain connectome research might hopefully point out a

common pathway for better understanding mental disorders and developing future diagnosis and treatment.

References

Bullmore E, Sporns O (2009) Complex brain networks: graph theoretical analysis of structural and functional systems. Nature reviews Neuroscience 10:186-198.

Collin G, van den Heuvel MP (2013) The ontogeny of the human connectome: development and dynamic changes of brain connectivity across the life span. The Neuroscientist : a review journal bringing neurobiology, neurology and psychiatry 19:616-628.

Filippi M, van den Heuvel MP, Fornito A, He Y, Hulshoff Pol HE, Agosta F, Comi G, Rocca MA (2013) Assessment of system dysfunction in the brain through MRI-based connectomics. Lancet neurology 12:1189-1199.

Hamilton JP, Etkin A, Furman DJ, Lemus MG, Johnson RF, Gotlib IH (2012) Functional neuroimaging of major depressive disorder: a meta-analysis and new integration of base line activation and neural response data. The American journal of psychiatry 169:693-703.

Meyer SE, Chrousos GP, Gold PW (2001) Major depression and the stress system: a life span perspective. Development and psychopathology 13:565-580.

Nabeshima T, Kim HC (2013) Involvement of genetic and environmental factors in the onset of depression. Experimental neurobiology 22:235-243.

Nosarti C, Reichenberg A, Murray RM, Cnattingius S, Lambe MP, Yin L, MacCabe J, Rifkin L, Hultman CM (2012) Preterm birth and psychiatric disorders in young adult life. Archives of general psychiatry 69:E1-8.

Salmaso N, Jablonska B, Scafidi J, Vaccarino FM, Gallo V (2014) Neurobiology of premature brain injury. Nature neuroscience 17:341-346.

Schmitz C, Rhodes ME, Bludau M, Kaplan S, Ong P, Ueffing I, Vehoff J, Korr H, Frye CA (2002) Depression: reduced number of granule cells in the hippocampus of female, but not male, rats due to prenatal restraint stress. Molecular psychiatry 7:810-813.

Stepanichev M, Dygalo NN, Grigoryan G, Shishkina GT, Gulyaeva N (2014) Rodent models of depression: neurotrophic and neuroinflammatory biomarkers. BioMed research international 2014:932757.

van den Heuvel MP, Sporns O (2011) Rich-club organization of the human connectome. The Journal of neuroscience : the official journal of the Society for Neuroscience 31:15775-15786.

Acknowledgements

I appreciate a lot my supervisors of thesis advisory committee - Dr. Afra Wohlschläger, Dr. Christian Sorg, and Prof. Dr. Hermann Müller for their continuous support during my whole doctoral study. The research time at TUM-NIC neuroimaging center and Neuroradiology department of TUM is enjoyable for me. The scientific insight and vision as well as dedication of Afra and Christian keep motivating me forward. I am also very thankful to all colleagues in our lab and all my coauthors in publications.

I would like to thank China Scholarship Council (CSC) which offers me first-3-year PhD study grant. I do appreciate GSN which offers excellent PhD training, guidance, and support as well as the international, multidisciplinary, and friendly platform.

I am deeply grateful to Xiyao and my parents for their love and support all the time as well as their patience throughout my studies.

Affidavit / Statutory declaration and statement

Hiermit versichere ich an Eides statt, dass ich die vorliegende Dissertation Brain Connectome in Major Depression and Preterm Born Individuals at Risk for Depression selbstständig angefertigt habe, mich außer der angegebenen keiner weiteren Hilfsmittel bedient und alle Erkenntnisse, die aus dem Schrifttum ganz oder annähernd übernommen sind, als solche kenntlich gemacht und nach ihrer Herkunft unter Bezeichnung der Fundstelle einzeln nachgewiesen habe.

I hereby confirm that the dissertation Brain Connectome in Major Depression and Preterm Born Individuals at Risk for Depression is the result of my own work and that I have only used sources or materials listed and specified in the dissertation.

München, den

Munich, date 28.08.2014

Chun Meng

Unterschrift signature

CV

Chun Meng

Born: 21.10.1980 Nationality: P.R.China

Education

2010.9 – 2014.8	**PhD** study	**Ludwig-Maximilians-Universität München**
	Graduate School of Systemic Neurosciences, LMU, Munich, Germany	
2007.5 – 2010.7	**MSc**	**Beijing Normal University**
	State Key Laboratory of Cognitive Neuroscience and Learning &	
	IDG/McGovern Institute for Brain Research, BNU, Beijing, China	
1999.9 – 2003.7	**BA**	**BeiHang University**
	School of Electronic and Information Engineering, BUAA, Beijing, China	

Work experience

2013.10 – 2014.6	**Research Scientist**	**Klinikum rechts der Isar,**
	TUM-NIC imaging center, TUM, Munich, Germany	
2011.4 – 2013.8	**Research Assistant**	**Klinikum rechts der Isar**
	Neuroradiology department, TUM, Munich, Germany	
2003.8 – 2007.4	**Electronic Engineer**	**China Aerospace**
	Institute of Information Technology, China Aerospace Science and	
	Industry Corporation, Beijing, China	

Awards and Fundings

2014 *PhD Grant* for thesis writing, GSN-LMU

2010 – 2013 *International Doctoral Scholarship* granted by China Scholarship Council (CSC)

2009 *Excellence Award*, State Key Laboratory of Cognitive Neuroscience and Learning, BNU

Publications

1. **C. Meng***, F. Brandl*, M. Tahmasian, J. Shao, A. Manoliu, M. Scherr, D. Schwerthoffer, J. Bäuml, H. Forstl, C. Zimmer, A. M. Wohlschlager, V. Riedl, C. Sorg, Aberrant topology of striatum's connectivity is associated with the number of episodes in depression. Brain 137, 598-609 (2014); published online EpubFeb (10.1093/brain/awt290). IF: 10.226

2. J. G. Bäuml, M. Daamen, **C. Meng**, J. Neitzel, L. Scheef, J. Jaekel, B. Busch, N. Baumann, P. Bartmann, D. Wolke, H. Boecker, A. M. Wohlschlager, C. Sorg, Correspondence Between Aberrant Intrinsic Network Connectivity and Gray-Matter Volume in the Ventral Brain of Preterm Born Adults. Cerebral Cortex, (2014); published online Epub Jun 16 (10.1093/cercor/bhu133). IF: 8.305

3. L. Pasquini, M. Scherr, M. Tahmasian, **C. Meng**, N. E. Myers, M. Ortner, M. Muhlau, A. Kurz, H. Forstl, C. Zimmer, T. Grimmer, A. M. Wohlschlager, V. Riedl, C. Sorg, Link between hippocampus' raised local and eased global intrinsic connectivity in AD. Alzheimer's & dementia : the journal of the Alzheimer's Association, (2014); published online EpubJul 17 (10.1016/j.jalz.2014.02.007). IF: 17.472

4. A, Manoliu, **C. Meng**, F. Brandl, A. Doll, M. Tahmasian, M. Scherr, D. Schwerthoffer, C. Zimmer, H. Forstl, J. Bauml, V. Riedl, A. M. Wohlschlager, C. Sorg, Insular dysfunction within the salience network is associated with severity of symptoms and aberrant inter-network connectivity in major depressive disorder. Front Hum Neurosci 7, 930 (2013) 10.3389/fnhum.2013.00930. IF: 2.9

5. A. Doll, C. Sorg, A. Manoliu, A. Woller, **C. Meng**, H. Forstl, C. Zimmer, A. M. Wohlschlager, V. Riedl, Shifted intrinsic connectivity of central executive and salience network in borderline personality disorder. Front Hum Neurosci 7, 727 (2013) 10.3389/fnhum.2013.00727. IF: 2.9

6. M. Tahmasian, D. C. Knight, A. Manoliu, D. Schwerthoffer, M. Scherr, **C. Meng**, J. Shao, H. Peters, A. Doll, H. Khazaie, A. Drzezga, J. Bauml, C. Zimmer, H. Forstl, A. M. Wohlschlager, V. Riedl, C. Sorg, Aberrant intrinsic connectivity of hippocampus and amygdala overlap in the fronto-insular and dorsomedial-prefrontal cortex in major depressive disorder. Front Hum Neurosci 7, 639 (2013) 10.3389/fnhum.2013.00639). IF: 2.9

7. J. Shao, N. Myers, Q. Yang, J. Feng, C. Plant, C. Bohm, H. Forstl, A. Kurz, C. Zimmer, **C. Meng**, V. Riedl, A. Wohlschlager, C. Sorg, Prediction of Alzheimer's disease using individual structural connectivity networks. Neurobiol Aging 33, 2756-2765 (2012); published online EpubDec (10.1016/j.neurobiolaging.2012.01.017). IF: 6.166

8. Y. Xuan*, **C. Meng***, Y. Yang, C. Zhu, L. Wang, Q. Yan, C. Lin, C. Yu, Resting-state brain activity in adult males who stutter. PloS one 7, e30570 (2012) 10.1371/journal.pone.0030570). IF: 3.73

9. L. Tian, **C. Meng**, H. Yan, Q. Zhao, Q. Liu, J. Yan, Y. Han, H. Yuan, L. Wang, W. Yue, Y. Zhang, X. Li, C. Zhu, Y. He, D. Zhang, Convergent evidence from multimodal imaging reveals amygdala abnormalities in schizophrenic patients and their first-degree relatives. PloS one 6, e28794 (2011)10.1371/journal.pone.0028794). IF: 3.73

* indicates equal contribution

List of publications and manuscripts

1. **C. Meng**, F. Brandl, M. Tahmasian, J. Shao, A. Manoliu, M. Scherr, D. Schwerthoffer, J. Bäuml, H. Forstl, C. Zimmer, A. M. Wohlschlager, V. Riedl, C. Sorg, **Aberrant topology of striatum's connectivity is associated with the number of episodes in depression**. Brain 137, 598-609 (2014); published online EpubFeb (10.1093/brain/awt290). **IF: 10.226**
2. **C. Meng**, J. G. Bäuml, M. Daamen, J. Jaekel, J. Neitzel, L. Scheef, B. Busch, N. Baumann, H. Boecker, C. Zimmer, P. Bartmann, D. Wolke, A. M. Wohlschläger, C. Sorg, **Extensive and interrelated subcortical white and gray matter alterations in preterm born adults**. Submitted
3. **C. Meng**, J. G. Bäuml, Y. He, X. Xie, J. Jaekel, M. Daamen, L. Scheef, B. Busch, N. Baumann, H. Boecker, P. Bartmann, D. Wolke, A. M. Wohlschläger, C. Sorg, **Altered functional brain connectome in very preterm born adults**. Submitted
4. **C. Meng**, F. Brandl, M. Scherr, D. Schwerthoffer, J. Bäuml, H. Forstl, C. Zimmer, A. M. Wohlschlager, V. Riedl, C. Sorg, **Aberrant microstructural white matter is associated with the number of episodes in major depression**. Drafting

Declaration of author contributions

Chun Meng designed the study, conceived whole analysis, scripted analytical programs, built all figures, carried out post analysis due to reviewers' comments, and wrote the paper **Meng et al (2014)**. Inside, Chun Meng carried out half of literature review, data preprocessing, quality control, and graph-based analysis. The other half was finished by Felix Brandl, whom Chun Meng supervised during his medical doctoral thesis. Christian Sorg (correspondence author), Felix Brandl, and Chun Meng conducted the result discussion and drafted the initial version of manuscript. Christian Sorg and Chun Meng revised the manuscript until final publishing. To note, Felix Brandl and Chun Meng contributed equally as marked in the publication resulting in a shared 1st authorship.
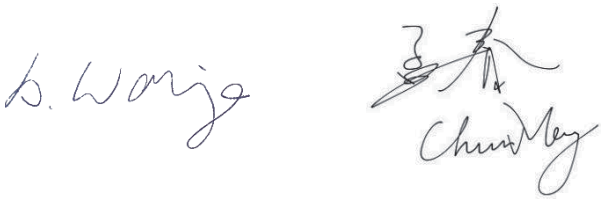
Chun Meng designed the study, analyzed the data and wrote three manuscripts **Meng et al (submitted[1], submitted[2], drafting)** as the 1st author.